https://dspace.org/

Green extraction technology for the extraction of iron from iron ore fines

Tshofu, Glawdis Shungu

2015-05-05
http://hdl.handle.net/10539/17610

Downloaded from a DSpace repository. https://dspace.org/

GREEN EXTRACTION TECHNOLOGY FOR THE EXTRACTION OF IRON FROM IRON ORE FINES

Glawdis Shungu Tshofu

A dissertation submitted to the Faculty of Engineering and the Built Environment, University of the Witwatersrand, in fulfilment of the requirements for the degree of Master of Science in Engineering.

Johannesburg, 2014

DECLARATION

I declare that this dissertation is my own unaided work. It is being submitted for the degree of Master of Science in Engineering to the University of the Witwatersrand, Johannesburg. It has not been submitted before for any other degree or examination in any other University.

……

Glawdis Shungu Tshofu

10 September 2014

ABSTRACT

Large quantities of iron ore fines accumulate near iron ore mining operations and cannot be used in conventional iron ore treatment processes. Existing iron ore fines processing techniques are associated with high costs, high energy consumptions and high greenhouse gas emissions. Greater environmental concern in the last few years creates the need to develop greener extraction techniques. In this study, a green method for the extraction of iron from iron ore fines using acetylacetone ($C_5H_8O_2$) was investigated and several processes for the utilization of the extraction products were proposed.

The extraction experiments were performed on iron ore fines containing 93 wt% of hematite. In the gas phase, it was found that the extraction increases with temperature and acetylacetone flowrate but decreases with bed weight. Very low extractions were observed at all the operating conditions under investigation. The highest extraction of only 3.88 % was obtained at 9 mL/min of acetylacetone after 6 hours. The low extractions were attributed to mass transfer limitations probably associated with the passivation of the active surface of the iron ore fines. In order to overcome these limitations the extraction experiments were performed in the liquid phase (leaching). Using a 2^k factorial design method, it was found that temperature and solid to liquid ratio had significant effects on the leaching process. The highest iron extraction of 97.7% was obtained at 140 °C, 0.025:1 solid to liquid ratio and a particle size of 106 to 150 µm after 48 hours. An adapted form of the shrinking core model was used for the kinetic analysis of the leaching process and the best fit was found to be the chemical reaction controlled model. However, the calculated activation energy from the modelling was 4.22 kJ/mol suggesting that the process might be controlled by diffusion. The extraction products were easily separated from unreacted acetylacetone using a Heidolph evaporator and iron(III) acetylacetonate crystals were formed in the process. A preliminary study showed that the gas phase recovery of iron from iron(III) acetylacetonate using hydrogen is practically feasible.

This work has shown that the proposed extraction method can be used as a platform for the development of two manufacturing processes; the production of iron nanoparticles and that of iron(III) acetylacetonate crystals. An economic feasibility study of the latter process was performed and the large net present value (NPV) of 1.153 Billion Rand, and high internal rate of return (IRR) of 63% were indicators of a profitable process.

PUBLICATIONS AND PRESENTATIONS

Conference proceedings

Tshofu, G S., van Dyk, L D., Ndlovu, S., Sibanda, V., 2013. Liquid phase extraction of iron from iron ore fines using acetyl acetone. Mineral Processing, Cape Town, South Africa, 7-8 August 2013

DEDICATION

To my mother

Therese Lukenge Kapwibwe.

ACKNOWLEDGMENTS

Thanks are due to the following people and organizations, their participation and support made this work possible:

- My supervisor, Dr Lizelle van Dyk, for her invaluable involvement at every stage of this work. Her guidance and support through trial times kept me going, even when unsure of the outcome. The useful criticism she gave during the process of writing this report are highly appreciated.
- Prof Sehlo Ndlovu, and Dr Vusi Sibanda, their insightful discussion during research meeting is acknowledge and appreciated.
- Undergraduate students; Juanita, Varisha and Fridaus for their involvement in some aspects of the experimental work.
- The Carnegie Foundation for funding this project through the Carnegie Transformation Research Award program at the University of the Witwatersrand.
- Kumba Iron Ore, for providing the iron ore fines used in this work.
- My siblings, Idriss, Brenda, Lys and Roselito for their love and support
- My special friend Christie, for her love, support, and suggestions

TABLE OF CONTENTS

DECLARATION ..... **ii**

ABSTRACT ..... **iii**

PUBLICATIONS AND PRESENTATIONS ..... **v**

DEDICATION ..... **vi**

ACKNOWLEDGMENTS ..... **vii**

LIST OF FIGURES ..... **xi**

LIST OF TABLES ..... **xv**

LIST OF ABBREVIATIONS AND SYMBOLS ..... **xvii**

1. INTRODUCTION **1**

1.1 Motivation and background 1

1.2 Aim and objectives 3

1.3 Dissertation layout 4

2 LITERATURE REVIEW **5**

2.1 Introduction 5

2.2 Review of conventional iron and steel production techniques 5

2.2.1 Blast furnace operations 6

2.2.2 Direct reduction 7

2.2.3 Direct smelting 7

2.2.4 Agglomeration techniques of iron ore fines 7

2.2.5 Energy use and gas emissions in the iron manufacturing industry 8

2.3 New techniques for the production of iron from iron ore fines 10

2.4 Chelating agent and the chelating effect 10

2.4.1 Description of chelating agents 10

2.4.2 Acetylacetone 12
2.5 Extraction of metals using chelating ligands 13
2.5.1 Extraction with acetylacetone 14
3 EXPERIMENTAL METHODS 19
3.1 Characterization of iron ore fines 19
3.1.1 Particle size distribution 19
3.1.2 Surface area characterization 19
3.1.3 Chemical and crystalline composition 20
3.2 Gas phase iron extraction 20
3.2.1 Experimental set up 21
3.2.2 Experimental method 23
3.3 Leaching of iron ore fines 23
3.3.1 Experimental set up 23
3.3.2 Experimental methods 24
3.3.3 Recovery of unreacted acetylacetone and iron(III) acetylacetonate from leach solution 26
3.4 Preliminary recovery of iron from iron(III) acetylacetonate 28
3.4.1 Experimental setup 28
3.4.2 Experimental method 29
4 RESULTS AND DISCUSSIONS 31
4.1 Characteristics of iron ore fines 31
4.1.1 Particle size distribution 31
4.1.2 Surface area characteristics 32
4.1.3 Chemical and crystalline composition of the iron ore fines 33
4.2 Gas phase extraction and recovery of iron 34

4.2.1 Effect of temperature on iron extraction 35

4.2.2 Effect of bed weight on iron extraction..... 36

4.2.3 Effect of acetylacetoneflowrate on iron extraction 37

4.3 Leaching of iron from iron ore fines 41

4.3.1 Identification of significant operating variables 41

4.3.2 Influence of significant operating variables on the leaching of iron from iron ore fines. 45

4.3.3 Kinetic analysis 48

4.3.4 Recovery of unreacted acetylacetone and iron(III) acetylacetonate from leach solution 58

4.4 Recovery of iron by hydrogen reduction of iron(III) acetylacetonate..... 60

4.5 Industrial applications of iron extraction using acetylacetone 62

4.5.1 The production of iron(III) acetylacetonate from iron ore fines 62

4.5.2 The production of iron nano-particles from iron ore fines..... 81

5 CONCLUSIONS AND RECOMMENDATIONS 83

5.1 Conclusions 83

5.2 Recommendations 85

6 REFERENCES..... 86

APPENDICES 93

Appendix A: Characteristics of solid samples 93

Appendix B: Gas phase extraction 95

Appendix C: Liquid phase extraction..... 105

Appendix D: Hydrogen reduction 118

Appendix E: Cost estimation..... 120

Appendix F: Matlab codes..... 139

LIST OF FIGURES

Figure 1.1: Block flow diagram for the extraction of iron from iron ore fines. 3

Figure 2.1: Block diagram illustrating the various process routes for the production of steel (Wright and Taylor, 1991). 6

Figure 2.2: Direct industrial CO_2 emissions by sector in 2006 (OECD, 2010). 9

Figure 2.3: Resonance stability of acetylacetone 11

Figure 2.4: Molecular structure of ethyl-diamine-tetraacetate (ChemEd, 2013)..... 12

Figure 2.5: The enol (a) and keto (b) stable form of acetylacetone..... 13

Figure 3.1: Fluidized bed reactor used for gas phase extraction 22

Figure 3.2: Experimental set up for the gas phase extraction process..... 22

Figure 3.3: Experimental set up for leaching experiments. 24

Figure 3.4: Heidolph 2 rotary evaporator for the recovery of unreacted acetylacetone, water and iron(III) acetylacetonate crystals. 28

Figure 3.5: Experimental set up for the hydrogen reduction process. 30

Figure 4.1: Cumulative particle size distribution of the iron ore fines sample..... 32

Figure 4.2: Micrograph of iron ore fines at 1350x magnification 33

Figure 4.3: The effect of temperature on the extraction of iron from iron ore fine particles (+106 to -150 µm) at 6 mL/min of acetylacetone flowrate. 35

Figure 4.4: The effect of bed weight on the extraction of iron at 250°C, 6 mL/min of acetylacetone, +106 to -150 µm particle size. 36

Figure 4.5: The effect of acetylacetoneflowrate on the extraction of iron at 250 °C from +106 to -150 µm particle size. 38

Figure 4.6: The effect of discontinuous acetylacetone flow and nitrogen feed on iron extraction at 250 °C and 6 mL/min for +106 to -150 µm particle size. 39

Figure 4.7: Iron extraction from iron ore fines and synthetic hematite at 250 °C and 6 mL/min for +106 to 1150 µm particle size. 40

Figure 4.8: Normal % probability plot of effects of operating variables (A-solid to liquid ratio, B-particle size, C-temperature) and their interaction effects (AB, BC and AC). 43

Figure 4.9: Half normal probability plot of effects of operating variables (A-solid to liquid ratio, B-particle size, C-temperature) and their interaction effects (AB, BC and AC)..... 44

Figure 4.10: The effect of temperature on leaching of iron at 0.025:1 and 0.127:1 solid to liquid ratio (S:L) from +106 to +150 µm particles after 48 hours. 45

Figure 4.11: The effect of solid to liquid ratio on leaching of iron ore fine at 140 °C with +106 to -150 and +400 to-600 µm particles after 48 hours..... 46

Figure 4.12: Leaching residue containing iron(III) acetylacetonate crystals..... 47

Figure 4.13: The effect of reaction time and temperature on leaching of iron at solid to liquid ratio of 0.025:1, 106 to 150 µm particles. 48

Figure 4.14: Model layer for mass transfer limitations..... 50

Figure 4.15: Experimental extraction kinetic data and fitted shrinking core model for chemical reaction controlled kinetics at various temperatures (+106 to -150 µm particle size and 0.025:1 solid to liquid ratio). 54

Figure 4.16: Arrhenius plot for leaching of iron ore fines at 0.025:1 solid to liquid ratio and particle size +106 to -150 µm. 56

Figure4.17: Experimental extraction kinetic data and fitted shrinking core model for diffusion controlled kinetics at various temperatures (+106 to -150 µm particle size and 0.025:1 solid to liquid ratio). 57

Figure 4.18: Picture of iron(III) acetylacetonate crystals formed during separation process. 58

Figure 4.19: X-Ray Diffractogram of iron(III) acetylacetonate crystals. 59

Figure 4.20: Picture of glass beads before and after hydrogen reduction experiments 61

Figure 4.21: Process flow diagram for the production of iron(III) acetylacetonate 65

Figure 4.22: Cumulative cash flow diagram for the iron(III) acetylacetonate production process. 72

Figure 4.23: Effect of acetylacetone price on the cumulative cash flow of the iron(III) acetylacetonate production process. 75

Figure 4.24: Effect of iron ore fines price on the cumulative cash flow of the iron(III) acetylacetonate production process. 76

Figure 4.25: Effect of iron(III) acetylacetonate selling price on the cumulative cash flow of the iron(III) acetylacetonate production process. 78

Figure 4.26: Effect of discount rate on the cumulative cash flow of the iron(III) acetylacetonate production process. 79

Figure 4.27: Cumulative cash flow diagram of the iron(III) acetylacetonate production process at different production rates. 80

Figure 4.28: Process flow diagram for the manufacture of iron nanoparticles..... 82

LIST OF TABLES

Table 3.1: Experimental level for controlled factors 25

Table 3.2: Experimental runs for 2^kfactorial design 26

Table 4.1: BET surface area of the iron ore fines 32

Table 4.2: Chemical composition of iron ore fines (Weight %) 34

Table 4.3: Crystalline composition of iron ore fines..... 34

Table 4.4: Iron extraction results the for 2^k factorial design..... 42

Table 4.5: Effect estimates and sum of squares for the 2^k full factorial design..... 43

Table 4.6: Regression coefficients of the various shrinking core models..... 53

Table 4.7: Reaction rate constants for different operating temperatures 55

Table 4.8: Activation energy for the different rate controlling mechanism (Habashi, 1969) 56

Table 4.9: Iron extraction using recycled acetylacetonate in the liquid phase..... 60

Table 4.10: Hydrogen reduction results 61

Table 4.11: Summary of bare module costs..... 68

Table 4.12: Summary of investment costs 69

Table 4.13: Raw material information 70

Table 4.14: Summary of annual production cost 70

Table 4.15: Profitability the process at different prices of acetylacetone 74

Table 4.16: Profitability of the process at different prices of iron ore 75

Table 4.17: Profitability of the process at different prices of iron(III) acetylacetonate 77

Table 4.18:Profitability of the process at different discount rates 78

Table 4.19: Profitability of the process at different production rates of iron(III) acetylacetonate 80

LIST OF ABBREVIATIONS AND SYMBOLS

AAS	Atomic Adsorption Spectrometry
ANOVA	analysis of variance
BET	Brunauer-Emmett-Teller
C_{acac}	Concentration of acetylacetone (moles per litre)
C_{BM}	Bare module cost (Rands)
C_{fluid}	Concentration of reagent in the fluid (moles per litre)
C_{GR}	Grass root cost (Rands)
C_{OL}	Cost of operating labour (Rands)
COM	Cost of manufacturing (Rands)
C_p^o	Purchased equipment cost (Rands)
C_{RM}	Cost of raw material (Rands)
C_{TM}	Total module cost (Rands)
C_{UT}	Cost of utilities (Rands)
C_{WT}	Cost of wate treatment (Rands)
DDD	1,2 dodecanediol
DRI	Direct Reduced Iron

E_a	Activation energy (Kilo joules per mole)
EDTA	Ethyl-Diamine-Tetraacetate
f	Shape factor
F_{BM}	Bare module factor
FCI	Fixed capital Investment
IRR	Internal rate of Return (%)
k	Reaction rate constant
M_{Al}	Mass of aluminium extracted (grams)
$M_{flyash(1-\delta)}$	Initial mass of aluminium contained in the flyash (grams)
$N_{Fe_2O_3}$	Number of moles of hematite (moles)
NPV	Net Present Value (Rands)
$\rho_{Fe_2O_3}$	Molar density of hematite in solid sample (moles per gram)
PID	Proportional-Integral-Differential
PSD	The particle size distribution
r	Reaction rate
R	Initial radius of iron ore particles (metres)
S	Surface area of solids particles (square metres)
SEM	Scanning Electron Microscopy
SRI	Smelting Reduced Iron

t	Reaction time (hours)
T	Temperature (degree Celsius)
TI	Temperature Indicator
TC	Temperature Controller
μ	Viscosity
τ	Completion time (hours)
$V_{Fe_2O_3}$	Volume of hematite (cubic metres)
W_{Al}	Weight of Aluminium in the reactor (grams)
$W_{Al_2O_3}$	Weight of Aluminium oxide in the reactor (grams)
x	Conversion of Iron
XRD	X-Ray diffraction (XRD) analysis
XRF	X-Ray fluorescence
N_{OL}	Number of operators per shift
P	Number of processing steps involving handling of particulate solids
N_{np}	Number of non-particulate processing steps

1. INTRODUCTION

1.1 Motivation and background

Mining operations and dressing of iron ore result in the production of large amounts of iron ore with particle size less than 4.75 mm. These particles are referred to as iron ore fines (ETSAP, 2010). Iron ore fines are mostly used in the manufacture of steel which is arguably one the most important and most used metals. The amount of iron ore fines produced worldwide is significantly large. For centuries conventional iron making techniques could not utilize most of the iron ore fines, and this resulted in the accumulation of stockpiles of iron ore fines around mining operations and processing plants. The amount of iron ore fines that is stockpiled as waste around the world can be estimated to millions of tonnes (ABC, 2013).

Conventional methods for processing iron ore fines include agglomeration techniques such as sintering and pelletizing. These techniques transform fines into agglomerates (pellets or sinters) of a desired size, and the agglomerates are then processed along with lump ores using conventional production techniques such as; blast furnace operations, direct reduction and smelting reduction for the manufacture of iron and steel (Biswas, 1981). However, agglomeration techniques are costly and energy intensive. The mentioned conventional iron manufacturing techniques are also associated with high energy consumptions and high greenhouse gas emissions (Plaul et al., 2009). Increasing environmental concerns have made current methods for the production of iron from iron ore fines less desirable which led to an increased interest in the use of greener processing techniques such as fluidized bed technologies. These technologies consist of a system of fluidized bed reactors inside which iron ore fines are directly reduced to elemental iron using non-coking coal or natural gas. Fluidized bed technologies provide an alternative iron manufacturing route without any agglomeration step (Plaul et al., 2009). The main challenge with the direct reduction of iron ore fines in a fluidized bed is scaling up the process and commercializing it.

The focus of this research is to propose a method for the extraction of iron from iron ore fines using acetylacetone. Previous work by van Dyk and co-workers (2010) showed that iron can be extracted from synthetic hematite using acetylacetone in the gas phase. The kinetics of the extraction process and effects of operating variables on extraction efficiency were also studied. Results showed that up to 87% of iron can be extracted after 4 hours at 250 °C from a synthetic mixture of 1 wt% Fe_2O_3 and silica atacetylacetone flowrate of 1 mL/min. It was also found that the process depends on temperature, ligand flowrate and metal oxide concentration. However, gas phase extraction of iron from real mineral systems has not been attempted.

Research on the extraction of metal using chelating agents has not been limited to gas phase operations. Apblett and Barber (2010) investigated the extraction of iron from iron ores using an acetylacetone-water mixture. Results showed that up to 99% of iron was extracted after 48 hours of operation at 140 °C and a solid to liquid mass ratio of 0.025:1. However, the kinetics of the leaching process and the effects of operating conditions such as temperature, solid-liquid mass ratio, and particle size were not investigated in the mentioned study.

The proposed process consists of reacting acetylacetone with iron ore fines to form iron(III) acetylacetone and water. This reaction can occur in gaseous or liquid phase according to the chemical reaction equation 1.1. The unreacted acetylacetone can easily be separated from iron(III) acetylacetonate by flash distillation and recycled back to the extraction process. Furthermore, Zhang and co-workers (2011) showed that the recovery of iron from iron(III) acetylacetonate is feasible by hydrogen reduction. Based on the mentioned information, this work will investigate the feasibility of the process proposed by the block flow diagram in Figure 1.1.

$$Fe_2O_3 + 6H(C_5H_7O_2)_{(f)} \rightarrow 2Fe(C_5H_7O_2)_{3(f)} + 3H_2O_{(f)} \qquad 1.1$$

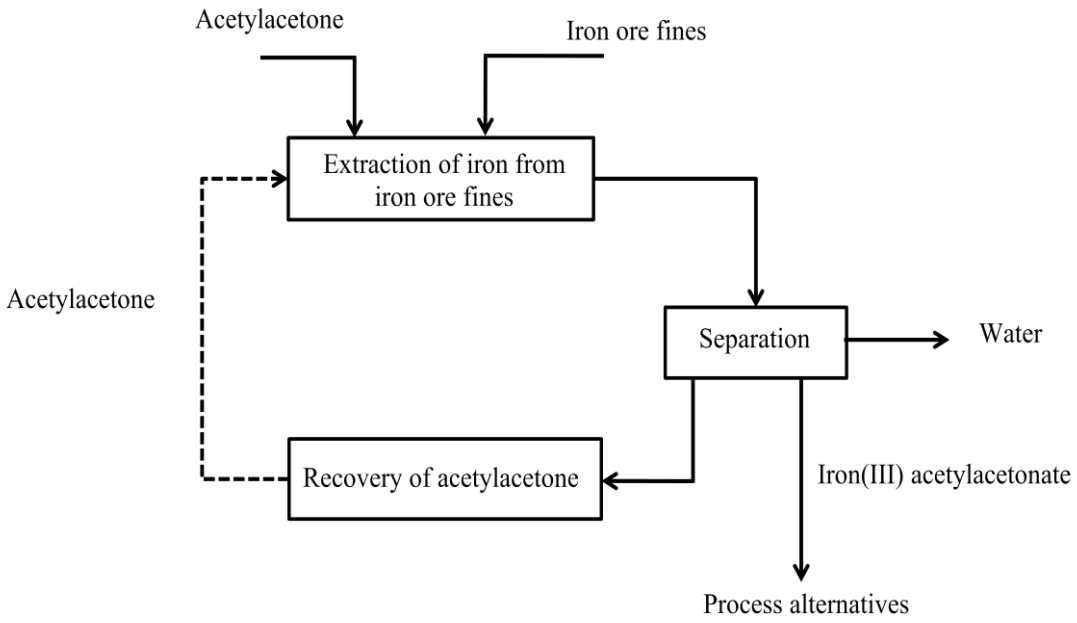

Figure 1.1: Block flow diagram for the extraction of iron from iron ore fines.

The extraction of iron from iron ore fines using acetylacetone is potentially more energy efficient. This is because the extraction occurs at operating temperatures below 300 °C compared to operating temperatures higher than 1000 °C used for all existing iron manufacturing processes. The process only produces water as a by-product, and therefore offers the advantage of extracting iron without any CO_2 emissions and slag production. These advantages have contributed to the growing interest in the extraction of metals using acetylacetone (Potgieter et al., 2006). This research work seeks to investigate the development of a process to utilize iron ore fines in an alternative way that is currently available.

1.2 Aim and objectives

The aim of this study is to propose an environmentally friendly extraction process for iron from iron ore fines using acetylacetone as an extractant.

This will be achieved through the following objectives:

1. To characterise iron ore fines in terms of its physical and chemical properties.
2. To study the influence of operating parameters on the extraction of iron from iron ore fines with acetylacetone (gas or liquid phase).

3. To investigate the practical feasibility of recovering iron from iron(III) acetylacetonate by hydrogen reduction.
4. To perform a kinetic analysis of the extraction process.
5. To investigate the recovery of unreacted acetylacetone and its reuse in the extraction process.
6. To identify alternative process options and study the economical feasibility.

1.3 Dissertation layout

The dissertation comprise of seven chapters and five appendices. Chapter two gives an overview of conventional iron production techniques. The chapter highlights the limitations of such techniques and the development being made in the production of iron from iron ore fines. A review of previous work on metal extraction using chelating agents and an overview of the uses of metal acetylacetonates are also included. Chapter three describes the materials, experimental set up and experimental methods used to achieve the above mentioned objectives. In chapter four the experimental results for the extraction of iron with acetylacetone in liquid and gas phase are presented. The kinetic data for the extraction in liquid phase are presented, discussed and used for kinetic modelling. Results of the recovery of unreacted acetylacetone and iron from iron(III) acetylacetone are included, as well as the economic feasibility study of the proposed iron(III) acetylacetonate manufacturing process. The conclusions and recommendations are both given in chapter five.

2 LITERATURE REVIEW

2.1 Introduction

Iron (Fe) is a dark silvery-gray metal, with an atomic weight of 55.847 g. It has a specific gravity of 7.874, a high melting point of 1535 °C and boiling point of 2750 °C. Pure iron is soft; it has high reactivity and corrodes very easily. Therefore it is mostly used in the form of alloys of which the most utilized is steel. Up to 98% of the iron produced is used in the form of steel (Wright and Taylor, 1991). For centuries, the use of steel has been unlimited, and it can easily be considered the backbone of industrialization. Due to its low cost and high strength, steel is still as important to modern society.

Iron is the fourth most abundant element in the earth's crust and is found in over 300 minerals. However, iron is mainly produced from oxide ores such as hematite (Fe_2O_3), magnetite (Fe_3O_4) and goethite ($Fe_2O_3H_2O$) (Yellishetty et al., 2010). The main mechanism for the formation of the mentioned types of iron deposits is through the precipitation of ferric iron from sea water. The world iron ore reserves were estimated at 165,345 MT in 2008, and it was estimated that at the high iron production rate, the world reserve of iron ore would last for another 79 years. Hence the need exist for alternative sources of iron in the production of steel (USGS, 2008). Iron ore fines which have been stockpiled as waste for centuries, appear to be an attractive alternative source for iron.

2.2 Review of conventional iron and steel production techniques

Conventional techniques for the manufacture of iron and steel can be classified into three process routes; blast furnace operations, direct reduction and direct smelting of iron ores. Figure 2.1 is a block flow diagram illustrating the various processing routes used to produce iron and steel. This section will briefly describe the various

possessing routes and highlight some of the progress being made in the iron manufacturing sector.

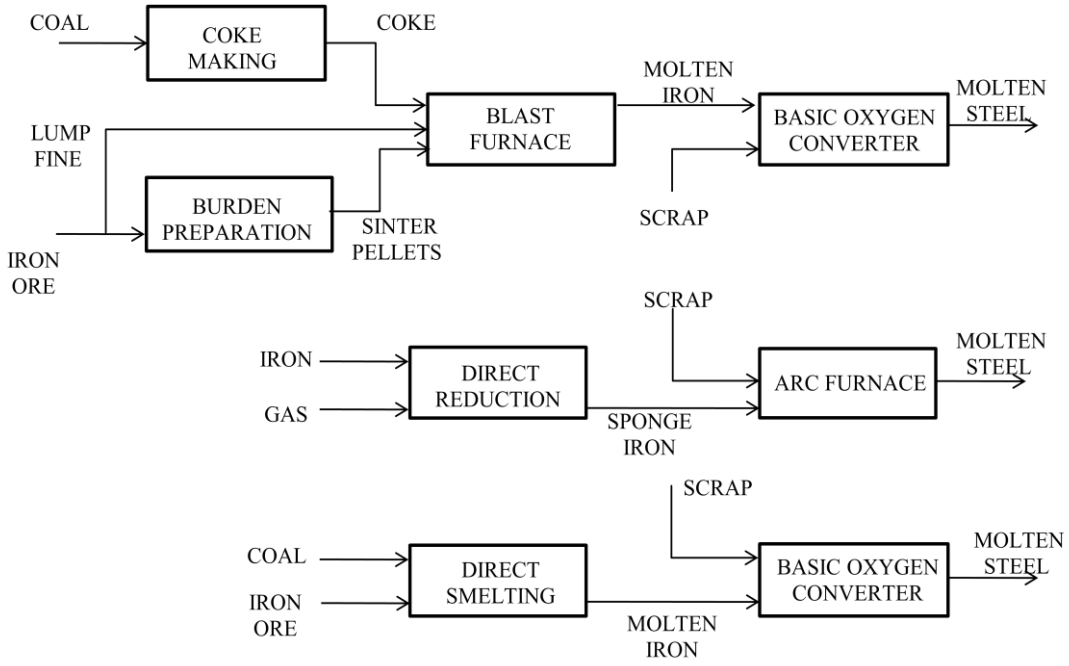

Figure 2.1: Block diagram illustrating the various process routes for the production of steel (Wright and Taylor, 1991).

2.2.1 Blast furnace operations

Even though several process routes for the production of iron have been developed throughout the years, most of the iron produced worldwide is still made using blast furnace operations. The furnace is built in a shape that ensures uniform flow of the thermally expanding gas and smooth descent of the burden. Iron ore, coke and fluxes (limestone) are charged from the top of the furnace, while air is blown from the bottom. Coke is oxidized to form carbon monoxide (CO) which reduces hematite (Fe_2O_3) to magnetite (Fe_3O_4) first, then to iron oxide (FeO) and finally to elemental Fe. The reduction of iron oxide in the blast furnace results in the formation of two layers at the bottom of the furnace; melted iron and slag (Biswas, 1981). Pig iron produced by blast furnace operations is still a major part of the iron produced worldwide. Its production produces approximately 1200 to 2000 m^3 of gas per ton of pig iron. These gases contain up to 28% of CO and 25% of carbon dioxide (CO_2).

Therefore, much work needs to be directed towards the improvement of the furnace efficiency and the reduction of gas emissions (ETSAP, 2010).

2.2.2 Direct reduction

Direct reduction processes also referred to as direct reduced iron (DRI) or sponge iron, are iron manufacturing techniques based on the direct reduction of iron oxide to elemental iron in the solid state. Most direct reduction processes use natural gas to reduce iron oxide while others use non-coking coal. The process is operated at temperatures lower than the melting temperature of iron ore. The most common of DRI processes is MIDREX. The feed to these processes can be a mixture of lump ores, pellets and up to 10% of iron ore fines. One of the main advantages of DRI processes is the low capital investment required for the small scale production; but these techniques are associated with low energy efficiency (ETSAP, 2010).

2.2.3 Direct smelting

Smelting iron, also known as smelting reduced iron (SRI) was developed as an alternative to the blast furnace and DRI processes. The technique is quite similar to the blast furnace process, but the main difference is the use of coal instead of coke as reducing agent (ETSAP, 2010). This is a process during which iron ore is pre-reduced by hot gas (CO-rich) prior to being fed into the smelter furnace where it flows counter-currently with the hot gas from the gasification of coal. Coal gasification occurs at the bottom section of the smelting vessel. The hot gas exiting the smelter is CO-rich and is used for the pre-reduction of iron ore. The main commercial process that uses direct smelting is the Corex process (Zervas et al., 1996). The advantages of such processes are its ability to utilize a variety of non-coking coal and the low capital investment required. However, SRI is a new process and its use is still limited (ETSAP, 2010).

2.2.4 Agglomeration techniques of iron ore fines

Iron ore fines constitute a large portion of the iron ore produced around the world, but cannot be used directly in most of the conventional iron production techniques. This is because fine materials clog the voids and consequently reduce the

permeability of the slag and decrease the production rate of furnaces (Biswas, 1981). For the production of iron from iron ore fines, agglomeration techniques are used to form agglomerates that can be processed along with lump ore using conventional methods.

Sintering and pelletizing are the two major techniques for the agglomeration of ore fines. During the sintering process, fines are mixed with solid fuel, and the mixture is heated in a grate in order to form agglomerates called sinters (Ball and Dartnell, 1973). The high permeability and reducibility of sinters improves the quality of hot metal, reduces the consumption of coke and increases the productivity of blast furnace operations.

Pelletizing is the process of transforming fines into pellets while upgrading its iron content. Using additives, fine particles are agglomerated into green balls which are then dried, heated and cooled. The pelletizing process also increases the productivity and efficiency of blast furnace operations (Ball and Dartnell, 1973). Although agglomeration techniques are found to increase the productivity of conventional ironmaking processes, these techniques are associated with additional cost, energy consumption, and greenhouse gas emissions. Below is a brief review of energy consumption and greenhouse gas emissions in the iron and steel industry.

2.2.5 Energy use and gas emissions in the iron manufacturing industry

The brief review of conventional iron production techniques has shown that the main challenges faced in the production of iron and steel are high energy consumption and high greenhouse gas emissions. Industries such as chemicals and petrochemicals, iron and steel, non-metallic minerals and non-ferrous metals are the biggest consumers of industrial energy in the United State (Gielen et al., 2008). These industries consumed 62% of the total 69.9 Exajoules of industrial energy used in 2008. The iron and steel industry was the second highest consumer, with energy use of up to 19% of the total energy consumed by the industrial sector. A survey by the organisation for economic co-operation and development (OECD, 2010) showed that the production of steel accounts for approximately 30% of the total CO_2 emissions. ,

The survey also revealed that the iron and steel industry was the highest contributor to the direct industrial CO_2 emissions, and this is illustrated by Figure 2.2.

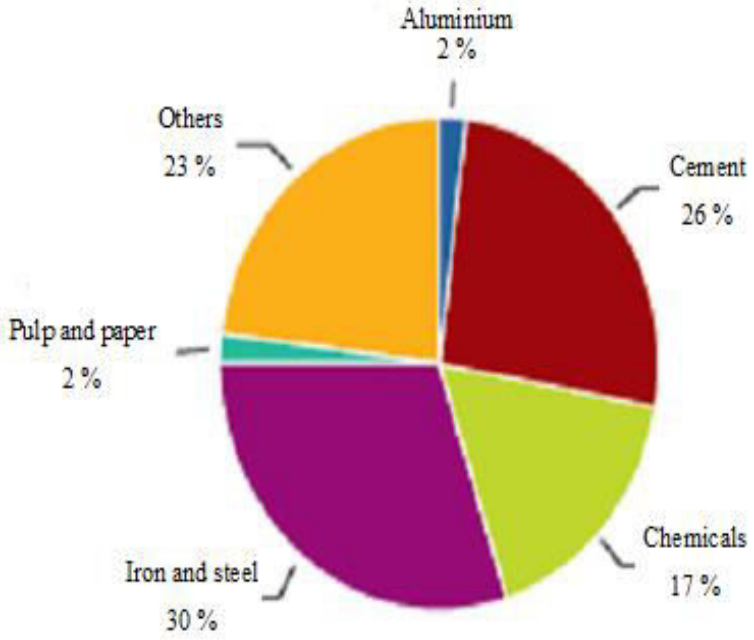

Figure 2.2: Direct industrial CO_2 emissions by sector in 2006 (OECD, 2010).

Because the feed to the blast furnaces requires specific properties (size and grade), more than 50% of the iron ore produced is converted to sinters. However, the heat consumed by the sintering process is 1.5-2 GJ per tonne of sinters and constitutes approximately 33% of the total heat consumption of an iron and steel plant (Gielen et al., 2008). The availability of iron ore fines and the high cost of agglomeration processes have created the need to improve existing ironmaking technologies or to develop new technologies that are both less expensive and less harmful to the environment. Processing techniques for the manufacture of iron from iron ore fines without any agglomeration stage will potentially result in lower energy consumption and lower gas emissions. These alternatives are discussed in the following sections.

2.3 New techniques for the production of iron from iron ore fines.

Amongst the emerging ironmaking techniques, the use of fluidized bed technologies appears to be the most attractive for processing iron ore fines. These fines can be processed by fluidized bed technologies without any pre-treatment process such as agglomeration. FINMET and FINEX are examples of processes that make use of thefluidized bed technology (Plaul et al., 2009). FINMET produces hot briquettes iron by direct reduction using natural gas, while FINEX is a process that utilize non-coking coal and iron ore fines to produce hot metal with qualities similar to the ones obtained from blast furnace operations. It was found that for the production of metallic iron using CO and H_2 as reducing gases, a two stages reduction process is needed to ensure high energy efficiency and low consumption of the reducing gases. However, future studies have to be directed to scale up these processes and to reduce greenhouse gas emissions (Plaul et al., 2009).

2.4 Chelating agent and the chelating effect

The aim of this work is to extract iron from iron ore fines with less energy consumption and low greenhouse gas emissions. To achieve this, the extraction using a chelating agent such as acetylacetone will be investigated. This section gives a brief description of chelating agents and their properties. It also provides information for a better understanding of the growing interest to use these ligands for metal extraction.

2.4.1 Description of chelating agents

The presence of ligand is required for the dissolution of metal solutes in solution, and for any chemical reaction to occur. The number of donor sites of a ligand dictates the number of atoms that can simultaneously bind to a metal ion. Based on the number of donor site they possess; ligands can be classified either as mono or poly-dentate. Poly-dentate ligands usually form a ring like structure and are referred to as chelating agents. The term chelate was derived from the claws of crustaceans; these

have similarities with heterocyclic ring structures (Morgan and Drew, 1920). The chelating effect can be described as the higher affinity that a metal ion or a cation has for a polydentate rather than a monodentate ligand.

The main advantage of using chelating agents for metal isolation is its ability to form very stable complexes. The high stability of these complexes is justified by the following factors (Huheey et al., 1993).

- The extent of dissociation of chelating complexes is less than that of ordinary complexes (mono-dentate).This is partly attributed to the probability that if a molecule dissociates from one end of a polydentate ligand, the other end can draw it back to its initial site. However, this is not the case for complexes made of monodentate ligands.
- Secondly, some chelating ligands have extra resonance stabilization resulting from the formation of six-membered rings with the central ion. Acetylacetone is an example of such a ligand. The presence of a ligand-metal π bond can enhance the delocalization of electrons and result in some resonance stability. This is illustrated by Figure 2.3.

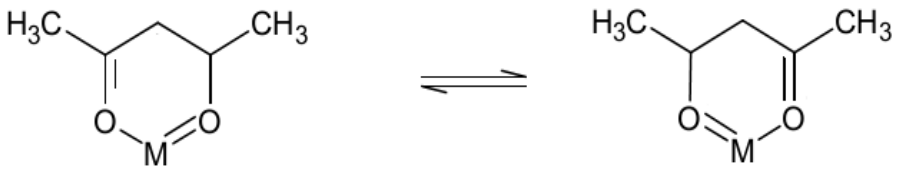

Figure 2.3: Resonance stability of acetylacetone

One of the most common and most important chelating agents is ethyl-diamine-tetraacetate (EDTA). As illustrated by Figure 2.4, EDTA is a hexa-dentate (six teeth) and each of its donor sites can bind to a metal ion. As a result, it is a very strong chelating agent that forms very stable complexes and is intensively used in industry. EDTA finds its use in the paper, textile, and agriculture industry. It is also used in medicine, cosmetic and for laboratory titration (Kolodynska, 2013).

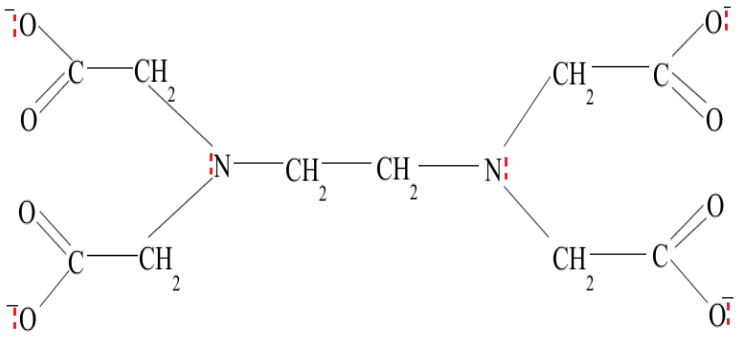

Figure 2.4: Molecular structure of ethyl-diamine-tetraacetate (ChemEd, 2013).

In general, chelating agents are intensively used in many fields of industry and their applications are unlimited. The prevention of brightness reversion in the pulp and paper production, the control of water hardness by the removal of calcium and magnesium in water treatment, and the separation of metal from metal contaminated waste by forming soluble metal-complexes are just a few examples of the numerous applications of chelating agents (Kolodynska, 2013). The chelating agent of interest to this study is acetylacetone. Below is a brief description of the ligand as well as its relevant chemical properties.

2.4.2 Acetylacetone

Acetylacetone ($C_5H_8O_2$), also referred to as 2-4-pentanedione, is a chelating agent of the family of β-diketones. It is a volatile liquid at room temperature with a density of 0.975 g/ml, and it boils at 140 °C under atmospheric pressure. At molecular level, it usually co-exists as an equilibrium mixture of the chelated enol and keto form. In liquid state, the relative amount of each of these two forms depends on factors such as temperature and the type of solvent used (Spencer et al., 1982). The molecular structures of the two tautomeric forms are represented in Figure 2.5. Acetylacetone is a bidentate because it can bond to the central ion via both oxygen atoms, as is illustrated in Figure 2.3.

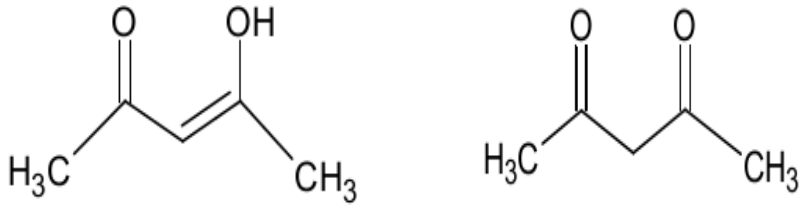

a) b)

Figure 2.5: The enol (a) and keto (b) stable form of acetylacetone

Equation 2.1 shows the reaction of acetylacetone with a trivalent metal such as iron.

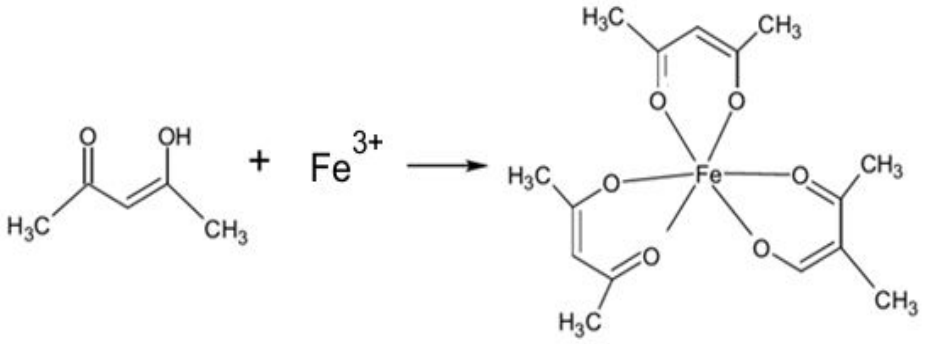

2.1

Acetylacetone finds its use in analytical extraction, in the isolation of metals due to its ability to selectively react with certain metals and to form gaseous metal complexes at low temperatures (Sievers and Sadlowski, 1978). The mentioned properties have spurred researcher's' interest in the use of acetylacetone for the extraction of metals. The following section gives a review of previous work on the extraction of metals using chelating ligands.

2.5 Extraction of metals using chelating ligands

In the past few decades, several researchers have directed their efforts to the investigation of metal extraction by organic volatiles. This is an emerging process for the recovery of heavy metals from industrial waste and other low grade sources (Allimann-Lecourt et al., 1999). This process entails reacting a chelating organic gas with a solid material containing metal oxides. The chelating organic selectively reacts with the metal of interest and forms volatile metal complexes. The products

are easily separated from the unreacted reagent due to their volatilities and distinct boiling temperatures. The metal complexes formed find numerous uses in industry; they are used as catalyst for several organic reactions, and also used for the production of metal oxides nanoparticles (Willis et al., 2007). Below is a brief review of the relevant extraction processes and the progress made in this area of study.

Cox and co-workers (1985) investigated the extraction of heavy metals from sediment using the SERVO process. The work showed that metals such as Zinc, Copper and Nickel can be effectively extracted from low grade ores or industrial waste using an organic compound that reacts selectively with the metals of interest. This process was developed at the University of Hertfordshire. In 2002, Allimann-Lecourt and co-workers (2002) pursued the research further by investigating the application of the SERVO process to the purification of combustion fly ash. The work mentioned above showed that the SERVO process can be used for the purification of solid residue and it also showed that the nature (properties) of the metal to be extracted is crucial in the extraction process.

2.5.1 Extraction with acetylacetone

Gas phase extraction

The feasibility of recovering valuable metals from solid oxide compounds by gas phase extraction in a fluidized bed was investigated by Potgieter and co-workers (2006). Their study showed that acetylacetone can be used to successfully extract aluminium, chromium, vanadium and iron from their solid oxides. Extraction of more than 60% of each metal was achieved. The extraction kinetics was investigated and it was found that the extraction of metals was dependent on temperature and reaction time

Further research was performed by van Dyk and co-workers (2010), and the focus was on the extraction of iron from synthetic iron(III) oxide in a fluidized bed. Acetylacetone was used as the extractant, and the extraction reaction is given by Equation 1.1. The effects of temperature, ligand flowrate and metal oxide

concentration were investigated. It was found that all these factors affect the extraction efficiency. The results showed that up to 87% of iron can be extracted after 4 hours at 250 °C using 1 wt% Fe_2O_3 mixture and 1 mL/min of acetylacetone. The extraction of aluminium from coal fly ash was also part of the mentioned work (Mpana, 2012). The study showed that up to 46.7% of aluminium can be extracted after 6 hours of gas phase extraction using aceylacetone at 250 °C.

From the research work mentioned above, it can be deduced that using acetylacetone as a ligand for the extraction of heavy metals in general and iron in particular is a promising process. However, most studies in this field have been performed on either low grade sources or synthetic metal oxides. It would be of industrial interest to investigate the efficiency of gas phase extraction processes on natural high grade sources of metal oxides. The study of metal extraction has not been limited to gaseous phase; other researchers have investigated the liquid phase route or leaching.

Leaching

Hamblin and Posner (1979) investigated the use of acetylacetone as a selective extractant of metal from soil. This study was performed using acetylacetone in both polar and non-polar solvents. Other work in this line of study includes the extraction of Zirconium and Hafnium with acetylacetone in the presence 3,5-dichlorophenol (Katsuta and Yanagihara, 1997), and the solvent extraction of iron from aluminium sulphate leach solution using acetylacetone-chloroform (Kamiriand and Gheadi, 2002). From all the work mentioned above it was found that various solutions of acetylacetone can be used to successfully extract metals from low grade sources.

Apblett and Barber (2010) investigated the extraction of iron from high grade sources. This work investigated the conversion of hematite into iron(III) acetylacetonate, and was performed by reacting a hematite ore with a refluxing mixture of acetylacetone and water at 140 °C for duration of 48 hours. Water was used in the process because it was found in previous work that small amount of water acts as catalyst to the extraction reaction (Apblett and Barber, 2010). The acetylacetone to water volume ratio used was of 9:1. This method provides an excellent green method for isolating iron from iron ores, with up to 99% iron

extraction achieved. The feasibility to regenerate acetylacetone by the use of a rotary evaporator was illustrated.

Kinetic modelling of acetylacetonate extraction processes

Previous studies have investigated the kinetics of metal extraction using acetylacetone. Mariba (2010) investigated the kinetics of the extraction of iron from synthetic hematite (Fe_2O_3) using acetylacetone in the gas phase. The kinetic analysis was based on the shrinking core model. The extraction reaction was assumed to be first order with respect to the concentration of acetylacetone, and the mathematical equation for the model if controlled by the chemical reaction is given by Equations 2.2 and 2.3. It was found that the extraction rate is chemically controlled at the lowest Fe_2O_3 concentration of 1 wt%, 1 mL/min of acetylacetone, and for a temperature range of 190 °C to 250 °C. Better fits of experimental data to the model were obtained at higher temperatures.

$$\frac{1}{S}\frac{d[\text{reactants}]}{\text{dt}} = kC_{Hacac} \qquad 2.2$$

$$kt = 1-(1-x)^{1/3} \qquad 2.3$$

Where k is the rate constant, t is the reaction time, and x the conversion of iron.

The kinetics of aluminium extraction from fly ash using acetylacetone in the gas phase was studied by Mpana (2012). In this study, a kinetic model was developed and fitted to the experimental data obtained at various operating conditions. The model assumed first order reaction with respect to the mass of Al_2O_3 available for extraction. Equation 2.4 and 2.5 shows the model developed in the study.

$$r = Sk_1 M_{flyash(1-\delta)} \qquad 2.4$$

$$M_{Al} = \mu\left(M^{o}_{flyash(1-\delta)} - M^{o}_{flyash(1-\delta)}e^{(-Sk_1 t)}\right)\frac{2\times W_{Al}}{W_{Al_2O_3}} \qquad 2.5$$

Where M_{Al} is the mass of aluminium extracted, $M^{o}_{flyash(1-\delta)}$ is the initial mass of aluminium contained in the flyash, S the surface area of the particle, and k_1 the

reaction rate constant. The model was found to fit to experimental data fairly well at a flowrate of 9 mL/min and various operating temperatures. However, when the model was used to predict extraction behaviour at different flowrates of acetylacetone, it did not fit the data very well. The model was only applicable to synthetic systems.

It was found that existing developed models using acetylacetone suffer from several shortcomings. The models did not take into account the flowrate and concentration of acetylacetone.

Recovery of metals (iron)

The various techniques for the synthesis of iron nanoparticles can be classified into physical and chemical synthesis methods. Physical synthesis methods include techniques such as high energy ball milling and inert gas concentration, while chemical vapour deposition and liquid chemical reduction can be named amongst chemical synthesis methods (Jamei et al., 2013). Chemical synthesis methods are the most advantageous because of their simplicity and ability to be studied at laboratory scale. Because of its high reducing ability, hydrogen reduction is an attractive method for the chemical synthesis of metal nanoparticles.

Hydrogen reduction can be used for the synthesis of many metals from their oxide compounds. However, at an industrial scale, it has only been applied in the synthesis of a few metals such as molybdenum and tungsten (Luidold and Antrekowitsch, 2007). Compared to other reduction techniques, hydrogen reduction presents several advantages; it has the ability to extract very pure metals from their oxide compounds, and it gives better contact between reducing agent and metal oxide to be reduced. Hydrogen is produced by either gasification of coal or electrolysis of water, and hydrogen reduction produces steam instead of carbon dioxide for carbon reduction. This makes the hydrogen reduction process a cleaner alternative for the environment (Luidold and Antrekowitsch, 2007).

Continuous efforts are being directed to develop and implement hydrogen reduction technology in large scale metal production. Charles and Haverlack (1969)

investigated the chemical vapour deposition characteristics of cobalt(II) on fused quartz substrate and observed that hydrogen was very essential as a reducing agent and carrier gas. Demopoulos and Distin (1985) looked at direct copper precipitation from a loaded chelating extractant by pressure hydrogen stripping. In the past few decades, intensive research on hydrogen reduction of different metals has been performed.

Several researchers have investigated the production of iron powder using hydrogen reduction. An example of such work is the study by Lee and Kim (2003). This research investigated the kinetics of the synthesis of iron nanoparticles by hydrogen reduction of ferrous chloride vapour. Results of this work showed that very high gas flow rate reduces conversion due to shorter retention time, and it was also found that the reduction rate is first order. The reduction reaction is illustrated by Equation 2.6.

$$FeCl_{2(s)} + H_{2(g)} \rightarrow Fe_{(S)} + 2HCl_{(g)} \qquad 2.6$$

The work performed by Zhang and co-workers (2011) is perhaps one that is more relevant to this study. The work focussed on the chemical synthesis of Fe nano-crystals via hydrogenation of iron(III) acetylacetonate. Experiments were performed in an autoclave at elevated temperature (260 °C to 300 °C) and pressure (6 MPa). High pressure was chosen to widen the solvent choice range; as higher pressure results in higher boiling points of organic solvents. However, it was observed that the outer layer of Fe nanoparticles was oxidized soon after being formed, hence the need for a stabiliser and appropriate operating temperature range. Results showed that 260 °C to 300 °C is the appropriate temperature range, 1,2 dodecanediol (DDD) is the stabiliser to use and the ratio of DDD to ferric acetylacetonateshould range from 1:1 to 2:1. This work proved the feasibility of recovering iron from iron (III) acetylacetonate via hydrogen reduction as per Equation 2.7.

$$Fe(C_5H_7O_2)_{3(s)} + \frac{3}{2}H_{2(g)} \rightarrow Fe_{(s)} + 3H(C_5H_7O_2)_{(g)} \qquad 2.7$$

3 EXPERIMENTAL METHODS

This study evaluated the feasibility of a novel process for the extraction of iron from iron ore fines using acetylacetone in the liquid and the vapour phase. The experimental methods used in this study are presented below. These include the characterization of iron ore fines, gas phase extraction and recovery from iron ore fines, liquid phase extraction (leaching), and recovery of unreacted acetylacetone.

3.1 Characterization of iron ore fines

The iron ore used for this study was obtained from the Sishen operations in South Africa, a division of Kumba Iron Ore, Anglo American. The ore was characterized with the following analytical techniques: sieves analysis, X-Ray Diffraction, X-Ray Fluorescence, Scanning Electron Microscopy (SEM), and Brunauer-Emmett-Teller (BET).

3.1.1 Particle size distribution

The particle size distribution was obtained bysieves analysis using a sieve shaker. A total mass of 24.03 kg of iron ore was received for this study, the whole sample was screened with sieves ranging from 45 µm to 5600 µm. A representative sample of the bulk was collected and sent for XRD analysis.

3.1.2 Surface area characterization

The surface area characteristics were obtained using Brunauer-Emmett-Teller (BET) and scanning electron microscopy (SEM) analytical methods. BET analysis was used for surface area measurement of the iron ore sample. This analytical method consists of passing nitrogen gas through the solid sample and fitting the amount of nitrogen adsorbed to the Brunauer-Emmett-Teller (BET) equation (Brunauer, 1943). The analysis was performed at -196 °C with a Micromeritics Tristar-Surface area and Porosity analyzer 3000 that was equipped with the Win 3000 software package.

The micrograph of the iron ore surface was obtained using scanning electron microscopy analysis (SEM) analysis. The sample was prepared using carbon coating, and analyzed with TESCAN equipped with the VEGA software package. The surface image was taken at a magnification of 1350.

3.1.3 Chemical and crystalline composition

The crystalline and chemical compositions of the ore were identified and quantified using X-Ray diffraction (XRD) analysis and X-Ray fluorescence (XRF) analysis as described below.

- The XRD analysis was performed to determine the crystalline composition of the iron ore fines. The sample was prepared using a back loading method, and analyzed with a PANanalyticalX'Pert Pro-powder diffractometer equipped with X'Celeratordetector, fixed divergence, and fixed receiving slits with Fe-filtered Co-Kα radiation. The use of metal foil filters such as Fe-filtered Co-Kα is to reduce the intensity of K β line in the X-ray spectrum, as the X-ray diffraction of powders requires a monochromatic X-ray source (Karl, 1997). The crystalline phases were identified using the X'PertHighscore plus software package.
- XRF analysis is a method that uses a beam of monochromatic X-Rays to determine the chemical composition of a sample. The XRF analysis of the iron ore fines was performed using the PANalyticalPW 2404 XRF spectrometer. The components of the sample were identified by major analysis using the super Q software package.

3.2 Gas phase iron extraction

Previous work by van Dyk and co-workers (2010) investigated the effects of operating variables such as temperature, acetylacetone flowrate, and hematite concentration on the gas phase extraction of iron from synthetic systems. Results from this study were used as a starting point for the choice of operating variables used in this study. The current gas phase extraction studies investigated the effects of these variables on the extraction of iron from iron ore fines. The operating

variables that were investigated include; temperature, acetylacetone flowrate and bed weight.

3.2.1 Experimental set up

A fluidized bed reactor (Figure 3.1) was used for the gas phase extraction of iron using acetylacetone. The reactor was made of a cylindrical glass column fitted with a ceramic frit at the bottom that served as a gas distributor. The dimensions of the reactor are given in Figure 3.1. A thermocouple was used to measure the temperature inside the column which had heating wire wrapped around it. The temperature was regulated with a proportional-integral-differential (PID) temperature controller connected to the thermocouple and heating wire. The column was insulated with ceramic wool for safety and to minimize energy losses to the environment.

The reactor described above was connected to a round-bowl flask which was heated using a heating mantle with adjustable heating rate. Acetylacetone was continuously fed to the flask with the use of a calibrated peristaltic pump. A cooling water condenser was connected to the top of the reactor to condense the unreacted acetylacetone and reaction products. A flask containing ethanol (20 mL) was placed in an ice bath and connected to the condenser to capture and dissolve the extraction products and unreacted acetylacetone. Figure 3.2 shows the described experimental set up.

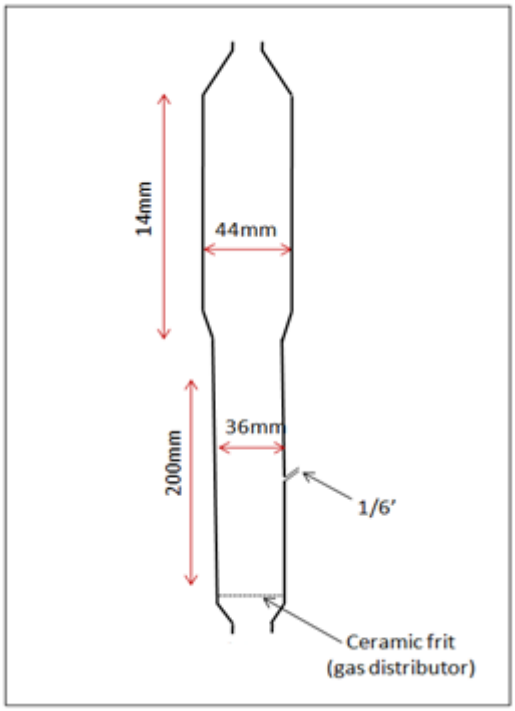

Figure 3.1: Fluidized bed reactor used for gas phase extraction

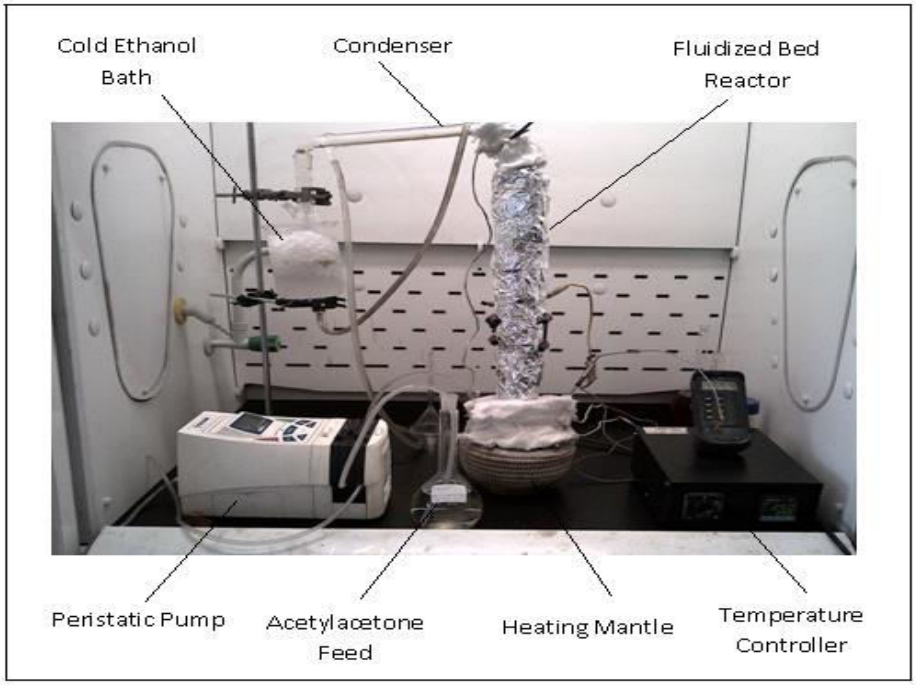

Figure 3.2: Experimental set up for the gas phase extraction process

3.2.2 Experimental method

A weighed mass of iron ore fines was placed inside the fluidized bed reactor. This mass was varied from 20 g to 50 g for different experimental runs. The reactor and necessary items were then assembled according to the experimental set up described above. The reactor temperature was set to the desired operating temperature of 160 °C, 250 °C, or 275 °C depending on the experimental run. The temperature of the vaporization flask was set within the range of 150 °C to 170 °C to ensure that acetylacetone is vaporized as it entered the flask. After the system was stabilized, and all the temperatures were at the set point, the peristaltic pump was switched on and acetylacetone was fed to the process at the desired flow rate. The extraction products and unreacted acetylacetone were captured in a cold bath containing 20 mL of ethanol. The ethanol mixture was exchanged at specific time intervals, diluted with distilled water, and analysed for its iron content by atomic adsorption spectroscopy (AAS) using the ICE 3000 series with the Solaar software package.

3.3 Leaching of iron ore fines

Apblett and Barber (2010) reported on the extraction of iron from different iron sources using a refluxing mixture of acetylacetone and water. The researchers failed to give details of the experimental set up or the influence of the extraction variables on the extraction kinetics. Because of the promising results obtained in the above mentioned study, the current work investigated the application of the proposed leaching process to iron ore fines. The investigation included the study of the effects of operating variables on the extraction of iron from iron ore fines and a kinetic analysis of the process. The experimental set up and methods used are described below.

3.3.1 Experimental set up

Liquid phase extraction experiments were performed in a 250 mL glass flask fitted to a reflux condenser. Laboratory clamps and supports were used to keep the glass flask immersed and suspended in a hot oil bath. The oil bath was kept over a heating plate equipped with a magnetic stirring. A peristaltic pump was used to circulate

cooling water through the condenser to ensure that most of the acetylacetone remained in the liquid phase. A type K thermocouple was placed in the oil bath and connected to a temperature controller in order to measure the oil temperature. Figure 3.3 shows the described experimental set up.

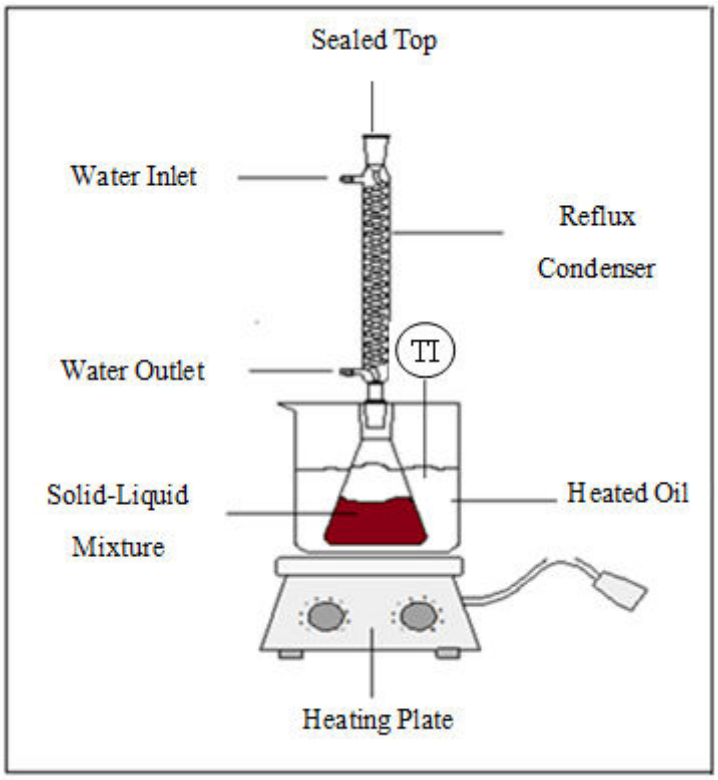

Figure 3.3: Experimental set up for leaching experiments.

3.3.2 Experimental methods

A 200 mL solution of acetylacetone –water mixture was placed in a flask containing a weighed mass of iron ore fines. The solution mixture was made up of acetylacetone and water with a mass ratio of 9:1. A known mass of iron ore fines (5, 7.5, 10, 15 or 25 g) were added for the various experiments. The flask was then connected to the condenser and suspended in the pre-heated oil. The cooling water pump was switched on, the heating rate was adjusted to meet the operating temperature and the stirring rate was set to 570 rpm. The leaching reaction was allowed to continue for different durations depending on the study performed. After each experiment the solution was filtered and the filtrate was diluted with distilled

water and the sample analyzed by AAS. Using the described experimental method, the following investigations were performed.

Identification of significant operating variables

The objectives of the preliminary liquid phase experiments were to identify the operating variables that have a significant effect on the extraction rate, and to estimate the extraction rate that is achievable at certain operating conditions. This analysis is usually achieved by the use of the factorial design method which utilizes statistics to identify the significance of the effects of operating variables and their combined effects (Montgomery, 2005). The combined effect of variables (factor interaction) is of great importance because the response caused by a specific variable may depend on the set values of constant variables (Myers et al., 2009). A 2 level factorial design method was applied for each variable, and can be defined as a 2^k factorial design. k represents the number of operating variables under investigation.

Experiments were performed based on random combinations of low and high level conditions for each of the chosen variables. For a full 2^k factorial design, a minimum of 2^k un-replicated runs were required. To identify the significant variables, statistical analysis methods such as analysis of variance, normal probability plot, and half normal probability plot were used.

The design of experiment method was performed using the Design Expert 6.0. Operating variables such as particle size, temperature and solid to liquid ratio were used in the design. The low and high levels used for each operating variables are shown in Table 3.1. Table 3.2 shows the standard layout of experimental runs performed for the 2^k full factorial design.

Table 3.1: Experimental level for controlled factors

Controlled Parameters	**Low level**	**High level**
Temperature [°C]	120	140
Particle Size Range [µm]	106 to 150	400 to 600
Solid to liquid ratio	0.025:1	0.127:1

Table 3.2: Experimental runs for 2k factorial design

	Factors				Factors	
Run	**A**	**B**	**C**	**S/L Ratio**	**Particle size [µm]**	**Temp [°C]**
I	-	-	-	0.025:1	+106-150	120
II	+	-	-	0.127:1	+106-150	120
III	-	+	-	0.025:1	+400-600	120
IV	+	+	-	0.127:1	+400-600	120
V	-	-	+	0.025:1	+106+150	140
VI	+	-	+	0.127:1	+106-150	140
VII	-	+	+	0.025:1	+400-600	140
VIII	+	+	+	0.127:1	+400-600	140

A (S/L ratio): 0.025:1 (-) and 0.125:1 (+); B (Particle size): +106-150 µm (-) and +400-600 µm (+); C (Temperature): 120 °C (-) and 140 °C (+)

Kinetic analysis

The kinetic study of any process is of great importance for the development of new processes, the design of process equipment and many other areas of engineering. In this study the kinetics of the leaching of iron from iron ore fines using acetylacetone was investigated. At constant temperature, leaching experiments were performed at a solid to liquid ratio of 0.025:1, +106-150 µm particles, and for the duration of 3 h, 6 h, 12 h, 18 h, 24 h, 36 h, and 48 h. Because previous studies have shown that reaction kinetics is dependent on temperature, the same experiments were repeated at 80 °C, 100 °C, 120 °C, and 140 °C. The kinetic data generated in this way was then used to develop a kinetic model of the leaching process that is applicable within the operating range of this study.

3.3.3 Recovery of unreacted acetylacetone and iron(III) acetylacetonate from leach solution

A leach solution and solid residue were obtained after each leaching experiment. The leach solution comprised of iron(III) acetylacetonate, water and unreacted acetylacetone, while the solid residue consisted of unreacted iron ore fines and other solid inert. A simple filtration method was used to separate unreacted iron ore fines

from the leach solution. The cake was washed in ethanol to recover any solid iron(III) acetylacetonate, and then stored for future analysis. The filtrate (leach solution) was further used in the separation and recovery process. The boiling points of water (100 °C), acetylacetone (140 °C), and the melting point of iron(III) acetylacetonate (182 °C) are distinctly different and this property was used to separate the products (NIST, 2013). Water and acetylacetone were recovered from iron(III) acetylacetonate by evaporation in a Heidolph rotary evaporator. The iron(III) acetylacetonate formed crystals while water and unreacted acetylacetone were separately recovered as the top products. After recovery, acetylacetone was recycled to the extraction process and this was repeated several times to assess the change in its reactivity. Iron(III) acetylacetonate crystals were subjected to XRD analysis, this was performed using a PANanalytical Empyrean diffractometer with PIXcel detector and fixed slits with Fe filtered Co-Kα radiation. Figure 3.4 shows the Heidolph evaporator used in this study.

The Heidolph evaporator was firstly operated at 110 °C to remove all the water from the solution. The separation of the acetylacetone from iron(III) acetylacetonate was then performed at 160 °C and a slow rotation speed of 70 rpm to produce acetylacetone and iron(III) acetylacetonate crystals. This is because the operating manual of the evaporator recommended a temperature difference of up to 20 °C in order to have sufficient distillation rate. The recovered acetylacetone was mixed with some fresh acetylacetone to make up the required volume, and it was used in the extraction process at 140 °C, 0.025:1 of solid to liquid ratio and for 48 hours duration.

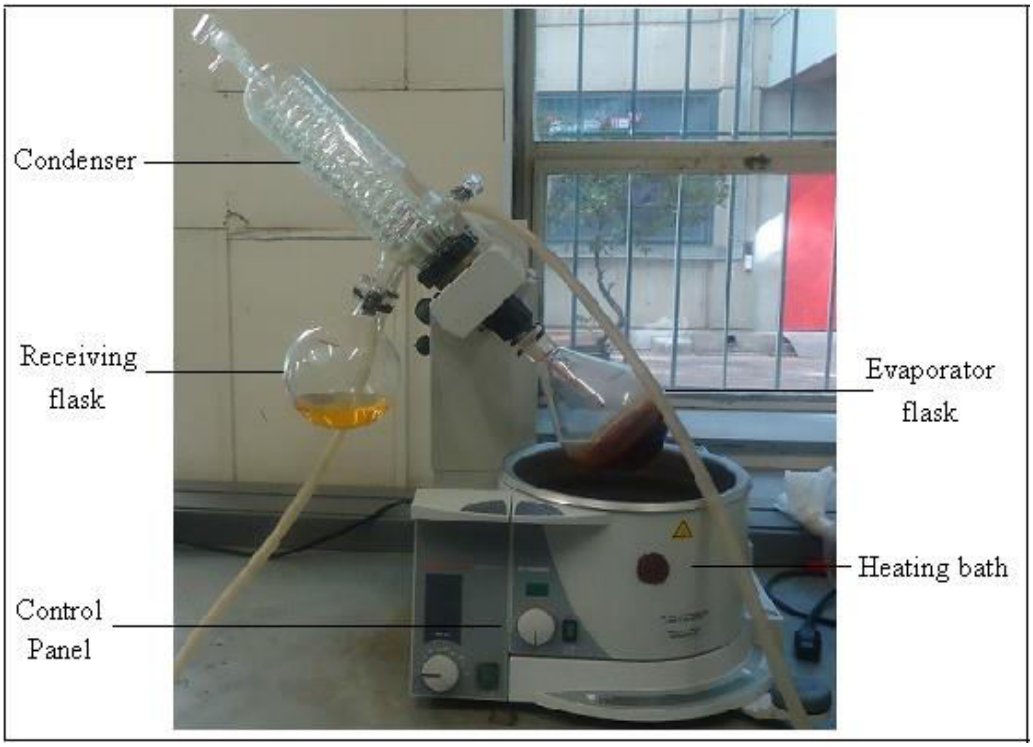

Figure 3.4: Heidolph 2 rotary evaporator for the recovery of unreacted acetylacetone, water and iron(III) acetylacetonate crystals.

3.4 Preliminary recovery of iron from iron(III) acetylacetonate

The experimental set up and method used for the recovery of iron from iron(III) acetylacetonate by hydrogen reduction in the gas phase are also presented below.

Hydrogen reduction was proposed as a method to recover elemental iron from the product, iron(III) acetylacetonate. This was a preliminary study to propose an experimental set up and assess the effect of operating temperature on the reduction efficiency. The experimental setup and procedure used for preliminary studies are as follows.

3.4.1 Experimental setup

The hydrogen reduction of iron(III) acetylacetonate was performed in a glass reactor of 2 cm diameter and 50 cm length. The reactor was filled with 4mm glass beads that served to increase the residence time of the gases and to provide a surface for the deposition of iron. Heating wire was wrapped around the column and connected to a

temperature controller in order to regulate the inside temperature of the reactor. The column was then insulated with ceramic wool and aluminium tape. A round bowl flask served as a region for the sublimation of iron(III) acetylacetonate, the flask was connected to the bottom of the reactor and heated using a heating mantle with adjustable heating rate. At a flowrate regulated by a mass flow controller, nitrogen gas was fed from a cylinder through a preheater into the round bowl flask to facilitate the sublimation of iron(III) acetylacetonate and to serve as a carrier gas in the reactor. Hydrogen gas was fed through a 1/16" stainless steel tube to the bottom of the reaction zone, just above the ceramic frit that separates the reactor from the sublimation zone. The described experimental set up is illustrated by Figure 3.5.

3.4.2 Experimental method

The method used to perform a hydrogen reduction experiment can be summarized as follow. The nitrogen pressure was set at 150 kPa and the flow was set to 400 cm^3/min. Once nitrogen was flowing through the system, the nitrogen heater was turned on and its temperature set at 250 °C. The temperature of the reactor was then set to the desired set point (250 °C, 270 °C, or 290 °C) and the heating mantle set to operate within the range of 110 °C-130 °C. This was to ensure that iron(III) acetylacetonate was kept below its melting temperature (182 °C). After the system was stabilized and all the temperatures were at the desired set point, 1 g of iron(III) acetylacetonate was placed in the round bottom flask, the hydrogen flow was set to 5 cm^3/min and the reaction was allowed to occur for 3 hours. To quantify the amount of iron formed, the glass beads were placed in 60 mL of 32% hydrochloric acid for aduration of 48 hours, and the resulting ferric chloride solution was analyzed for iron content with an AAS.

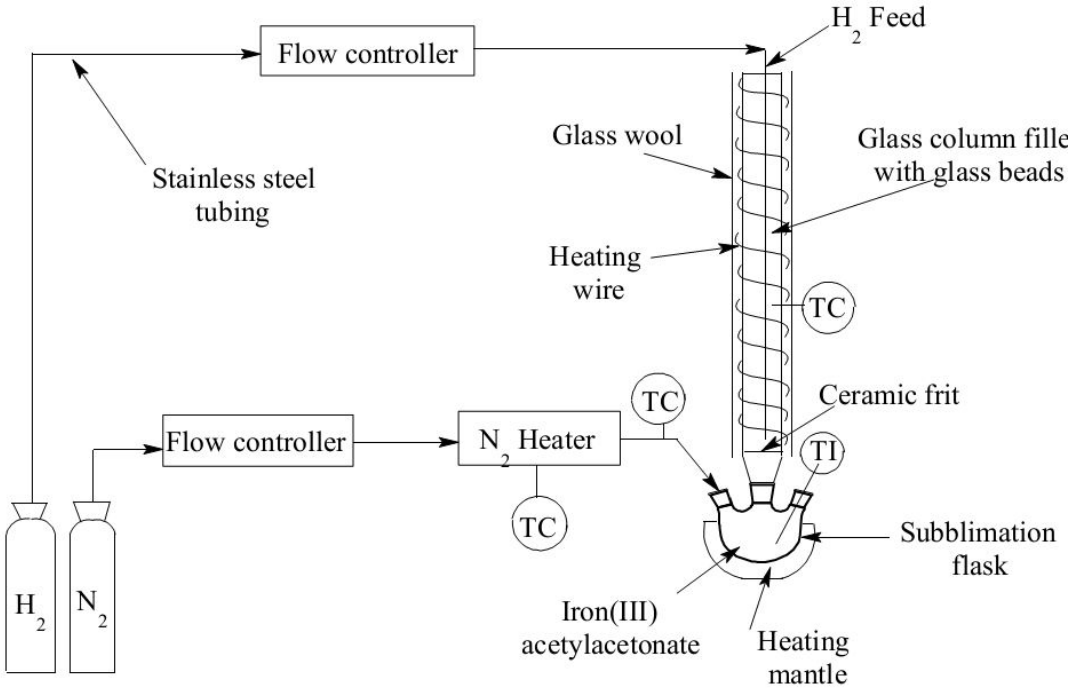

Figure 3.5: Experimental set up for the hydrogen reduction process.

4 RESULTS AND DISCUSSIONS

The main aim of this study was to develop an environmentally friendly extraction process to recover iron from iron ore fines. In order to achieve this aim, iron ore fines were characterized and a series of iron extraction (gas and liquid phase) and recovery experiments were performed.

4.1 Characteristics of iron ore fines

Iron ore fines were characterized by its particle size distribution (sieve analysis), surface area, surface morphology (SEM), and chemical analysis. These physical properties were useful in the design of the fluidized bed reactor and the interpretation of extraction results.

4.1.1 Particle size distribution

The particle size distribution (PSD) was determined by sieves analysis and is given in appendix A (Table A.1). The cumulative particle size curve is shown in Figure 1.1. The lowest sieve size was 45 µm, and only 0.05% of the iron ore fines were smaller than this size. 96.59% of the iron ore was smaller than the biggest sieve size (5600 µm). As shown on Figure 4.1, the d_{50} which is the particle size that gives a cumulative passing of 50% was found to be 2512 µm. Because most agitation leaching are performed on particles smaller than 500 µm (Salmi et al., 2010; Cao et al., 2006; Knorr et al., 2011), it can be deduced that the iron ore fines might have to be subjected to further milling prior to leaching. Larger particles are not recommended for agitation leaching because they have a high settling velocity and do not remain in suspension.

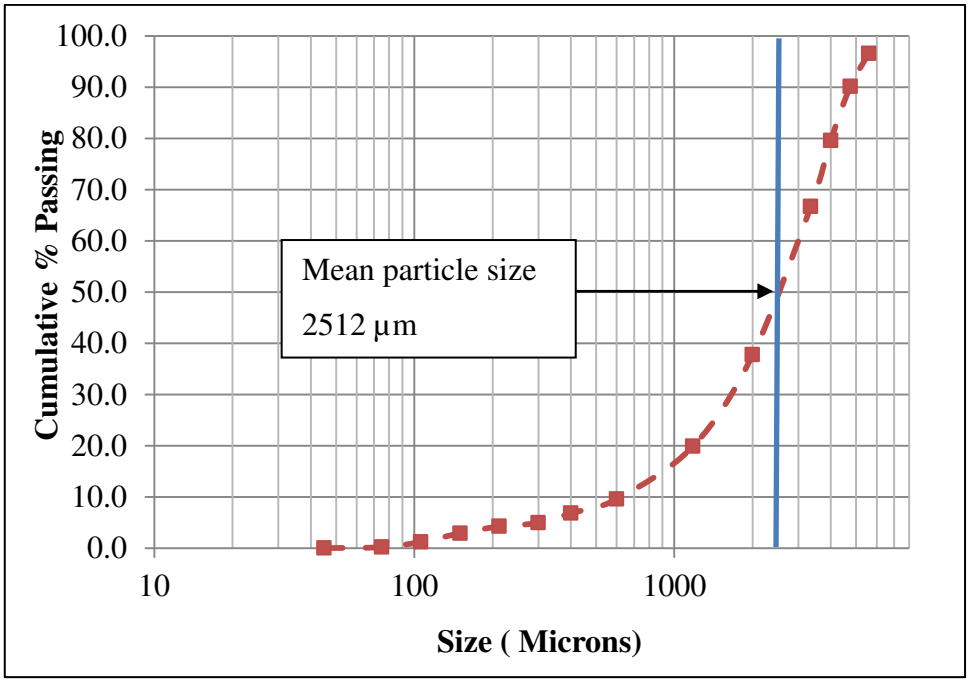

Figure 4.1: Cumulative particle size distribution of the iron ore fines sample.

4.1.2 Surface area characteristics

The Brunauer-Emmett-Teller (BET) analysis was used to determine the surface area of the iron ore fines. The analysis was performed on three iron ore fines samples of distinct particle sizes (+106-150 µm, +300-400 µm and +1180-2000 µm), and the results are presented in Table 4.1. The surface area for each sample was determined, and the results are presented in Table 4.1. The BET results show that a decrease in particle size results in an increase of the available surface area per gram of iron ore, and as leaching is a surface reaction in this case, a larger surface area would lead to more efficient leaching.

Table 4.1: BET surface area of the iron ore fines

Sample particle size [µm]	**Surface area [m^2/g]**
+106 -150	3.1724
+300 -400	2.6450
+1180 -2000	1.2029

Scanning electron microscopy (SEM) analysis is widely used to obtain micrograph images of solid materials. An SEM image of 106 to 150 µm iron ore particles was taken at 1350X magnification, and the micrograph obtained is presented in Figure 4.2. It can be seen that the iron ore particles are of irregular shapes and that the particle size distribution is not homogeneous.

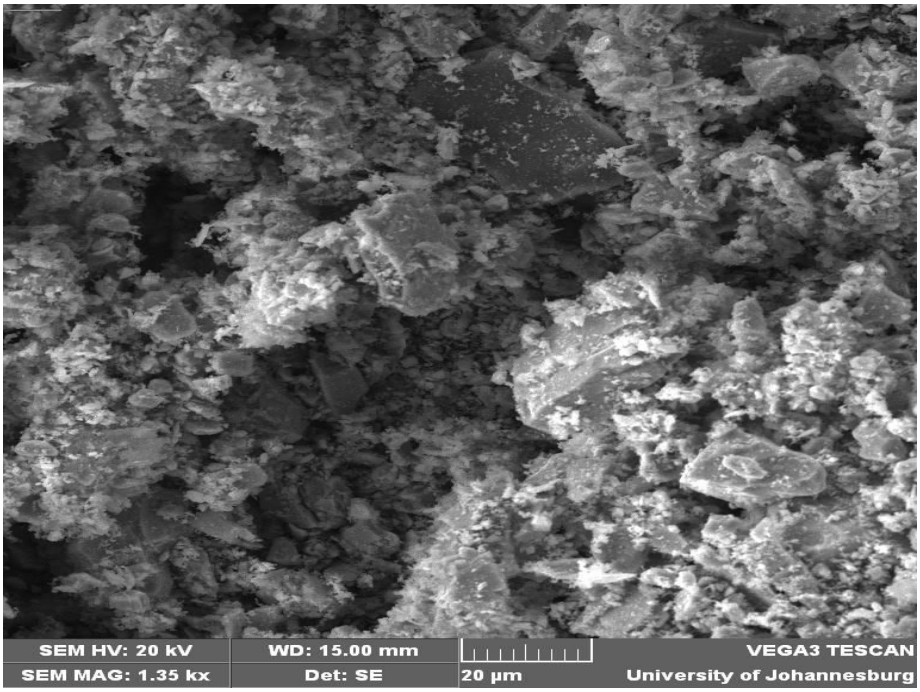

Figure 4.2: Micrograph of iron ore fines at 1350x magnification

4.1.3 Chemical and crystalline composition of the iron ore fines

The chemical composition of the iron ore fines was determined using XRF analysis, and the results of this analysis are presented in Table 4.2. These results show that the iron ore fines contain 93.09% of iron(III) oxide, 5.06% silicon dioxide, 1.30% of aluminium(III) oxide and other oxides in trace amounts. It is known that silica does not react with acetylacetoneand it can therefore be assumed that most of the acetylacetone consumed during the extraction process will be due to its reaction with iron.Acetylacetone can also react with aluminium(III) oxide to form aluminium(III) acetylacetonate (Mpana, 2012). However, aluminium is contained in the muscovite mineral and it is unlikely to be leached from this crystalline phase.

Table 4.2: Chemical composition of iron ore fines (weight %)

Fe_2O_3	Al_2O_3	SiO_2	CaO	K_2O	P_2O_5	TiO_2	MnO	Cr_2O_3	NiO	Na_2O
93.09	1.30	5.06	0.20	0.26	0.14	0.10	0.06	0.04	0.01	0.24

The XRD analysis shows that the constituents of the iron ore can be grouped into three major crystalline phases. These crystalline phases are hematite, muscovite and quartz. The crystalline composition of the iron ore is presented in Table 4.3. The hematite concentration obtained from XRD (93.91%) analysis is similar to the concentration of iron(III) oxide obtained from XRF (93.09%). The XRD analysis also showed that aluminium, potassium and some silica obtained are part of the Muscovite phase detected by XRD.

Table 4.3: Crystalline composition of iron ore fines

Crystalline Phases	Formula	Weight (%)
Hematite	Fe_2O_3	93.91
Muscovite	$KAl_2(Si_3Al)O_{10}(OH,F)_2$	2.17
Quartz	SiO_2	3.92

4.2 Gas phase extraction and recovery of iron

The gas phase extraction of iron was performed by reacting vaporised acetylacetone with iron ore fines in a fluidized bed reactor at elevated temperatures as was given by reaction Equation 1.1 as was given in section 1.1.

$$Fe_2O_{3(s)} + 6H(C_5H_7O_2)_{(g)} \rightarrow 2Fe(C_5H_7O_2)_{3(g)} + 3H_2O_{(g)} \qquad 1.1$$

Gas phase extraction experiments were designed with the objective to investigate the effects of operating parameters on the extraction efficiency of iron from iron ore fines. The effects of reaction temperature, acetylacetone flowrate, and bed weight on the extraction reaction were investigated and each experiment was performed for a total duration of 6 hours.

4.2.1 Effect of temperature on iron extraction

The effect of temperature was investigated by performing gas phase extraction experiments at 160 °C, 250 °C, and 275 °C. These experiments were carried out at a constant bed weight of 20 g, a constant acetylacetone flowrate of 6 mL/min and a total duration of 6 hours. The boiling temperature of acetylacetone is 140°C. In order to ensure that acetylacetone remains in the vapour phase, 160 °C was chosen as the lowest operating temperature. 275 °C was chosen as the highest operating temperature because iron(III) acetylacetonate volatilizes over a range of 92 °C to 275 °C (Potgieter et al., 2006). The results are presented in Figure 4.3. The cumulative percentage of iron extracted refers to the total mass of iron extracted over the total mass of iron initially in the fluidized bed reactor.

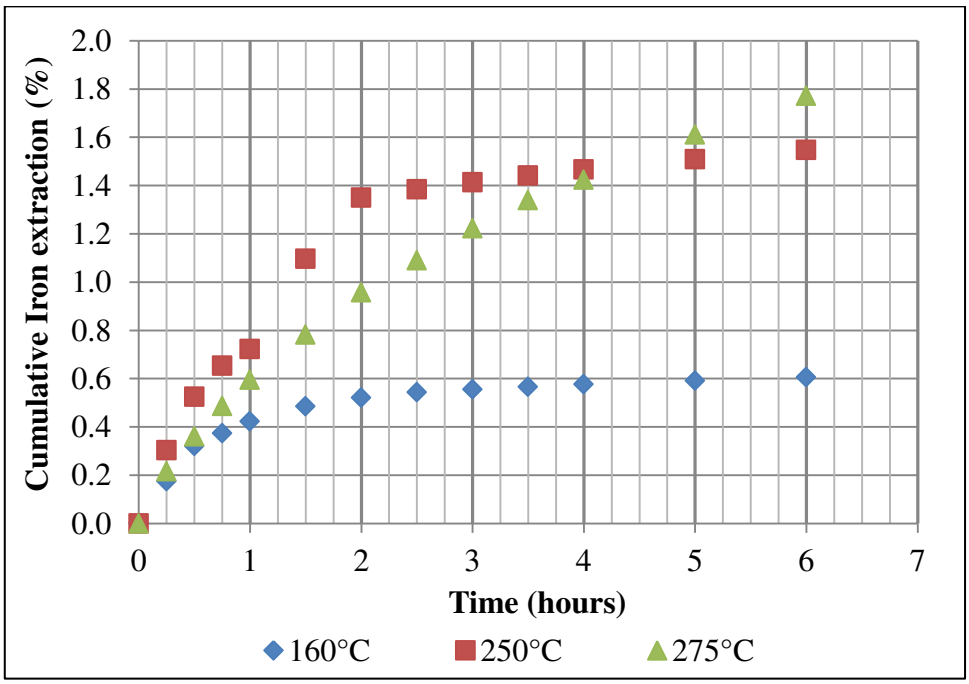

Figure 4.3: The effect of temperature on the extraction of iron from iron ore fine particles (+106 to -150 µm) at 6 mL/min of acetylacetone flowrate.

It can be seen from the results in Figure 4.3 that iron extraction is dependent on temperature. It is also clear that the extraction was very low at all operating temperatures. At the lowest operating temperature (160 °C), only 0.6% of iron was

extracted after 6 hours. At the highest operating temperature (275 °C), less than 2% cumulative iron extraction was achieved after 6 hours. It was also found that the extraction rate decreased considerably and began to plateau after 1h 30 minutes when operating at 160 °C, and after 2 hours at 250°C. This trend was not observed at 275 °C. At this temperature, the extraction of iron did not vary much throughout the experiment. The decrease in extraction rate with time was attributed to the possible formation of a product layer (iron(III) acetylacetonate) on the solid surface. Additional studies should be performed in order to validate this claim.

4.2.2 Effect of bed weight on iron extraction

The effect of bed weight on iron extraction was investigated by performing extraction experiments at bed weights of 20 g and 50 g, at a constant temperature of 250 °C, acetylacetone flowrate of 6 mL/min and for a total duration of 6 hours. Results are presented in Figure 4.4.

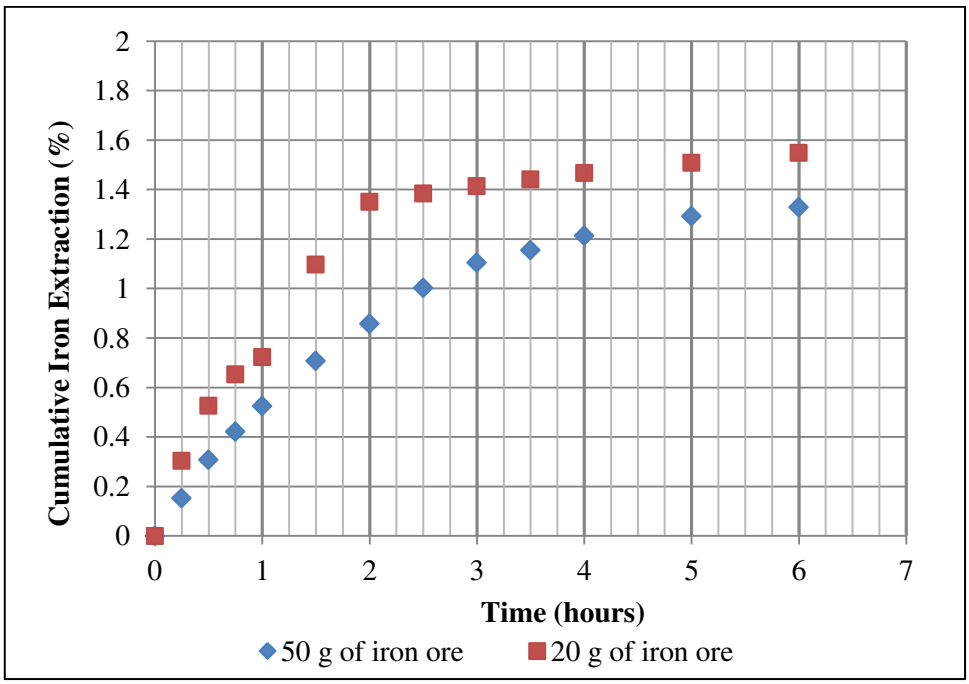

Figure 4.4: The effect of bed weight on the extraction of iron at 250°C, 6 mL/min of acetylacetone, +106 to -150 µm particle size.

It can be seen from Figure 4.4 that the extraction of iron is dependent on the bed weight. An increase in the bed weight resulted in a decrease in iron extraction. The

mass ratio of acetylacetone to iron ore inside the reactor was higher for a smaller bed weight; hence each iron ore particle had the probability to collide with more molecules of acetylacetone. This trend agreed with previous studies by van Dyk et al. (2010) and Mpana (2012). Results also showed that iron extraction slowed down faster for a bed of 20 g compared to the bed weight of 50 g. It was suspected that the overall low extraction of iron was caused by the probable formation of a product layer (iron(III) acetylacetonate) on the surface of iron ore particles. As a result, a smaller bed with fewer particles will have less available surface area for extraction that could passivate faster than a larger bed. This is because it will take longer to form enough iron(III) acetylacetonate to cover the entire surface area of the larger bed.

4.2.3 Effect of acetylacetoneflowrate on iron extraction

Previous studies by Potgieter et al. (2006) and van Dyk et al. (2010) have shown that the flowrate of the ligand has a significant influence on the extraction of iron from synthetic hematite. van Dyk and co-workers (2010) found that the extraction of metals from their oxides increases with the ligand flowrate. The effect of acetylacetone flowrate was investigated by performing gas phase extraction experiments at 2, 6 and 9 mL/min of acetylacetone. This investigation was carried out at a constant temperature of 250 °C, and a constant bed weight of 20 g for 6 hours. The choice of acetylacetone flowrate was governed by the design of the evaporator and the fluidized bed reactor. 9 mL/min was used as the highest acetylacetone flowrate because it was the maximum evaporation rate of the evaporator and no elutriation of the particles was observed at this condition. The results are presented in Figure 4.5.

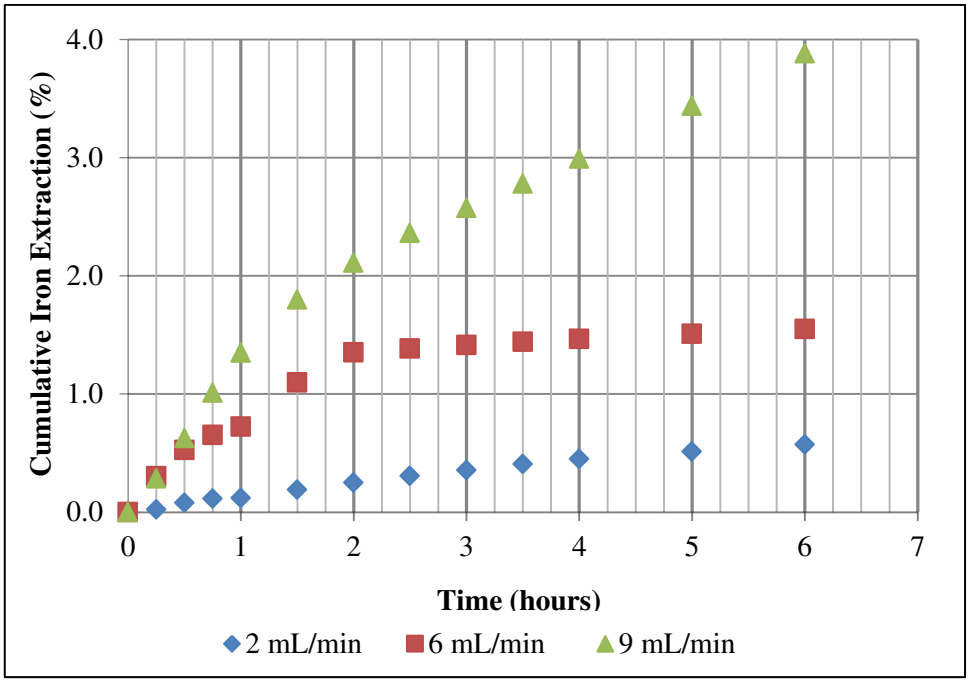

Figure 4.5: The effect of acetylacetoneflowrate on the extraction of iron at 250 °C from +106 to -150 µm particle size.

Figure 4.5 shows that the extraction of iron is dependent on the acetylacetone flowrate, and it can be seen that an increase in acetylacetone flowrate results in higher extractions. At 2 mL/min of acetylacetone, extraction appears linear throughout the experiment. However, the reaction slowed down considerably after 3 hours of extraction at a flowrate of 6 mL/min. A different trend was observed at 9 mL/min as the decrease in extraction is not as significant with time. The overall increase in extraction with increasing acetylacetone flowrate is in agreement with previous studies on the extraction of metals using acetylacetone (Potgieter et al., 2006; van Dyk et al., 2010). At higher acetylacetone flowrates, more acetylacetone were in contact with the iron ore fines, and this could have contributed to the slightly higher extraction rate observed. Furthermore, for mass transfer limited solid-fluid reactions, the rate of reaction is directly proportional to the flowrate (Fogler, 2006). At higher flowrates, the linear velocity of the gas is increased and the mass transfer resistance reduced. However, the overall extraction rate of iron was also found to be slow, with only 3.88% extraction achieved at the highest flowrate of 9 mL/min after 6 hours of extraction.

To test the passivation theory, an additional gas phase extraction experiment was performed using a modified extraction method. The acetylacetone feed was stopped after 3 hours for a duration of 30 minutes. During this period the reactor temperature was raised to 300 °C to sublimate the iron(III) acetylacetonate and nitrogen was fed to the reactor to flush out the gas inside the reactor. The operating temperature was then returned to 250 °C and the extraction was continued. This procedure was repeated after the 4th, 5th, and 6th hour of reaction. The results were then compared to the results of gas phase extraction with continuous feed of acetylacetone (Figure 4.6).

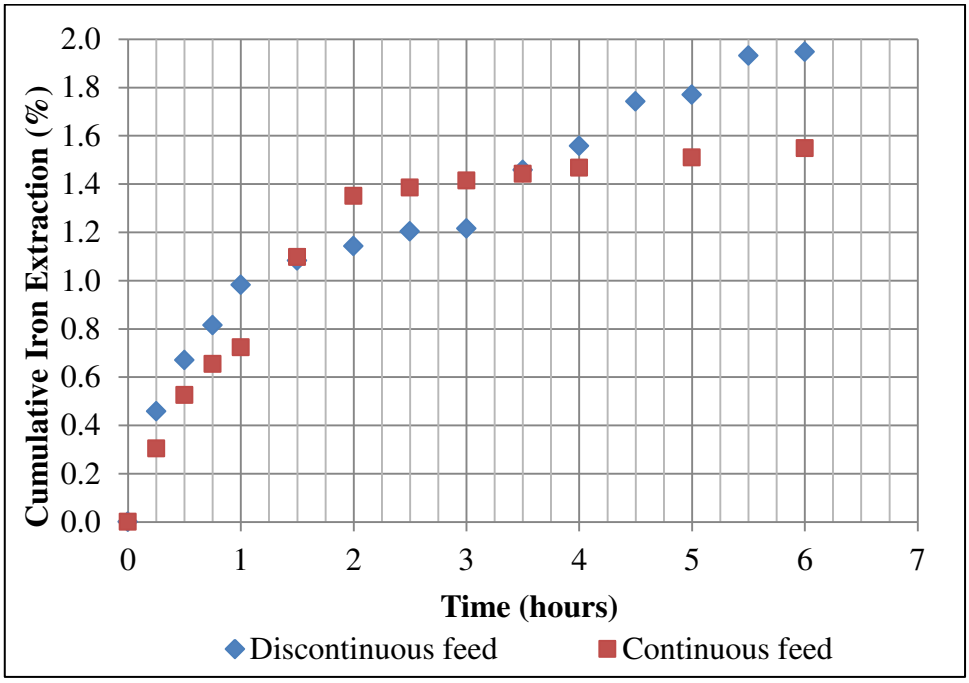

Figure 4.6: The effect of discontinuous acetylacetone flow and nitrogen feed on iron extraction at 250 °C and 6 mL/min for +106 to -150 µm particle size.

From Figure 4.6 it can be seen that both graphs have similar trends for the first 3 hours. The extraction began with a higher rate and then slowed down considerably. However, when the heating program was followed it looks as though there was a small step increase after each nitrogen treatment step. The increase in extraction was, however, very small and therefore this method was not a viable option to increase the efficiency of the extraction process.

The results presented above showed that gas phase extraction of iron from iron ore fines using acetylacetone was low at all the conditions under investigation. This is contrary to what was expected as previous studies at low metal concentrations achieved higher extractions from synthetic mixtures of iron(III) oxide and silica (Mariba, 2010). In addition to the heat treatment test, an additional experiment was performed using synthetic hematite (93 wt%) at 250 °C and similar flowrates as used for the iron ore fines experiments. A comparison of the extractions obtained from the two sources is presented in Figure 4.7.

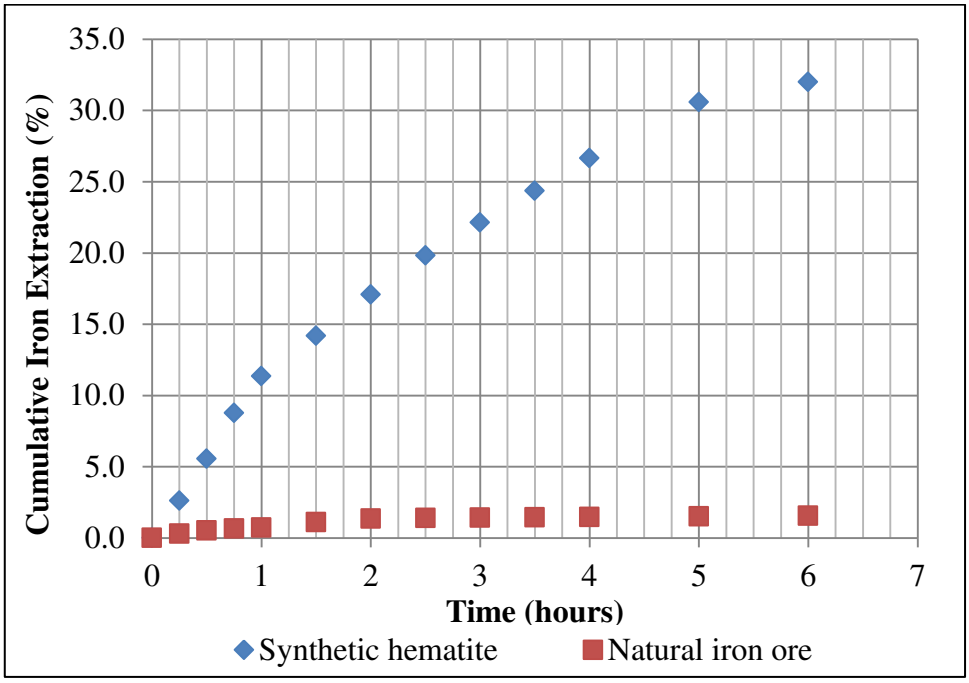

Figure 4.7: Iron extraction from iron ore fines and synthetic hematite at 250 °C and 6 mL/min for +106 to 1150 µm particle size.

Figure 4.7 shows that the extraction of iron from a synthetic system was much higher than the extraction from iron ore fines. After 6 hours of extraction, up to 32% of iron was extracted from the synthetic system compared to 1.55% extracted from the iron ore fines. A similar trend was observed in previous studies on aluminium extraction by Mpana (2012), as 46.7% of aluminium was extracted from a synthetic system compared to 17.9% of aluminium extraction achieved from fly ash at 250 °C and 6mL/min of acteylacetone. An XRD analysis of the synthetic hematite revealed that the hematite was very pure +99.9% (Figure A.1, Appendix A). The synthetic

hematite and the iron ore fines therefore only differ in the fact that iron ore fines contains small amounts (6-7%) of impurities which might react with the acetylacetone and cause surface passivation. This theory will have to be investigated further.

4.3 Leaching of iron from iron ore fines

In order to increase the extraction efficiency it was decided to investigate the liquid phase route. Extraction experiments in the liquid phase were designed with the objective to identify the significant operating variables, to study their effect on the extraction of iron and to perform a kinetic analysis of the extraction process. The results of these investigations are presented and discussed below.

4.3.1 Identification of significant operating variables

The 2^k full factorial design method was used to identify the operating parameters that have significant effects on the efficiency of the extraction process. The identification of significant operating variables is an important screening process that reduces the cost and duration of research by eliminating the time consuming process of investigating non-significant variables (Montgomery, 2005). The effects of temperature, particle size and solid to liquid ratio were determined and used to identify the significant operating variables. Experiments were performed at the operating conditions as described in the experimental section. Because the extraction of iron with acetylacetone is strongly dependent on temperature, the highest operating temperature for this investigation was chosen as 140 °C. This is the boiling temperature of acetylacetone under atmospheric conditions, and the highest temperature at which most of the acetylacetone stayed in the liquid phase. The results of the batch leaching tests are presented in Table 4.4.

Table 4.4: Iron extraction results the for 2^k factorial design

Run	Solid: Liquid ratio	Particle size [µm]	Temperature [°C]	Iron extraction [%]
I	0.025:1	+106-150	120	52.3
II	0.127:1	+106-150	120	35.5
III	0.025:1	+400-600	120	33.1
IV	0.127:1	+400-600	120	36.7
V	0.025:1	+106+150	140	97.7
VI	0.127:1	+106-150	140	34.5
VII	0.025:1	+400-600	140	90.2
VIII	0.127:1	+400-600	140	36.6

The results presented in Table 4.4 show that acetylacetone can be used to successfully extract iron from iron ore fines in the liquid phase. Up to 97.7% of iron was extracted after 48 hours at 140 °C, at a solid to liquid ratio of 0.025:1, and particle size of +106 to -150 µm. As shown in Table 4.4, low extractions were achieved at the lower temperature (120 °C) and high solid to liquid ratio (0.127:1).

The results were used to calculate the effects of the various operating variables and their combined effects on the extraction of iron from iron ore fines. The calculation of effect estimates and the analysis of variance (ANOVA) were performed using Matlab and the design expert software. The relevant calculations can be found in section C.1 (Appendix C) and the results are presented in Table 4.5.

It can be seen that solid to liquid ratio (A), operating temperature (C), and their interaction (AC) have considerably bigger effects and sums of squares. This served as a first indication that temperature and solid to liquid ratio have significant effects of the extraction of iron. However, the significance of operating variables is usually confirmed by the use of either a normality plot, or a half normality plot which are presented in Figure 4.8 and Figure 4.9 respectively.

Table 4.5: Effect estimates and sum of squares for the 2^k full factorial design

Source of variation	Effect Estimate	Sum of Squares	Percent Contribution
A	-32.5	2,112.5	42.96
B	-5.85	68.445	0.46
C	25.35	1,285.2	26.75
AB	7.5	112.5	0.97
AC	-27.78	1,542.9	26.75
BC	3.15	19.845	1.15
ABC	-2.7	14.58	0.95

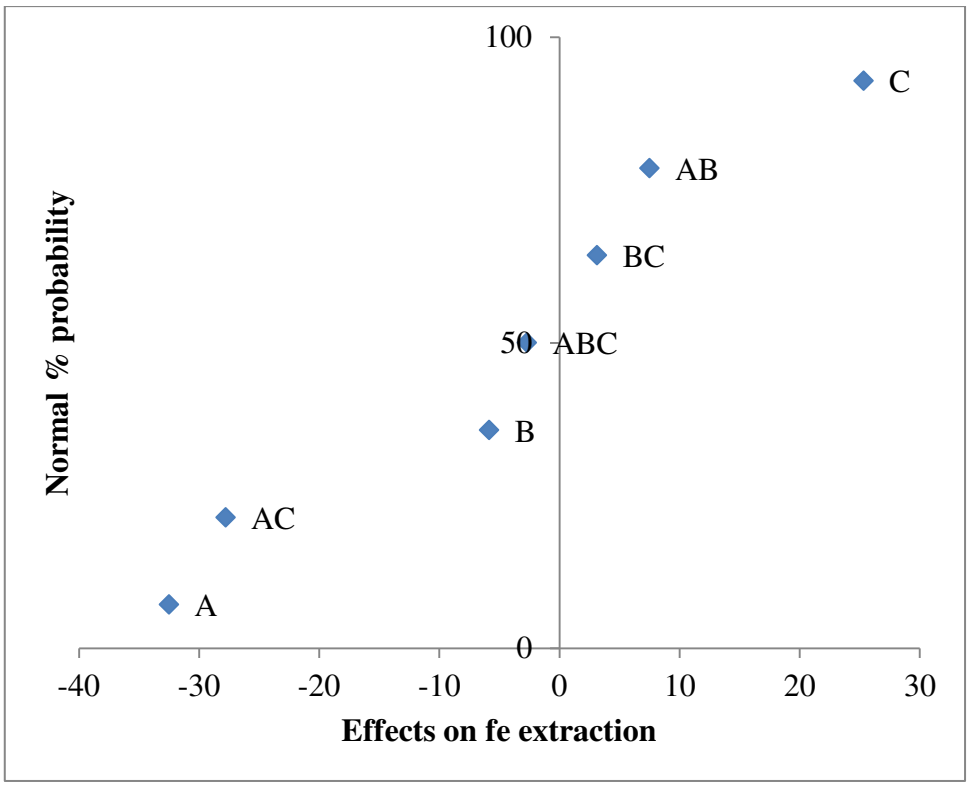

Figure 4.8: Normal % probability plot of effects of operating variables (A-solid to liquid ratio, B-particle size, C-temperature) and their interaction effects (AB, BC and AC).

The normal probability plot (Figure 4.8) was used to identify the operating variables that have significant effects on iron extraction. On a normal probability plot, such

variables are identified as being the furthest away from the zero mean line (Daniel, 1959). It can be seen that the solid to liquid ratio (A) and temperature (C) are significant operating variables of the leaching process. The normal probability plot also shows that the interaction of temperature and solid to liquid ratio has a significant effect on iron extraction. Within the chosen operating range, particle size distribution (B) and the other interactions between operating variables (AB, BC and ABC) have no significant effect on the extraction process. This result is confirmed by the half normal probability plot (Figure 4.9) as the significant variables lie the furthest away from the line.

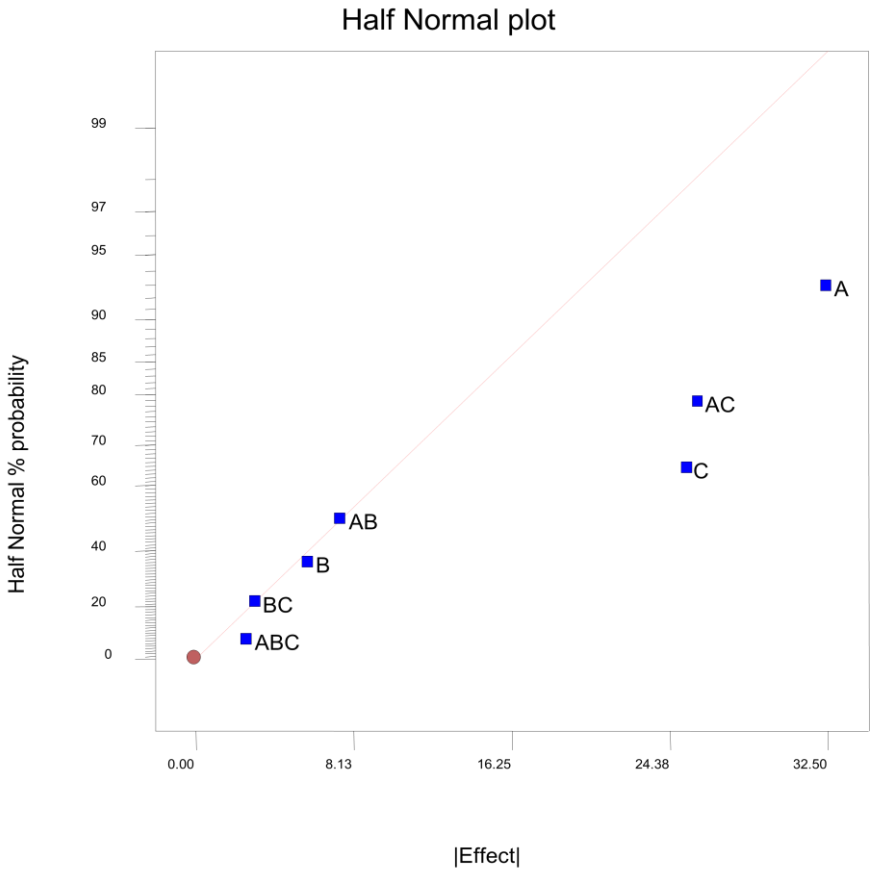

Figure 4.9: Half normal probability plot of effects of operating variables (A-solid to liquid ratio, B-particle size, C-temperature) and their interaction effects (AB, BC and AC).

Additional experiments were performed to study the influence of the significant operating variables on the leaching of iron from iron ore fines using acetylacetone. The results obtained are presented and discussed below.

4.3.2 Influence of significant operating variables on the leaching of iron from iron ore fines.

Effect of temperature

The effect of temperature on iron extraction from iron ore fines was investigated by performing leaching experiments at 100 °C, 120 °C, 140 °C, and 160 °C. These experiments were performed at a low (0.025:1) and a high solid to liquid ratio (0.127:1) for a duration of 48 hours. Figure 4.10 shows the effect of temperature on leaching.

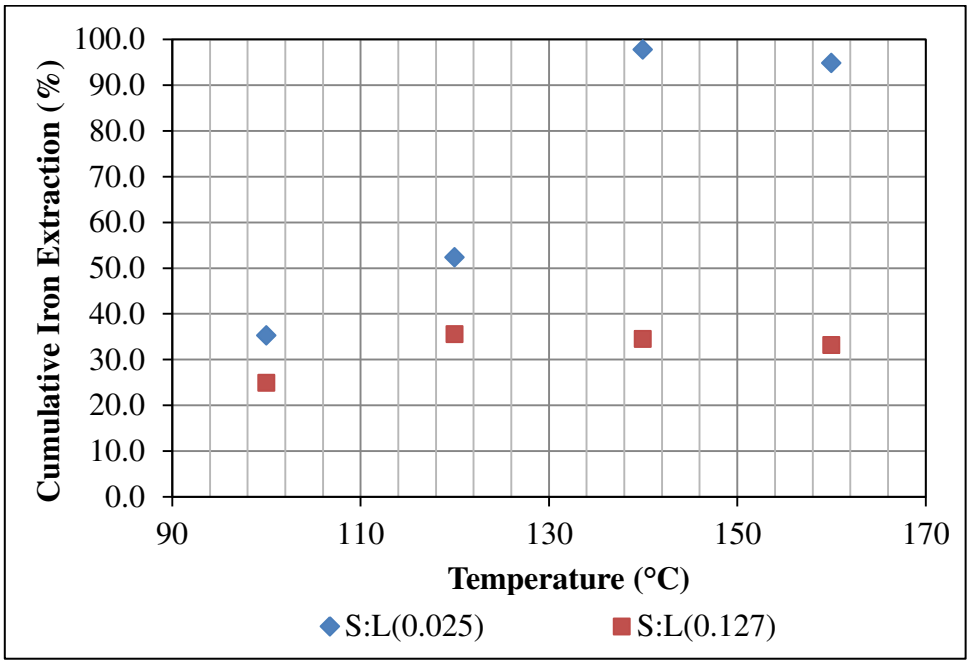

Figure 4.10: The effect of temperature on leaching of iron at 0.025:1 and 0.127:1 solid to liquid ratio (S:L) from +106 to +150 µm particles after 48 hours.

Figure 4.10 shows that iron extraction is strongly dependent on the temperature at the low solid to liquid ratio (0.025:1). An increase from 35.2% to 97.7% iron extraction is observed when the operating temperature was raised from 100 °C to 140 °C. At higher temperatures, molecules possess higher internal energy and more collisions between reactants occur resulting in faster reactions. The same trend was observed in previous gas phase studies by van Dyk and co-workers (2012). The effect of

temperature on iron extraction is less pronounced at the high solid to liquid ratio (0.127:1). This trend is further discussed along with the effect of solid to liquid ratio in the next section. It can also be seen that increasing the temperature beyond the boiling temperature of acetylacetone (140 °C) resulted in lower extractions. At temperatures above the boiling point, more liquid evaporated and was in reflux. Consequently, less acetylacetone remained in liquid phase to react with the iron ore fines and this resulted in lower iron extraction.

Effect of solid to liquid ratio

The effect of solid to liquid ratio was studied by performing liquid phase experiments at solid to liquid ratios of 0.025:1, 0.038:1, 0.051:1, 0.076:1 and 0.127:1. These experiments were performed on +106 to -150 µm and +400 to -600 µm iron ore fines particles at 140 °C for 48 hours. The results are presented in Figure 4.11.

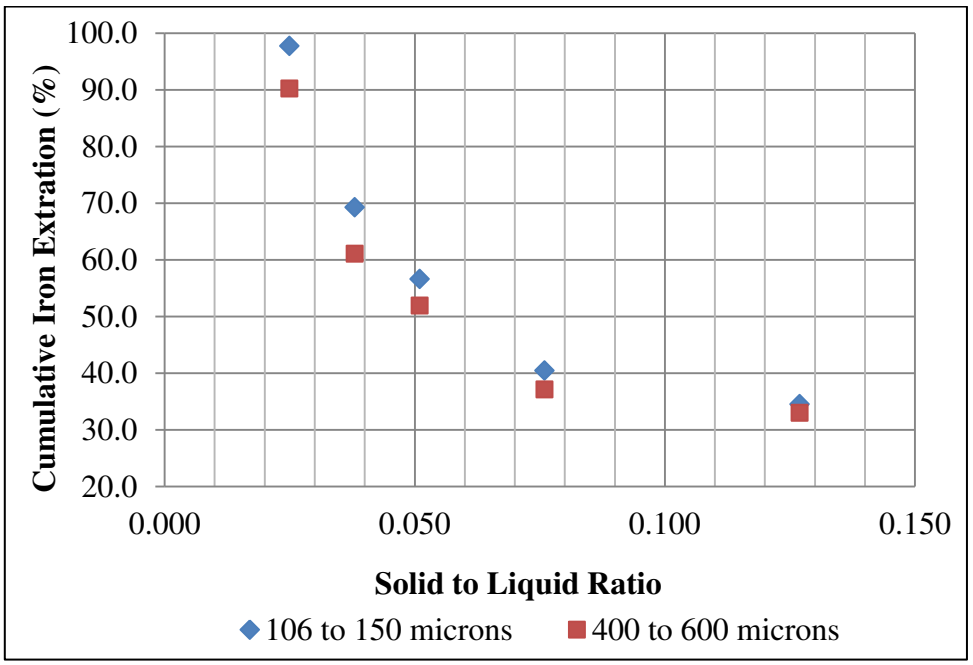

Figure 4.11: The effect of solid to liquid ratio on leaching of iron ore fine at 140 °C with +106 to -150 and +400 to-600 µm particles after 48 hours.

It can be seen from Figure 4.11 that percentage of iron extracted decreased with an increase in solid to liquid ratio. The curve is non-linear and also shows that the

effect of solid to liquid ratio on extraction decrease with an increase in solid to liquid ratio. The same overall trend was observed for +106 to -150 µm and +400 to -600 µm particles. At low solid to liquid ratios, particle size had a larger effect on iron extraction than at high solid to liquid ratios. 97.7% and 90.2% iron extraction were achieved for +106 to- 150 µm and +400 to - 600 µm particles at the solid to liquid ratio of 0.025:1, as opposed to 36.7% and 36.6% iron extraction achieved at the solid to liquid ratio of 0.127:1. This is an indication that the extraction is not controlled by the surface chemical reaction at higher solid to liquid ratio and may be mass transfer limited.

Iron(III) acetylacetonate is fairly soluble in acetylacetone. The higher the solid to liquid ratio, the more iron(III) acetylacetonate was formed. 35.49 g of iron(III) acetylacetonate was formed at a solid to liquid ratio of 0.127:1 as opposed to only 20.09 g formed at the ratio of 0.025:1. Even though the amount of liquid was in stoichiometric excess, the solution became saturated with iron(III) acetylacetonate and iron(III) acetylacetonate crystals formed. These crystals could have also formed on the surface of the unreacted iron ore particles. Figure 4.12 shows the presence of iron(III) acetylacetone in the solid residue after extraction. Such solid residues were washed in ethanol and the resulting solutions were also analyzed with AAS to quantify the total amount of iron(III) acetylacetonate formed. As a consequence the acetylacetone molecules would not reach the surface of the particle for the reaction to take place, and the reaction might become mass transfer limited and results in low iron extractions. At an industrial scale, it might be necessary to have more than one leaching stage instead of one reactor in order to increase the overall leaching rate.

Figure 4.12: Leaching residue containing iron(III) acetylacetonate crystals

4.3.3 Kinetic analysis

A kinetic study was performed with particles in the size range of +106 to -150 µm at different operating temperatures (80 °C, 100 °C, 120 °C and 140 °C) and constant solid to liquid ratio (0.025:1). At a solid to liquid ratio of 0.025:1, no crystallization of the products was observed previously over the entire temperature range. Figure 4.13 shows the extraction of iron from iron ore fines over time at different temperatures.

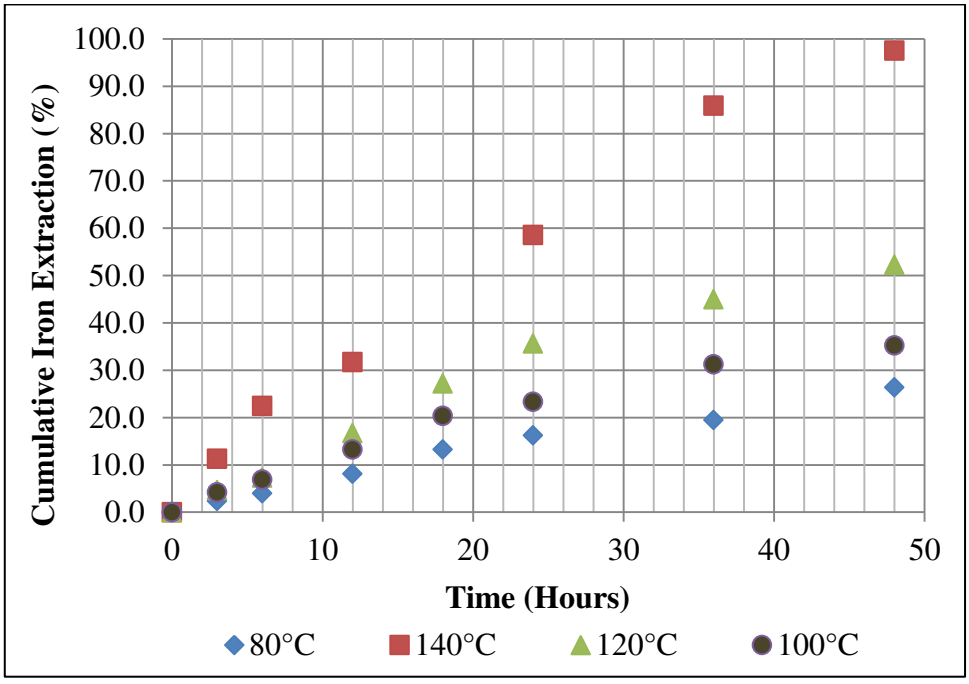

Figure 4.13: The effect of reaction time and temperature on leaching of iron at solid to liquid ratio of 0.025:1, 106 to 150 µm particles.

It can be seen from Figure 4.13 that iron extraction increased with time for all temperatures. As previously observed, the extraction increased with an increase in temperature. The different slopes of the curves in Figure 4.13 implied that distinct extraction rates were obtained at the various operating temperatures. The results also showed that at all operating temperatures, the extraction of iron was not completed after 48 hours. Higher extraction could be achieved after longer leaching periods.

Kinetic modeling of the leaching process

The results presented in Figure 4.13 were used to model the solid/liquid reaction between iron(III) oxide and acetylacetone. Chemical reaction usually occurs through sequential steps and the overall rate is governed by the slowest step (limiting step). This can either be a mass transfer step or the actual chemical kinetics of the reaction.

The reaction between iron(III) oxide and acetylacetone can be described by the following steps:

1. Diffusion of acetylacetone molecules from the bulk solution to the film of solution surrounding the iron ore particles.
2. Penetration of acetylacetone molecules through the film to the solid surface.
3. Absorption of acetylacetone molecules on the surface of the iron ore particles.
4. Reaction of actetylacetone with iron on the solid surface to form iron(III) acetylacetonate and water.
5. Dissolution of iron(III) acetylacetonate into acetylacetone.
6. Diffusion of the products through the product layer, through the film and fluid surrounding the particles and back to the bulk solution.

During the reaction the iron ore particle is consumed and the surface area available for leaching decreases. This together with the steps presented above is in good agreement with the traditional shrinking core model except that the dissolution of iron(III) acetylacetonate plays a significant role in the overall kinetics.

The analysis of kinetic data was performed using the shrinking core model. Diffusion through the fluid film, chemical reaction and diffusion through the product layer are the three main rate limiting steps on which the conventional shrinking core model is based. The model also assumes that the leaching process is a surface reaction which is first order with respect to the concentration of the fluid reagent (acetylacetone). Figure 4.14 illustrates the layers contributing to mass transfer limitation.

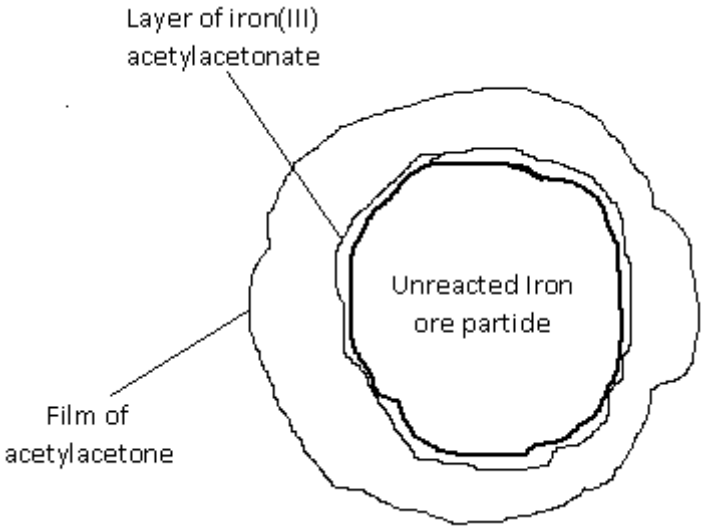

Figure 4.14: Model layer for mass transfer limitations

To minimize mass transfer limitations, the kinetic analysis was performed using kinetic data obtained at the low solid to liquid ratio of 0.025:1, and it was assumed that the leaching rate is limited by chemical reaction at this operating condition. At higher solid to liquid ratio the presence of iron(III) acetylacetonate crystals was observed, and in such conditions the reaction rate will most likely be controlled by the diffusion through the product layer (iron(III) acetylacetonate) or the dissolution of iron(III) acetylacetonate crystals in a solution of acetylacetone. The derivation of the adapted shrinking core model (chemical reaction) and its application to the leaching of iron(III) oxide with acetylacetone is shown below.

The leaching of iron from iron(III) oxide using acetylacetone was given by Equation 1.1.

The chemical reaction rate of a solid-liquid reaction is usually expressed in the mathematical equation shown in Equation 4.2 (Levenspiel, 1972).

$$\frac{1}{S}\frac{d[\text{reactants}]}{\text{dt}} = kC_{fluid} \qquad 4.2$$

Relating Equation 4.2 to the leaching of iron ore fines with acetylacetone, Equation 4.3 was obtained.

$$\frac{1}{S}\frac{dN_{Fe_2O_3}}{dt} = -kC_{Acac} \qquad 4.3$$

Where :S is the surface area of solid available for reaction (m^2)

$N_{Fe_2O_3}$ is the numberof moles of iron oxide (Fe_2O_3)

k is the reaction rate constant

C_{Acac} is the concentration of acetylacetone in mole/L

Because the iron ore particle is shrinking as the reaction proceeds, the number of moles of iron can be expressed in terms of the changing iron ore particle size (radius *r*). A shape factor *f* was used to account for the irregular shape of the iron ore particles. This is illustrated by Equation 4.4.

$$N_{Fe_2O_3} = \rho_{Fe_2O_3} V_{Fe_2O_3} = \rho_{Fe_2O_3}\left(f\frac{4}{3}\pi r^3\right) \qquad 4.4$$

Differentiating both sides of Equation 4.4 gives Equation 4.5

$$dN_{Fe_2O_3} = \rho_{Fe_2O_3} f 4\pi r^2 dr \qquad 4.5$$

Substituting Equation 4.5 into Equation 4.3 gives the following expression:

$$\frac{1}{S}\rho_{Fe_2O_3} f 4\pi r^2 dr = -kC_{Acac}dt \qquad 4.6$$

Integration of both sides of Equation 4.6 yields Equations 4.7 and 4.8.

$$f\rho_{Fe_2O_3}\int_R^r dr = -kC_{Acac}\int_0^t dt \qquad 4.7$$

$$\frac{f\rho_{Fe_2O_3}}{kC_{Acac}}(R-r) = t \qquad 4.8$$

Where R is the initial radius of the particle and *r* is the radius after *t* hours of leaching.

Equation 4.8 can be rearranged into Equation 4.9.

$$\left(1-\frac{r}{R}\right)=\frac{kC_{Acac}}{Rf\rho_{Fe_2O_3}}t \qquad 4.9$$

The conversion of Fe_2O_3 can be written in terms of volume fraction as follows

$$X=1-\left(\frac{\text{Volume of unreacted core}}{\text{Total initial volume of particle}}\right) \qquad 4.10$$

Assuming that the particles have irregular shapes, Equation 4.10 can be rearranged into Equation 4.11.

$$X=1-\frac{\frac{4}{3}\pi r^3 f}{\frac{4}{3}\pi R^3 f}=1-\left(\frac{r}{R}\right)^3 \qquad 4.11$$

Equation 4.11 can be rearranged into Equation 4.12 which can then be substituted into Equation 4.9 to get an equation of conversion as function of time (Equation 4.13).

$$\frac{r}{R}=(1-X)^{1/3} \qquad 4.12$$

$$X=\left[1-\left(1-\frac{kC_{Acac}}{Rf\rho_{Fe_2O_3}}t\right)^3\right] \qquad 4.13$$

Using the number of moles of Fe_2O_3 consumed in the reaction, the total iron extraction is then expressed as shown in Equation 4.14**.**

$$\text{Iron extraction} = \left[1-\left(1-\frac{kC_{Acac}}{Rf\rho_{Fe_2O_3}}t\right)^3\right]\times 100\% \qquad 4.14$$

The shrinking core models for diffusion through product layer and for diffusion through fluid film controlled processes are given by Equations 4.15 and 4.16 respectively.

$$\frac{t}{\tau} = 1-3(1-X_B)^{2/3}+2(1-X_B) \qquad 4.15$$

$$\frac{t}{\tau} = 1-(1-X_B)^{2/3} \qquad 4.16$$

These models were also fitted to the experimental data presented in Figure 4.15. The graphs showing comparison between the kinetic models and the experimental data can be found in Figures C.1 – C.4 (Appendix C). The regression coefficients of the three possible shrinking core models were calculated and the results are presented in Table 4.6. The regression coefficient is a statistical mean to measure how well a mathematical model fits to a set of data. The results in Table 4.6 was used as a first guess for the model to best describe the controlling step and hence the activation energy of the reaction was calculated using the shrinking core model for chemical reaction controlled kinetics.

Table 4.6: Regression coefficients of the various shrinking core models

Temperature [°C]	**Regression coefficients (R^2)**		
	Diffusion through product layer	Diffusion through fluid film	Chemical reaction
80	0.963	0.988	0.992
100	0.970	0.982	0.987
120	0.944	0.991	0.995
140	0.872	0.994	0.995

The kinetic model given by Equation 4.14 was fitted to the experimental data obtained at different operating temperatures (80 °C, 100 °C, 120 °C, and 140 °C) for iron ore fines particle size of +106 to-150 µm and solid to liquid mass ratio of

0.025:1. Figure 4.15 shows the fitted shrinking core model of a chemical reaction controlled process.

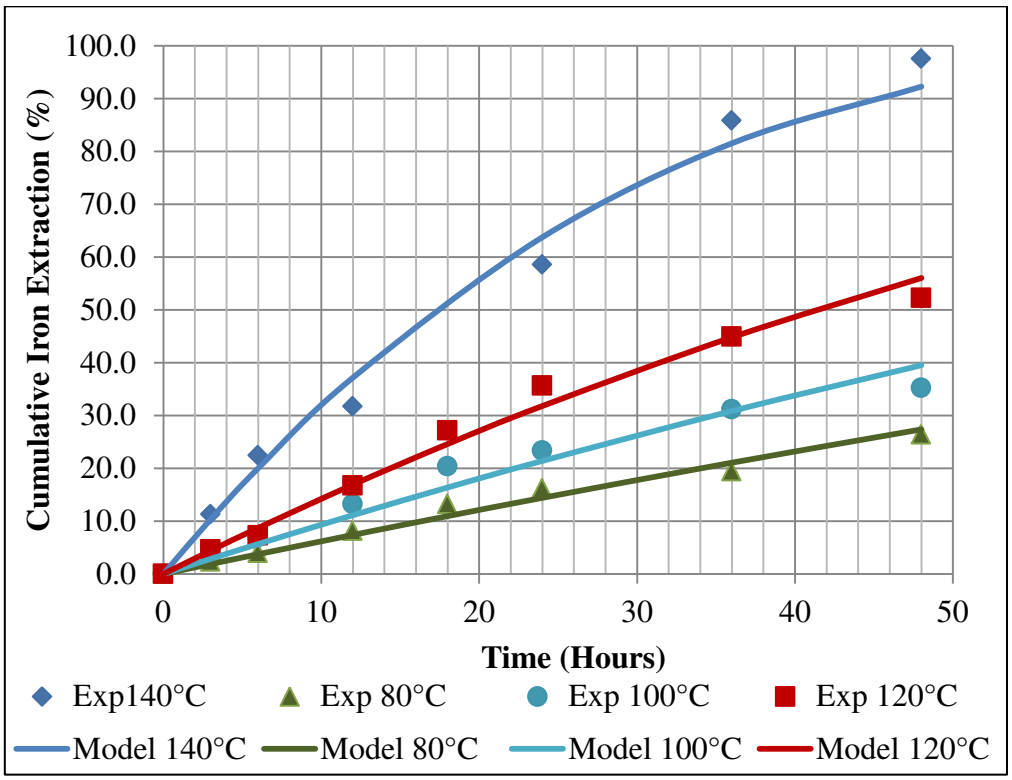

Figure 4.15: Experimental extraction kinetic data and fitted shrinking core model for chemical reaction controlled kinetics at various temperatures (+106 to -150 µm particle size and 0.025:1 solid to liquid ratio).

The activation energy was calculated from the results of the fitted model in order to assess the effect of temperature on the rate constant of the chemical reaction kinetics. After fitting the kinetic model to experimental data as shown in Figure 4.15, the reaction rate constants were found at each temperature and the results are presented in Table 4.7.

Table 4.7: Reaction rate constants for different operating temperatures

Temperature [°C]	**Rate constant [$m^{-2}hr^{-1}$]**
80	0.00014
100	0.00021
120	0.00033
140	0.00079

The mathematical function relating the reaction rate constant to the reaction temperature is given by the Arrhenius equation shown below.

$$k = Ae^{-\frac{E_a}{RT}} \qquad 4.17$$

This equation can be linearised by taking the natural logarithm of each side of Equation 4.17.

$$\ln k = -\frac{E_a}{RT} + \ln A \qquad 4.18$$

Using Equation 4.18 and a plot of $\frac{1}{T}$ versus ln(k), the activation energy can be calculated from the slope of the curve (Figure 4.16) and was found to be 4.22 kJ/mol. This result indicates that within the chosen operating range, the extraction rate is not strongly affected by temperature. Figure 4.16 shows the Arrhenius plot for leaching of iron ore fines at 0.025:1 solid to liquid ratio and particle size +106 to -150 µm.

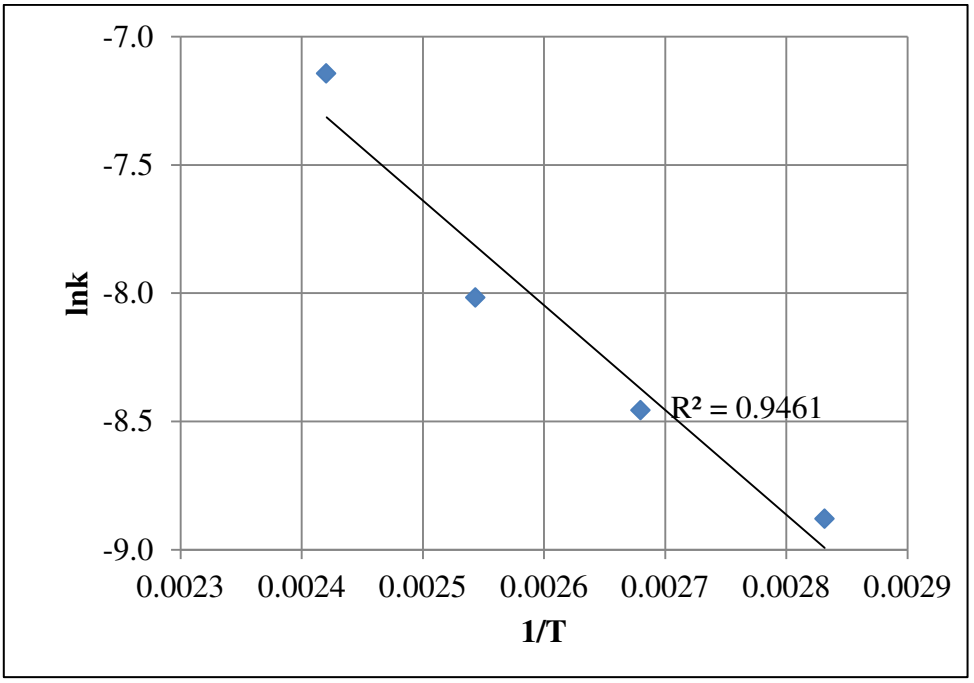

Figure 4.16: Arrhenius plot for leaching of iron ore fines at 0.025:1 solid to liquid ratio and particle size +106 to -150 µm.

In general, chemically controlled processes are strongly dependent on temperature while diffusion controlled processes are only slightly affected by the reaction temperature (Habashi, 1969). Table 4.8 shows typical activation energy ranges for various rate controlling mechanisms.

Table 4.8: Activation energy for the different rate controlling mechanism (Habashi, 1969).

Rate controlling step	Activation energy [kJ/mole]
Diffusion controlled	4.18 to 12.36
Intermediate process	12.54 to 41.8
Chemically controlled	>41.8

It can be seen that the activation energy of 4.22 kJ/mole calculated using a chemical kinetics controlled relationship is considerably lower than what is expected. The deviation of this value from a typical value greater than 41.8 kJ/ mole suggests that the overall reaction rate might be controlled by diffusion. In order to test this theory,

the diffusion controlled model was fitted to the experimental data (Figure4.17). It can be seen that the model fits the experimental data similarly to the model for chemical reaction controlled processes.

However, to determine the activation energy required for a diffusion controlled process additional experimental work is necessary. The proposed model should also be extended to include the effect of solid to liquid ratio and dissolution kinetics of iron(III) acetylacetonate in acetylacetone.

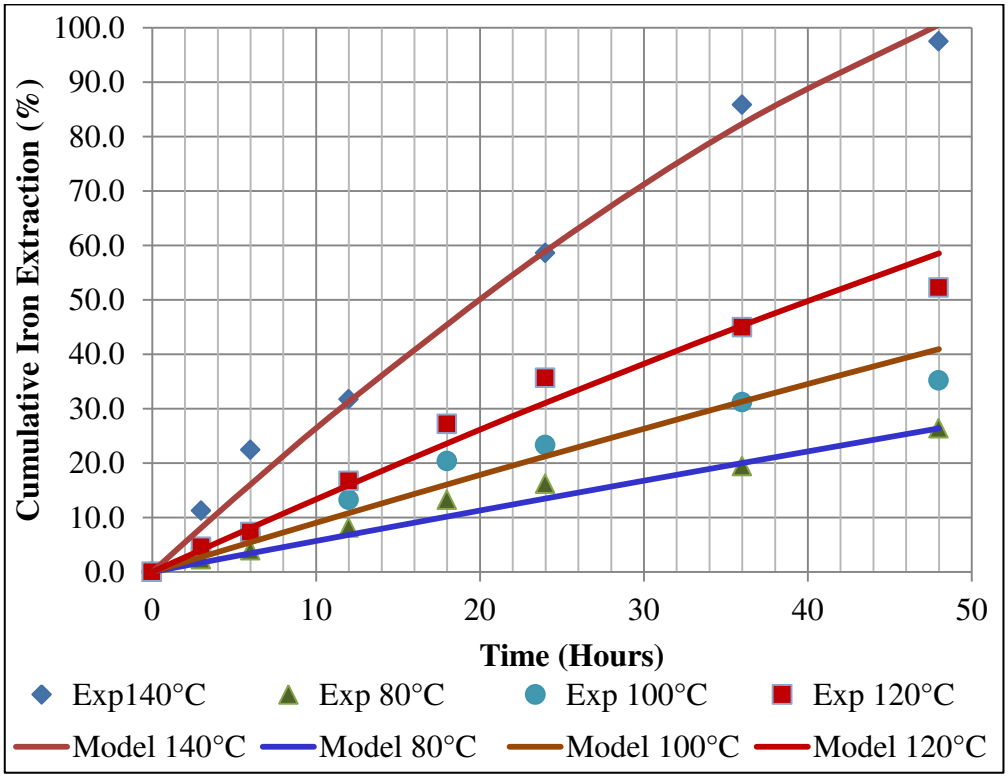

Figure4.17: Experimental extraction kinetic data and fitted shrinking core model for diffusion controlled kinetics at various temperatures (+106 to -150 µm particle size and 0.025:1 solid to liquid ratio).

4.3.4 Recovery of unreacted acetylacetone and iron(III) acetylacetonate from leach solution

The leach liquor and solid residue obtained from the leaching process were separated by filtration. The leach liquor comprised of dissolved iron(III) acetylacetonate, unreacted acetylacetone and water. These constituents have distinct boiling temperatures and were easily separated by the use of a Heidolph evaporator. Acetylacetone and water were recovered by distillation and a solid residue of iron(III) acetylacetonate was formed. The evaporator was firstly operated at 110 °C to remove all the water from the solution and then at 160 °C to separate acetylacetone from iron(III) acetylacetonate.

The iron(III) acetylacetonate crystals recovered through this process is shown in Figure 4.18. To confirm the qualitative composition of the crystals, it was characterized using X-ray diffraction (XRD) analysis. Figure 4.19 shows that the peak list of the formed crystals fit the crystallographic data of synthetic iron(III) acetylacetonate quite well.

Figure 4.18: Picture of iron(III) acetylacetonate crystals formed during separation process.

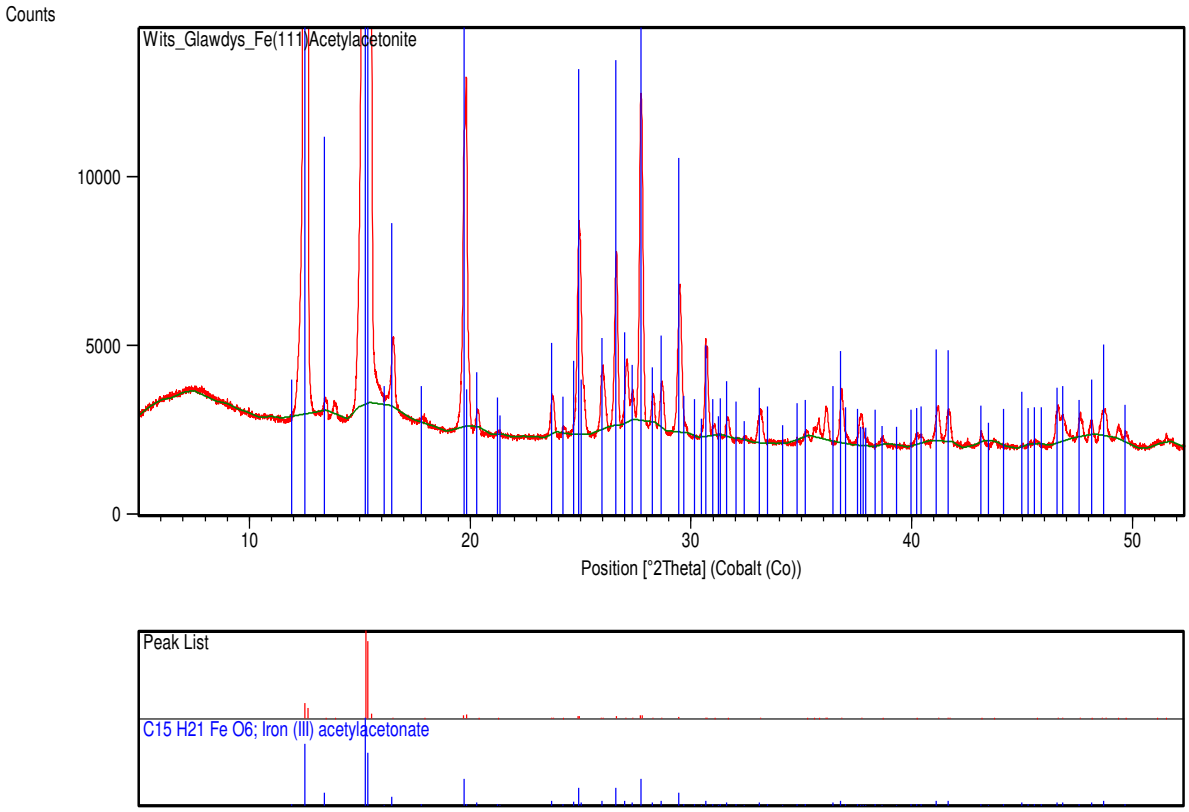

Figure 4.19: X-Ray Diffractogram of iron(III) acetylacetonate crystals.

The iron(III) acetylacetonate crystals can be further purified by sublimation. Previous studies by Stabnikov and co-workers (2007) showed that Fe, Al, Mn, and In acetylacetonate can be purified at a pressure of 1.10^{-2} Torr and over a temperature range of 200 °C to 210 °C (Stabnikov et al., 2007).

In order to determine whether the recovered acetylacetone can be reused additional leaching experiments at 140 °C, 0.025: 1 solid-liquid ratio with +106 to -150 µm particles were performed with recycled acetylacetone. The results are shown in Table 4.9. From these results it can be seen that the reactivity of acetylacetone is not strongly affected by the separation process. When using recycled acetylacetone, it was found that the variation in iron extraction was within 5% of the extraction achieved with fresh acetylacetone.

Table 4.9: Iron extraction using recycled acetylacetonate in the liquid phase

	Fresh feed	1st Recycle	2nd Recycle
Iron extraction (%)	97.72	92.91	94.38

4.4 Recovery of iron by hydrogen reduction of iron(III) acetylacetonate

The products of the extraction process is iron(III) acetylacetonate and water. A preliminary study was performed to investigate the possibility of recovering iron from iron(III) acetylacetonate by reducing it with hydrogen in the gas phase. Zhang and co-workers (2011) investigated the synthesis of iron nanocrystals in an autoclave by the hydrogenation of iron(III) acetylacetonate at high pressure (6 MPa) and a temperature of 300 °C. Pure iron nanocrystals smaller than 10 nm were formed in this study to show the feasibility of the reduction process in the liquid phase (Zhang, et al., 2011).

A gas phase route was chosen as it can easily be incorporated in series with a gas phase extraction unit. The hydrogenation reaction is given by Equation 2.7 and the reduction experiment was conducted as described in section 3.4.

$$Fe(C_5H_7O_2)_{3(g)} + \frac{3}{2}H_{2(g)} \rightarrow Fe_{(s)} + 3H(C_5H_7O_2)_{(g)} \qquad 2.7$$

The synthesis of elemental iron using hydrogen reduction of iron(III) acetylacetonate was performed in a temperature range of 250 °C to 290 °C. Results showed that the recovery of iron using this process is feasible at the mentioned operating conditions. The visual evidence was the acute colour change of the glass beads observed after the hydrogen reduction experiment (Figure 4.20). Such a colour change was only evident after hydrogen gas was fed to the reactor. It was caused by vapour deposition of elemental iron on the glass beads. Using concentrated hydrochloric acid, iron particles were dissolved from the glass beads and the solution was analysed using AAS. The results are presented in Table 4.10.

Figure 4.20: Picture of glass beads before and after hydrogen reduction experiments

Table 4.10: Hydrogen reduction results

Temperature [°C]	**Fe recovery [%]**
250	46.4
270	23.7
290	29.0

The highest recovery of iron was 46.4% at 250 °C and this was equivalent to only 2.93 mg of iron recovered after 3 hours. Table 4.9 also shows a fluctuation of iron recovery with temperature. Previous studies on hydrogen reduction of iron oxides showed that the reduction process is enhanced by high temperatures and high hydrogen flowrates (Wagner et al., 2006). For safety reasons, a high nitrogen to hydrogen feed rate (80:1) was used in this study which resulted in a very low hydrogen concentration in the reactor. This could be the reason for the low recoveries. It was also difficult to sublimate the iron(III) acetylacetonate and the sublimation rate of iron(III) acetylacetonate was very slow. Only 4.8% of the initial mass of iron(III) acetylacetonate was sublimated after 3 hours. If the efficiency of the gas phase extraction process can be improved a continuous extraction and

recovery process will overcome this problem. It should also be noted that this is the first time that the recovery from iron(III) acetylacetonate was attempted in the gas phase.

4.5 Industrial applications of iron extraction using acetylacetone

The aim of this section is to identify and explore feasible process routes to utilise iron ore fines. The results of the experimental work will be used as a basis for calculations. It should be emphasized that at this stage the proposed processes is not intended to replace existing iron making techniques, but to add value to various deposits of iron ore fines by proposing a novel value added process with less energy consumption and no green house gas emissions compared to existing processes. This study proposes two value added processes; the production of or iron nanoparticles from iron ore fines. A detailed economic evaluation was performed on the production of iron(III) acetylacetonate.

4.5.1 The production of iron(III) acetylacetonate from iron ore fines

Process description

The results of the leaching and iron(III) acetylacetonate recovery experiments were used to come up with a conceptual design of a process for the production of iron(III) acetylacetonate from iron ore fines. A description of the proposed manufacturing process (Figure 4.21) is presented below.

The acetylacetone-water mixture and iron ore fines are fed to a mixer M-101 to form an homogeneous slurry. The iron ore fines are fed to the mixer using a screw conveyor (C-101) at a rate that ensures a solid to liquid mass ratio of 0.025:1 (stream 4). The slurry is pre-heated to 130 °C before being fed to a series of 4 leaching reactors that operate isothermally at 140 °C. This is to ensure the feed to the reactor remains mostly in the liquid phase. The reactors are identical in size and sized to yield a total slurry residence time of 48 hours or 12 hours per reactor. Based on the experimental results, iron extraction of up 97% is expected at the end of the leaching

process. The hot product stream (slurry) is drained from the bottom of the last reactor (R-104), cooled to a lower temperature using a heat exchanger (E-102), and then fed to a decanter (D-101) to recover most of the clear solution (stream 11). The decanter underflow stream (stream 12) is filtered to recover the remainder of the solution entrained with the solid residue (stream 13).

The solution containing iron(III) acetylacetonate, acetylacetone and water (stream 15) is fed to a forced convection crystallizer where iron(III) acetylacetonate crystals are produced by vaporization of acetylacetone and water. The vapour stream containing water and acetylacetone (stream 17) is then partially condensed at 110 °C (E-103) and fed to a flash drum for vapour-liquid separation. The vapour stream (stream 20) that is rich in water is condensed (E-104) and a portion of the stream is purged from the process to avoid the accumulation of water in the process. The objective of the separation process is to minimize the amount of acetylacetone lost with the purge stream. Stream 24 and stream 21 are then mixed and recycled back to the leaching process.

A mass and energy balance of the process was performed and the results are also presented in Figure 4.21. The calculations were based on an annual iron(III) acetylacetnate production rate of 9600 tons. This rate was chosen because it was the highest supply capacity from the various iron(III) acetylacetonate suppliers (Alibaba., 2014). The assumptions made for the mass and energy balance calculation are as follows.

1. The plant was assumed to operate for 351 days a year and 24 hours a day. This is to allow for a typical annual shut down period of 2 weeks for maintenance purposes (Turton et al., 2008).
2. The cumulative conversion after each reactor was taken as that obtained after 12 h, 24 h, 36 h and 48 h of iron extraction at the solid-liquid ratio of 0.025:1 and 140 °C. From the experimental work this was 32 %, 58 %, 86 % and 97 % respectively.
3. To separate the solution and the solid residue from the stream exiting the last reactor, a decanter was first used. This is because the % solid of stream 9 is

very low (0.058%), and is not suitable for filtration. The % solid was raised to 9% in the decanter underflow (Sinnot, 2005).

4. The underflow of the decanter was then filtered using a top feed drum filter to produce a cake with 2% moisture (Richardson, et al., 2002). The choice of solid-liquid separator was performed using Figure 10.10 from Sinnot (2005).
5. The forced convection crystallizer was assumed to operate perfectly such that all of the acetylacetone and water are vaporized and only dry iron(III) acetylacetonate crystals are recovered in stream 16.
6. The separation of the acetylacetone-water mixture is governed by the vapour-liquid equilibrium of the binary mixture. The separation process was simulated using Aspen Plus v8.4. A Txy phase diagram of the mixture was also generated during the simulation process and is given in Figure E.1 (Appendix E)
7. No heat losses occur to the environment.
8. Physical data used for energy balance calculations are presented in Table E.1 (Appendix E).

The results of the mass and energy balance calculations were then used to perform a profitability analysis of the proposed process which included a sensitivity analysis.

.

C-101	M-101	E-101	R -101	R -102	R -103	R -104	E-102	D-101	F-101	CR-101	E-103	V-101	E-105	E-104
Screw conveyor	Mixer	Heater	Leaching Reactor	Leaching Reactor	Leaching Reactor	Leaching Reactor	Cooler	Decanter	Drum Filter	Crystallizer	Condenser	Flash Drum	Cooler	Condenser

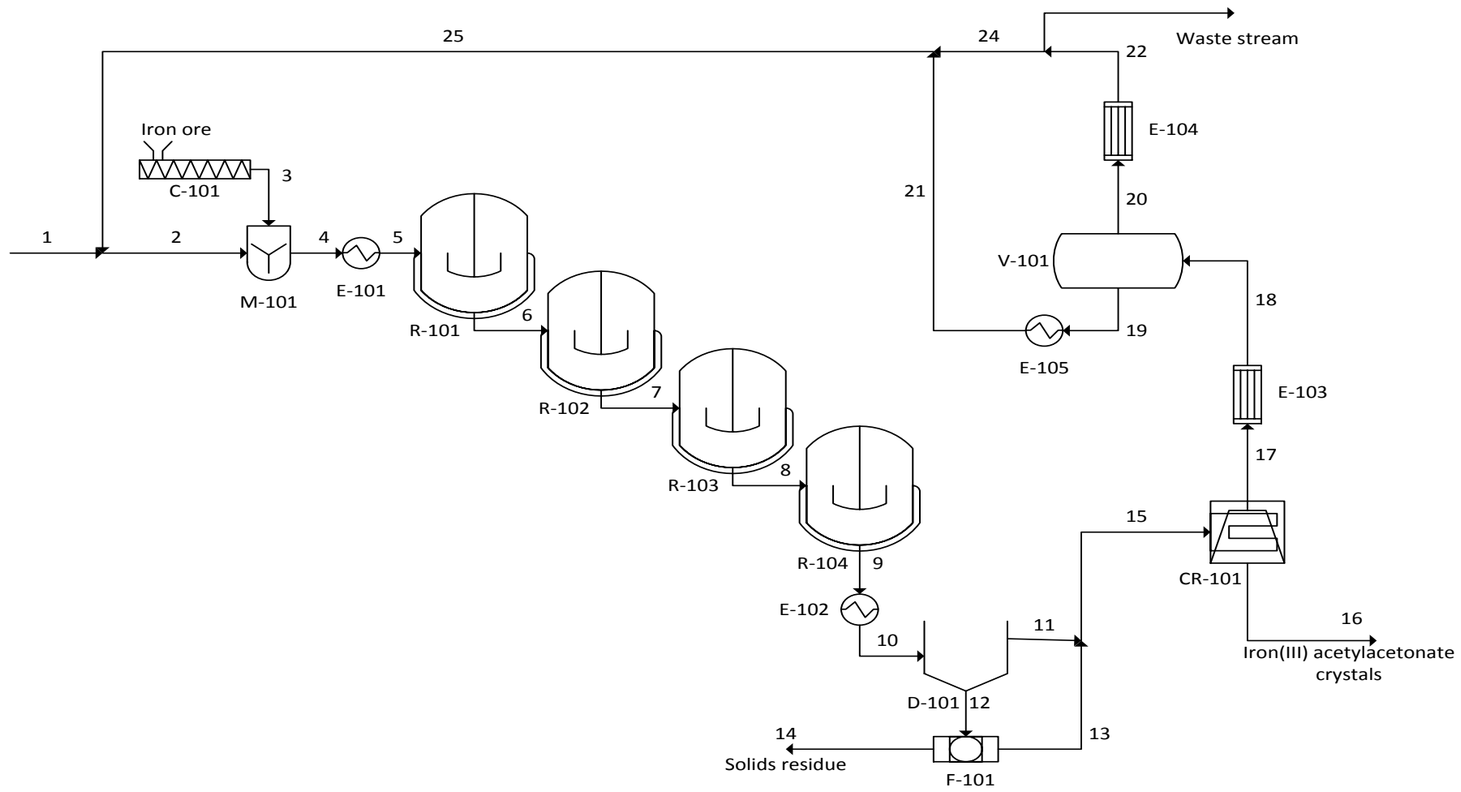

Streams	1	2	3	4	5	6	7	8	9	10	11	12	13	14	15	16	17	18	19	20	21	22	23	24	25
Temp (°C)	**25**	**75.8**	**25**	**75.1**	**130**	**140**	**140**	**140**	**140**	**60**	**60**	**60**	**60**	**60**	**60**	**140**	**140**	**110**	**110**	**110**	**81**	**80**	**80**	**80**	**79.9**
H (MJ/s)	**-1.36**	**-15.12**	**-0.38**	**-15.50**	**-14.63**	**-14.49**	**-14.22**	**-13.92**	**-13.46**	**-14.72**	**-14.63**	**-0.09**	**-0.08**	**-0.015**	**-14.70**	**-0.02**	**-12.76**	**-13.8**	**-12.57**	**-1.25**	**-12.86**	**-1.46**	**-0.56**	**-0.87**	**-13.76**
$C_5H_8O_2$	1.148	9.275	0.000	9.275	9.275	8.955	8.694	8.414	8.304	8.304	8.256	0.048	0.043	0.005	8.299	0.000	8.299	8.299	7.854	0.445	7.854	0.445	0.172	0.273	8.127
H_2O	0.000	1.057	0.000	1.057	1.057	1.085	1.109	1.133	1.144	1.144	1.138	0.006	0.006	0.000	1.144	0.000	1.144	1.144	0.921	0.223	0.921	0.223	0.086	0.136	1.058
Fe_2O_3	0.000	0.000	0.265	0.265	0.265	0.179	0.110	0.036	0.006	0.006	0.000	0.006	0.000	0.006	0.000	0.000	0.000	0.000	0.000	0.000	0.000	0.000	0.000	0.000	0.000
$Fe(C_5H_7O_2)_3$	0.000	0.000	0.000	0.000	0.000	0.376	0.682	1.011	1.141	1.141	1.133	0.007	0.006	0.001	1.140	1.140	0.000	0.000	0.000	0.000	0.000	0.000	0.000	0.000	0.000
Total(ton/h)	**1.148**	**10.331**	**0.265**	**10.596**	**10.596**	**10.595**	**10.595**	**10.595**	**10.595**	**10.595**	**10.527**	**0.068**	**0.055**	**0.012**	**10.583**	**1.140**	**9.443**	**9.443**	**8.775**	**0.668**	**8.775**	**0.668**	**0.258**	**0.409**	**9.185**

Figure 4.21: Process flow diagram for the production of iron(III) acetylacetonate

Economic analysis

In order to evaluate the feasibility of this process from an economic point of view, a preliminary economic evaluation of the process was performed. This included a cost estimation, a profitability analysis, and sensitivity analysis. The results obtained are presented below, together with brief descriptions of the methods used in the calculations.

Estimation of the total capital investment costs

Using the mass and energy balance data, the size and cost of the major pieces of equipment were determined. The fixed capital investment (FCI) was estimated using the module costing technique and was then used to estimate the working capital (WC) and the total capital investment (TCI) as per Equation 4.19.

$$TCI = FCI + WC \quad 4.19$$

The working capital was taken as 20% of the fixed capital investment (Turton, et al., 2008). The fixed capital investment was estimated using Equation 4.20 and Equation 4.21.

$$C_{TM} = \sum_{i=1}^{n} C_{TM,i} = 1.18 \sum_{i=1}^{n} C_{BM,i} \quad 4.20$$

Where C_{TM} is the total module cost of all the major pieces of equipment.

C_{BM} is the bare module cost of each piece of equipment.

The total module costs (C_{TM}) refers to the capital investment cost required to make expansions or alterations on an already existing facility. The fixed capital investment required to build a plant from undeveloped land is referred to as grass roots costs and was calculated as shown below (Turton et al., 2008).

$$C_{GR} = C_{TM} + 0.50 \sum_{i=1}^{n} C_{BM,i} \quad 4.21$$

The bare module cost of each piece of equipment was calculated by determining the purchased cost first. This process was performed using various methods as described in Appendix E. The purchased cost was obtained at base conditions; carbon steel equipment operating at 1 atm. To account for the difference in material of construction, installation and other miscellaneous costs, bare module factors (F_{BM}) were used as illustrated by Equation 4.22.

$$C_{BM} = C_p^o \times F_{BM} \qquad 4.22$$

Where C_p^o is the purchased cost of the equipment

F_{BM} is the bare module factor

The cost of a piece of equipment is also strongly dependant on the material of construction. One of the reagents of the proposed process is acetylacetone, it is in large excess and is a very corrosive chemical. Several studies on the corrosion resistance of various materials found that stainless steel, monel, and aluminium are metals that are not corroded by acetylacetone at ambient conditions (1 atm, 20 °C) (Yamada, 2014; burkert, 2007). However, the corrosion resistance of these metals at higher temperatures (up to 140 °C) is yet to be determined. During the experimental work, severe corrosion of stainless steel tubes by acetylacetone was observed at 140 °C. Hence the corrosion resistance properties of the other metals at higher temperatures are uncertain. The use of glass-lined steel appears to be the most suitable option. This is because Pyrex glassware was used for all experimental work and showed excellent resistance to acetylacetone. It also presents the advantage of easy cleaning, less contamination and long operating life (De Dietrich, 2013).

The bare module cost of each piece of equipment was estimated using historical data and was then projected to the current year using Equation 4.23. The cost were then converted from US dollards to the local currency (ZAR) using a conversion rate of R10.56/$ (Exchange Rates UK, 2014).

$$\text{Cost in year A} = \text{Cost in year B} \times \frac{\text{Cost index in year A}}{\text{Cost index in year B}} \qquad 4.23$$

The bare module cost of the major pieces of equipment was obtained and the results are presented in Table 4.11.

Table 4.11: Summary of bare module costs

Process unit	**Cost (million Rands)**
Conveyor (C-101)	0.017
Mixer (M-101)	0.305
Heater (E-101)	1.338
Reactor (R-101)	22.956
Reactor (R-102)	22.956
Reactor (R-103)	22.956
Reactor (R-104)	22.956
Cooler (E-102)	1.431
Decanter (D-101)	1.763
Filter (F-101)	0.361
Crystallizer (CR101)	64.366
Condenser (E-103)	1.359
FlashDrum (V-101)	0.849
Cooler (E-104)	0.221
Cooler (E-105)	1.434
Total bare module cost	**165.265**

The total bare module cost was then used to estimate the total module cost (Equation 4.20) which was then used to calculate the fixed capital investment (Equation 4.21). Results of the total capital investment calculations (Appendix E) are summarized in Table 4.12.

Table 4.12: Summary of investment costs

Capital investments	**Cost (million Rands)**
Fixed capital investment (FCI)	277.645
Working capital [20% FCI] (WC)	55.529
Total capital investment (TCI)	**333.174**

Estimation of manufacturing cost

The estimation of the manufacturing cost of a product is a vital step toward the assessment of the economical feasibility of its manufacturing process. The major factors affecting the manufacturing costs are; raw material costs, utilities costs, waste treatment costs and cost of operating labour. Equation 4.24 shows how these factors are combined to calculate the total manufacturing costs (Turton et al., 2008).

$$COM = 0.280FCI + 2.73C_{OL} + 1.23\left(C_{UT} + C_{WT} + C_{RM}\right) \quad 4.24$$

Where COM is the cost of manufacturing

FCI is the fixed capital investment

C_{UT} is the costs of utilities

C_{WT} is the costs of waste treatment

C_{RW} is the costs of raw materials

The total manufacturing cost was calculated for a year of production (351 days). The raw materials requirement was obtained from the mass balance, and it was used along with the unit cost of each raw material to obtain the total raw material costs. The cost of acetylacetone was obtained using the market price from Alibaba.com (Alibaba, 2014). The aim of this process is to add value to the large stockpiles of iron ore fines considered as waste. Therefore, the plant should be situated next to the mentioned stockpiles, and the only cost associated with iron ore would be the solid handling cost. This cost was taken as 10 % of the iron ore price obtained from Alibaba.com (Alibaba, 2014). In addition the effect of fluctuations in the costs of iron ore was investigated in the sensitivity analysis in a later section. The total raw material costs were calculated and the results are presented in Table 4.13.

Table 4.13: Raw material information

Raw material	Annual feed rate (tons)	Unit cost (R/ton)	Cost (million Rands)
Acetylacetone	9669.127	39072.00	377.792
Iron ore	2229.343	65.28	0.146
Total cost of raw materials			377.938

To calculate the labour cost, it was assumed that the workers will work for 24 hours a day and 365 days a year. It was also assumed that a single operator works for 49 weeks a year and 5 shifts a week (Turton et al., 2008). Using the mentioned information, it was found that the proposed process will require 78 operators. Assuming a monthly income of R 13500 per operator (Salary survey, 2014), the total annual labour cost was found to be 12.636 million Rand.

The utilities comprised of cooling water, low pressure steam and electricity. Physical properties such as specific heat capacity and enthalpies were used along with energy balance results to calculate the required feed rates of cooling water and steam. The cost of cooling water was taken as R 21.91 per m^3 (Johannesburg municipality, 2014). The costs of steam and electricity tariffs were taken as R 399.575 per ton (Turton et al., 2008) and 0.6942 R/kWh (Eskom, 2014) respectively. The waste treatment cost was calculated as the cost for treating non-hazardous solid waste and hazardous waste water. The solid residue of the proposed process is comprised of inert metal oxides, mainly SiO_2, contained in the iron ore fines and the waste water stream contains some acetylacetone. These costs were taken as R 519.304/ ton and R 28850.196 per m^3 respectively (Turton et al., 2008). The total annual production costs are given in Table 4.14.

Table 4.14: Summary of annual production cost

Variable costs	Cost (million Rands)
Raw materials	377.938
Operating labour	12.636
Utilities	54.175
Waste treatment	62.935
Total Manufacturing costs	**721.145**

Sales and revenue

The revenue of the process is generated by the sale of the product, iron(III) acetylacetonate. It was assumed that all the product are sold and the revenue was then calculated as follows.

Revenue = Selling price of iron(III) acetylacetonate x Annual production rate

Annual iron(III) acetylacetonate production rate = 9600 tonnes

Cost of iron(III) acetylacetone = R 116.16 per kg ($ 11/ kg) (Alibaba, 2014)

The total revenue from the sales of iron(III) acetylacetonate was calculated at 1130.511 million Rands per annum.

Profitability analysis

The profitability of a chemical plant is a very important factor as it governs the choice of investing in a certain project as opposed to not investing. Amongst several methods for profitability analysis, cash flow diagrams and internal rate of return (IRR) were chosen for this study. To draw the cash flow diagram, it was assumed that the plant design and construction will take 2 years and production will start at the end of the second year. Therefore, the fixed capital investment was spread over the first 2 years. The plant life was taken as 10 years.

The depreciation was calculated using the straight line method over the operating life of the plant assuming that the plant had no salvage value. It was also assumed that the working capital is not recovered at the end of the plant life (worst case scenario). A taxation rate of 28% was assumed (SARS, 2014) and a discounted rate (r) of 12% was used (Turton et al., 2008). The net cash flow at the end of each year was calculated using Equations 4.25 – 4.28.

$$\text{Expenses} = \text{Total Manufacturing Costs} + \text{Depreciation} \quad (4.25)$$

$$\text{Income Tax} = (\text{Revenue} - \text{Expenses}) \times \text{Tax Rate} \quad (4.26)$$

$$\text{Net Profit} = \text{Revenue} - \text{Expenses} - \text{Income Tax} \quad (4.27)$$

$$\text{Cash Flow} = \text{Net Profit} + \text{Depreciation} \quad (4.28)$$

To account for the time value of money, the annual net cash was discounted as follows.

$$PV = \frac{\text{Cash flow in year n}}{(1+r)^n} \quad (4.29)$$

Where r is the discount rate.

The net present value (NPV) of the investment is the total cumulative net cash flow at the end of the plant life, and it is calculated as follows.

$$NPV = \sum_{n=1}^{n=12} \frac{PV}{(1+r)^n} \quad (4.30)$$

Figure 4.22 shows the plot of the non-discounted and the discounted cumulative cash flow diagram of the proposed project.

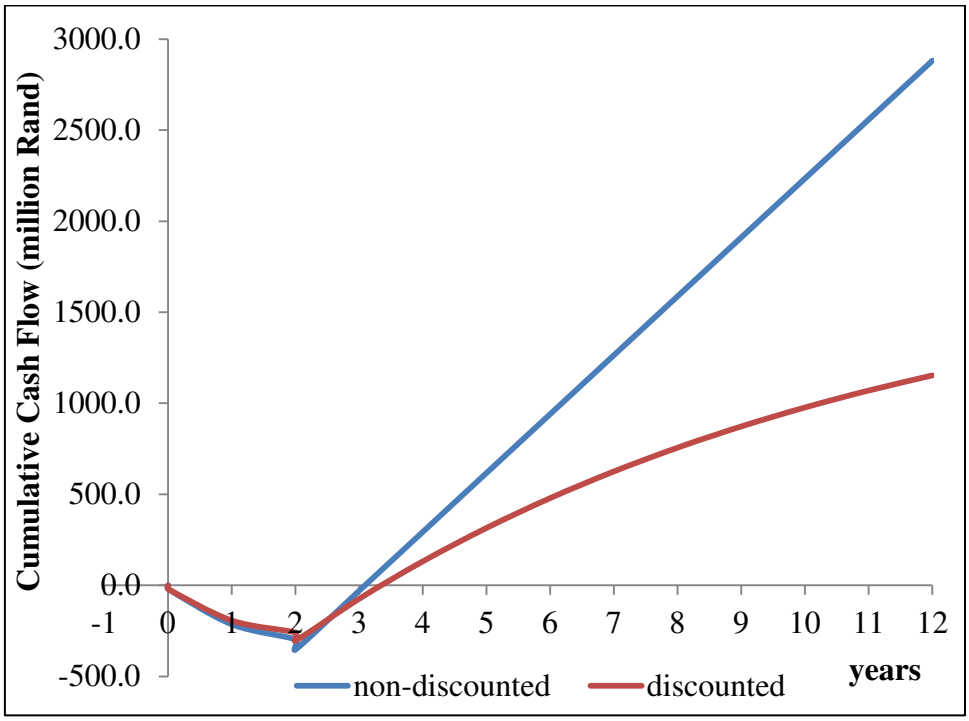

Figure 4.22: Cumulative cash flow diagram for the iron(III) acetylacetonate production process.

From the discounted cash flow diagram (Figure 4.22) it can be seen that the proposed process breaks even before 4 year from the start of the project and less than 2 years from the start of production. The graph also shows that the project would have made a net profit of more than 1 billion rand (1.153 billion Rand).

An alternative method to measure the profitability of a project is through the use of the internal rate of return (IRR). The IRR is the discounted rate that makes the NPV at the end of the plant life equals to zero. The IRR is evaluated through an iterative process during which the rate is varied until the NPV calculated using Equation 4.30 equals zero.

The IRR of the proposed process was found to be as high as 63%. This is well above typical investment return rates in the chemical industry and it indicates that the proposed manufacturing process will be a highly profitable investment. This is also illustrated by the relatively short payback period and the large NPV at the end of the plant life.

The high profitability of the iron(III) acetylacetonate manufacturing process is mostly due to high value (selling price) of iron(III) acetylacetonate (R 116160.00 per tonne) compared to acetylacetone (R 39072.00 per tonne) and iron (Alibaba, 2014). In addition, the production process is a simple process that requires a small capital investment and operates at a relatively low cost.

Sensitivity analysis

The economic analysis presented above was performed under the assumption that all the cost variables are known with absolute certainties. However, most factors do not remain constant during the entire lifetime of the plant, and are subjected to a certain level of changes (Turton et al., 2008). The construction time, plant capacity, price of product, interest rates, inflation rates, raw material price and plant capacity are just a few examples of the numerous variables that can influence the profitability of the process. This study focused on the sensitivity of the process to fluctuations in raw

material prices, product price, and plant capacity. The results of the mentioned sensitivity analysis are presented and discussed below.

Raw materials costs

Cost of acetylacetone

The sensitivity of the profitability of the iron(III) acetylacetonate manufacturing process to variations in the price of acetylacetone was investigated. A probable variation of the raw material price of -20% to +50% was chosen. This was based on forecasts over a 10 year plant life (Turton et al., 2008). The NPV and IRR at different acetylacetone prices within the chosen range were calculated and the results are presented in Table 4.15.

Table 4.15: Profitability of the process at different prices of acetylacetone

Cost of Acetylacetone (R/ton)	**NPV (million Rands)**	**IRR (%)**
29304.00 (-25%)	1421.420	71.7
39072.00 (Base)	1039.470	59.7
48840.00 (+25%)	657.520	45.9
58608.00 (+50%)	275.569	28.2

The results presented above show that the profitability of the manufacturing process is strongly affected by variations in the price of acetylacetone. Table 4.15 shows that a 25% decrease in the price of acetylacetone will increase the NPV at the end of the plant life from 1039.47 million Rands to 1421.42 million Rands. It can also be seen that a price increase of 50% will decrease the NPV to 275.569 million Rands. Even though the profitability of the process is strongly affected by variations in the price of acetylacetone, the process remains profitable over the entire price range as the NPV remains positive and the IRR relatively high. The payback period ranges from 3 to 5 years for the entire price range and this is illustrated by Figure 4.23.

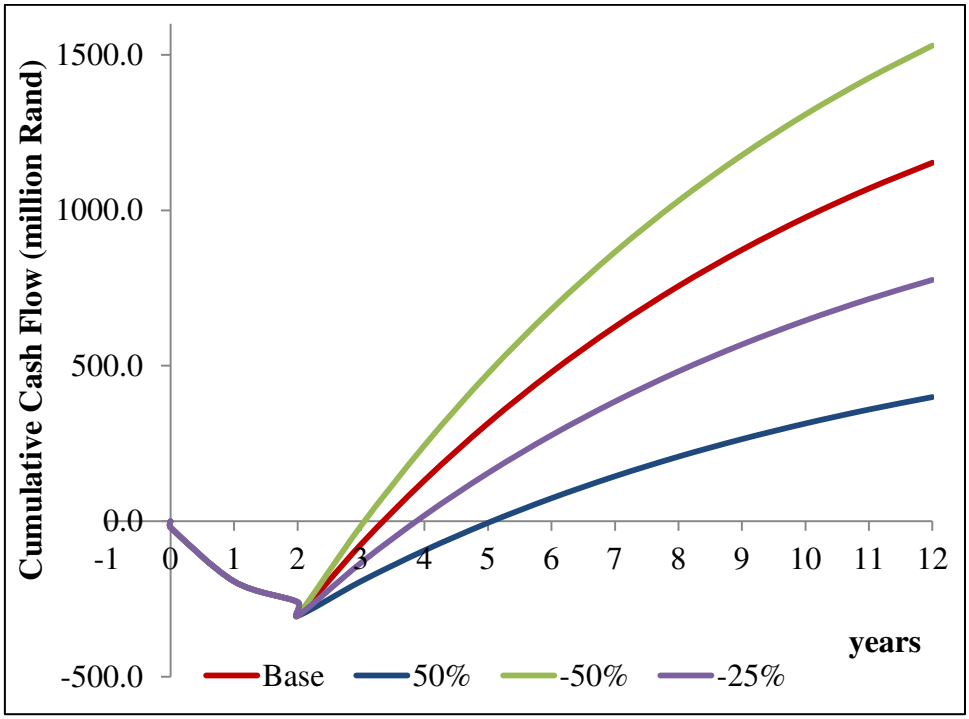

Figure 4.23: Effect of acetylacetone price on the cumulative cash flow of the iron(III) acetylacetonate production process.

Cost of iron ore fines

The sensitivity of the manufacturing costs to variations in the cost of the iron ore fines was also investigated. The cost of the iron ore fines was varied from zero (free) to the full market price of iron ore (0%-100% of R 652.80 per ton). The NPV and IRR at the different prices of iron ore fines are presented in Table 4.16.

Table 4.16: Profitability of the process at different prices of iron ore

Cost of iron ore fines (R/ton)	**NPV (million Rands)**	**IRR (%)**
0	1153.406	63
65.28 (10)%	1152.825	63
163.20 (25 %)	1151.954	63
326.40 (50 %)	1150.503	63
652.80 (100 %)	1147.601	62.90

The results presented in Table 4.16 show that the cost of iron ore fines has a small effect on the overall profitability. The NPV and IRR remain almost constant through the entire variation range. This is mainly because the feed rate and cost of iron ore are significantly lower than those of acetylacetone. This implies that price of acetylacetone is a more significant cost variable. The small effect of the cost of iron ore on the profitability of the project is also illustrated by Figure 4.24.

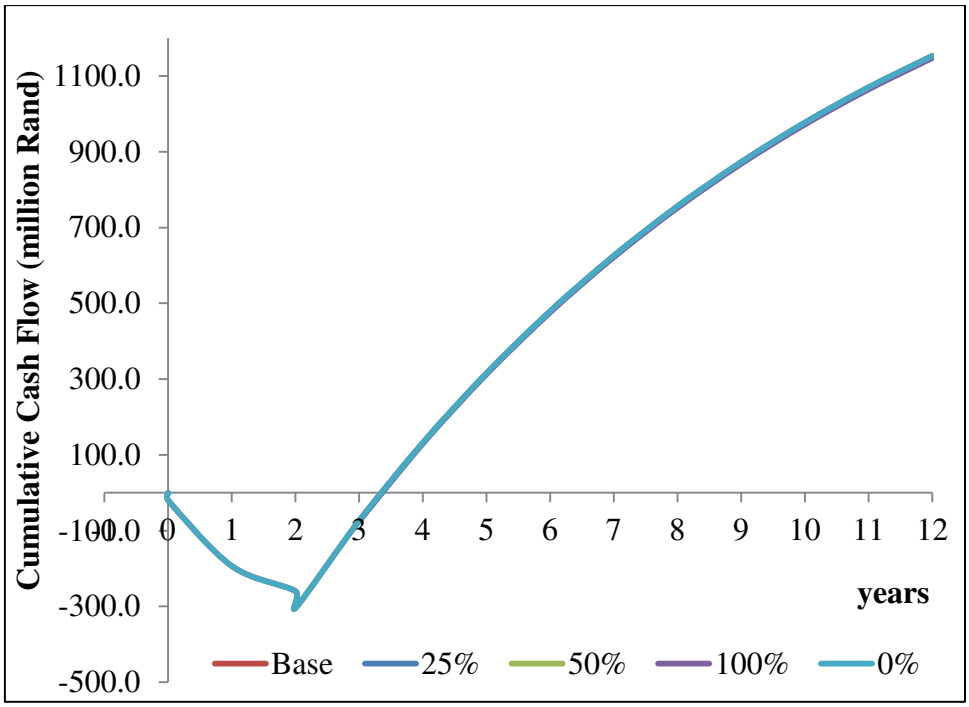

Figure 4.24: Effect of iron ore fines price on the cumulative cash flow of the iron(III) acetylacetonate production process.

Market price of the product

The sensitivity of the profitability of the process to variations in product price was performed for a variation range of -50% to +20% (Turton et al., 2008). The NPV and IRR at different selling prices of iron(III) acetylacetonate within the chosen variation range were calculated and the results are presented in Table 4.17.

Table 4.17: Profitability of the process at different prices of iron(III) acetylacetonate

Cost of iron(III) acetylacetonate R/ton	**NPV (million Rands)**	**IRR (%)**
58,080.00 (-50%)	-592.151	-
87,120.00 (-25%)	463.683	36.6
116,160.00 (Base)	1152.825	63
139,392.00 (+20%)	2156.025	92.7

Table 4.17 shows that the NPV and IRR of the manufacturing process vary significantly with fluctuations in the selling price of iron(III) acetylacetonate. A 20% increase in the product price will almost double the NPV at the end of the plant life (from 1152.825 million Rands to 2156.025 million Rands). The results also show that the process will still be profitable after a 25% decrease in selling price. However, a 50 % decrease in iron(III) acetylacetonate price will make the process unprofitable as it results in a negative NPV. The price of iron(III) acetylacetonate also has a large effect on the payback period as is illustrated by Figure 4.25. Therefore, a meticulous analysis of trends in the selling price of iron(III) acetylacetonate should be conducted prior to the design and construction of the proposed plant.

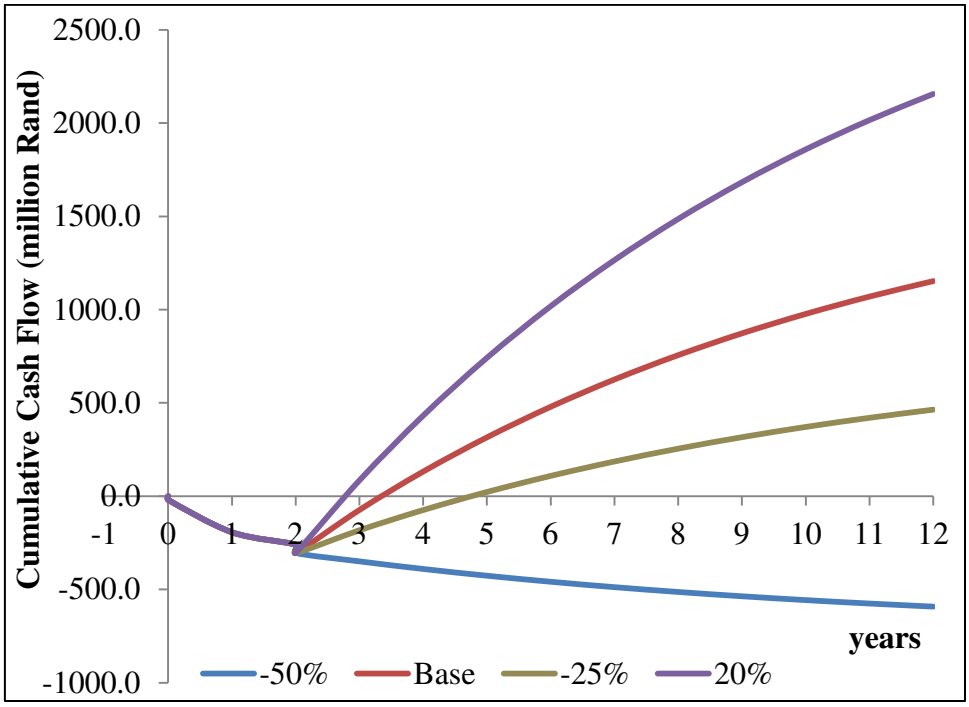

Figure 4.25: Effect of iron(III) acetylacetonate selling price on the cumulative cash flow of the iron(III) acetylacetonate production process.

Discount rate

The sensitivity of the profitability of the process to variations in discount rates was investigated. A discount rate fluctuation range of -50% to +50% was considered (Turton et al., 2008). The results obtained are presented in Table 4.18.

Table 4.18: Profitability of the process at different discount rates

Discount rate	**NPV (million Rands)**
Non-discounted (0 %)	2881.544
6%	1791.984
12%	1152.825
18%	759.627

Table 4.18 shows that the NPV of the project decreases considerably with increasing discount rate. As it can be seen, a discount rate of 6% reduces the non-discounted NPV by more than a billion (2.88 to 1.79 billion Rands), while a discount rate of

12% reduces the NPV by more than half (2.88 billion Rands to 1.15 billion Rands). Because the IRR of this process was found to be 63% at the base conditions, any discount rate lower than 63% will yield a positive NPV and hence a profitable project. Figure 4.26 shows the effect of the discount rate on the cumulative cash flow diagram of the project.

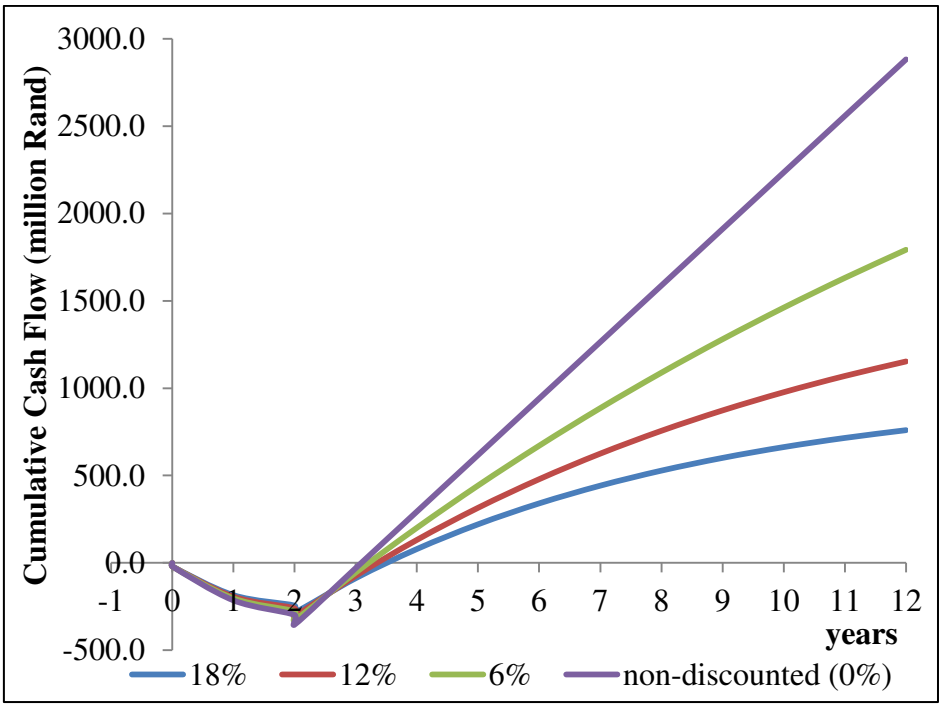

Figure 4.26: Effect of discount rate on the cumulative cash flow of the iron(III) acetylacetonate production process.

Plant capacity

The effect of plant capacity on the profitability of the process was also investigated. An additional mass and energy balance was performed for an annual iron(III) acetylacetonate production rate of 4800 tons (half the initial production capacity). The economic analysis of the smaller plant was also performed using the methods described above. The results obtained are presented in Table 4.19.

Table 4.19: Profitability of the process at different production rates of iron(III) acetylacetonate

Plant capacity (ton/year)	NPV (million Rands)	IRR (%)
4800	427.973	40.1
9600	1152.852	63

The results presented in Table 4.19 shows that a process plant of half the production capacity will have a smaller NPV and a lower IRR. It can also be seen from the cumulative cash flow diagram (Table 4.19) that the payback period will be slightly longer for the smaller process plant (between 4 to 5 years).

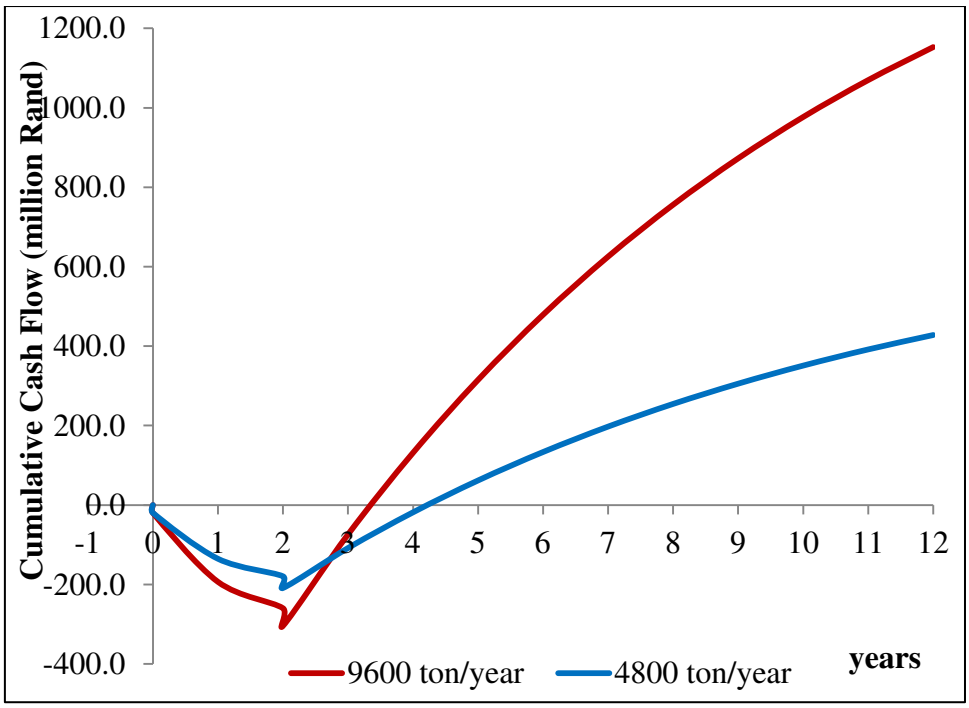

Figure 4.27: Cumulative cash flow diagram of the iron(III) acetylacetonate production process at different production rates.

From the results of the economical analysis, it appears that the production of iron(III) acetylacetonate is a viable value added process to utilize iron ore fines.

4.5.2 The production of iron nano-particles from iron ore fines

This study showed that the extraction of iron from iron ore fines using acetylacetone in the liquid phase is feasible and the proposed manufacturing process appears highly profitable. Studies by Zhang and co-workers (2011) showed the technical feasibility of recovering iron from iron(III) acetylacetonate in the liquid phase. This process step was combined with the results from the current study (leaching and recovery of iron(III) acetylacetonate crystals) to develop a conceptual process for the production of iron nanoparticles from iron ore fines.

Figure 4.28 is the process flow diagram for the proposed method of production of iron nanopartices. In this process, a concentrated solution of iron(III) acetylacetonate is produced using the iron(III) acetylacetonate manufacturing process (Figure 4.21) described above. The concentrated solution of iron(III) acetylacetonate (stream 16) is mixed with solvents (oleic amine and 1,2-dodecanediol) and then fed to the hydrogen reduction reactor (R-105). Hydrogen gas is fed to the reduction reactor (R-105) which is operated at 6 MPa and 300 °C as suggested by Zhang and co-workers (2011). The solvents are used to ensure that the iron particles are of uniform size and to avoid oxidation of the particles. The iron nanoparticles formed are separated from the solvents by filtration (F-102), the particles are then washed and dried to produce pure iron nanoparticles.

From a technology perspective the production of iron nanoparticles from iron ore fines is possible, however, for a complete economic evaluation of the process, additional research is required to determine the kinetics of the hydrogen reduction process.

C-101	M-101	E-101	R -101	R -102	R -103	R -104	E-102	D-101	F-101	CR-101	E-103	V-101	E-105	E-104	M-102	R-105	F-102	E-106
Screw conveyor	Mixer	Heater	Leaching Reactor	Leaching Reactor	Leaching Reactor	Leaching Reactor	Cooler	Decanter	Drum Filter	Crystallizer	Condenser	Flash Drum	Cooler	Condenser	Mixer	H2 reduction reactor	Filter	Dryer

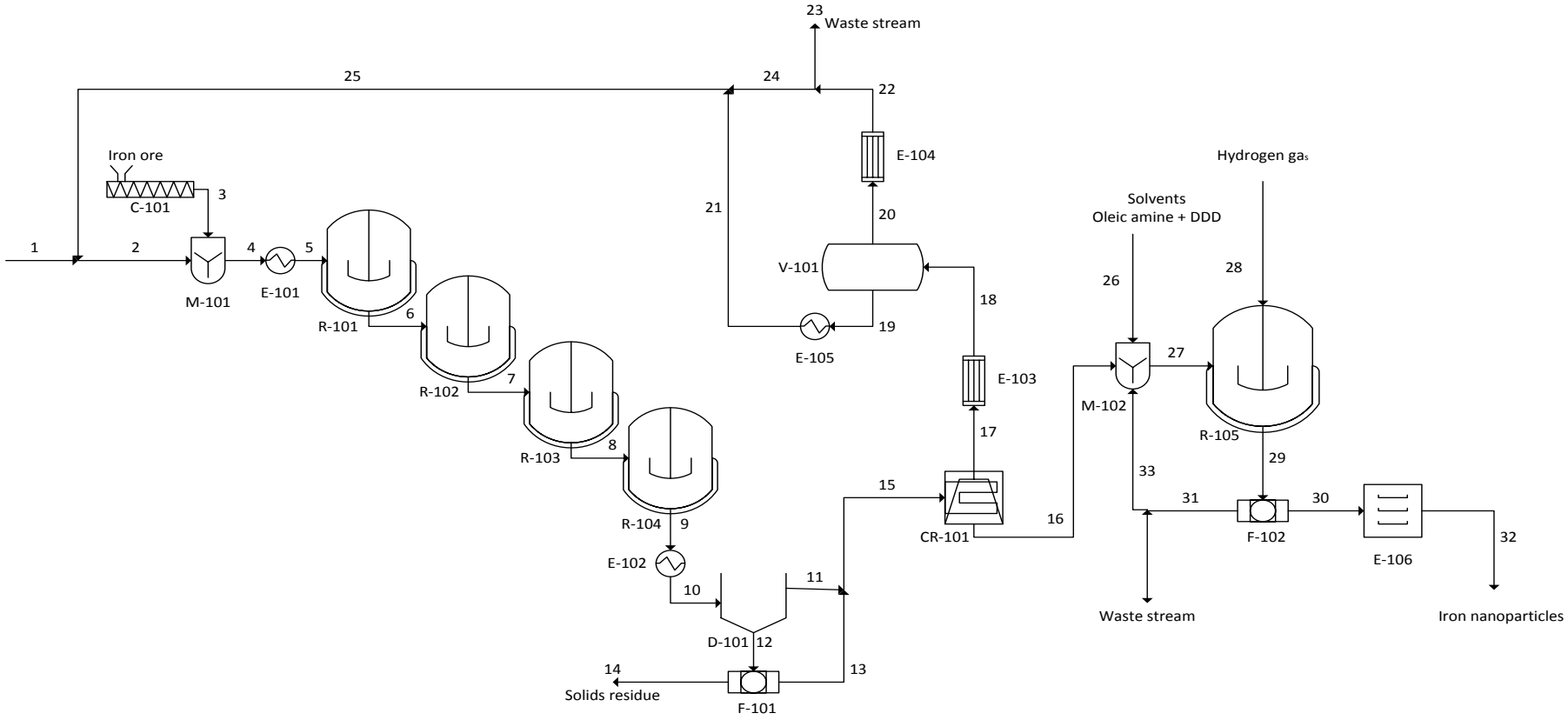

Figure 4.28: Process flow diagram for the manufacture of iron nanoparticles

5 CONCLUSIONS AND RECOMMENDATIONS

5.1 Conclusions

The aim of this work was to propose a green extraction process for the extraction of iron from iron ore fines. The following conclusions were drawn from the results.

It was found that iron ore fines are mostly hematite (93%), the iron particles are of irregular shape and the average particle size is 2512 µm. The extraction of iron from iron ore fines using acetylacetone in the gas phase was found to increase with temperature and acetylacetone flowrate, but decreased with bed weight. Gas phase extraction of iron was generally very slow and the highest iron extraction of 3.88% was achieved at 9 mL/min of acetylacetone at 250 °C after 6 hours. The low extraction in the gas phase was attributed to mass transfer limitations and the possible formation of a product layer (iron(III) acetylacetonate) on the surface of iron ore particles. Leaching by agitation was then chosen because acetylacetone act as a solvent of iron(III) acetylacetonate in the liquid phase.

The identification of the significant operating variables of the liquid phase extraction (leaching) was performed using the 2^k factorial design method, and it was found that within the chosen operating range, temperature and solid to liquid ratio have significant effects on the leaching efficiency. High iron extractions were achieved at low solid to liquid ratio and high temperature. Up to 97% of iron was extracted at the solid to liquid ratio of 0.025:1 at 140 °C for a total duration of 48 hours. The increase in iron extraction with increased temperature was attributed to the increased internal energy resulting in more collision between reacting molecules. The decrease in iron extraction observed at higher solid to liquid ratio was attributed to the formation of iron(III) acetylacetonate crystals in solution. These could form on the surface of unreacted iron ore particle and slow the extraction reaction. The kinetic analysis using a shrinking core model showed that the best initial fit was that of chemical reaction controlled kinetics. However the calculated activation energy from the modelling was 4.22 kJ/mol suggesting that the process might be controlled by diffusion. Furthermore, the

shrinking core models do not take into account the effect of solid to liquid ratio and the dissolution of iron(III) acetylacetonate in acetylacetone.

From the experimental results it can be concluded that the constituents of the leach solution resulting from the leaching of iron ore fines with acetylacetone can easily be separated using a Heidolph evaporator. Through this separation method unreacted acetylacetone was successfully recovered with little effects on its reactivity. Iron(III) acetylacetonate crystals were produced during this process. This could also be used as a platform for the development of a new method to synthesize iron(III) acetylacetonate crystals.

The recovery of iron by hydrogen reduction of iron(III) acetylacetonate in the gas phase was found to be possible. This was a first attempt in the gas phase. Low iron recoveries were obtained because of the low flowrate and concentrations of hydrogen used in this study. This was in agreement with previous studies on hydrogenation processes that showed that the reduction efficiency rates increases with hydrogen flowrate. However the experimental set up still needs to be optimized.

An industrial process to produce iron nanoparticles from the extraction and recovery of iron from iron ore fines with acetylacetone and hydrogen reduction was proposed conceptually. Such a process is technically possible based on the results presented in this study and another by Zhang et al. (2011). However, its economic feasibility is yet to be assessed. The kinetics of the hydrogen reduction process should be investigated in order to generate sufficient data to perform the investigation.

In addition, the experimental results were also used to conceptually design and evaluate a process that uses iron ore fines to produce iron(III) acetylacetonate. The production of iron(III) acetylacetonate by leaching of iron ore fines using acetylacetone was found to be economically feasible. The results from the sensitivity analysis indicated that the price of iron ore has negligible effects on the profitability, while the prices of acetylacetone and iron(III) acetylacetonate strongly affects the NPV and IRR of the process. The process remained profitable for large fluctuations in the price of acetylacetone and is more profitable for a large scale production process. However,

fluctuations in the iron(III) acetylacetonate price could negatively affect the economics of such a process and therefore a thorough market analysis is necessary.

5.2 Recommendations

Based on the knowledge gained from this project, the following can be recommended for future studies.

- The design of the gas phase experimental set up should be improved such that the effects of much higher acetylacetone flowrates can be investigated.
- The study of gas phase experiments should be performed on various types of iron ore in order to identify the characteristics that enhance extraction in the gas phase.
- Additional liquid phase experiments should be performed at higher pressure in order to expand the study of temperature influence, and to develop a kinetic model that covers a wider range of operating conditions.
- More efficient sublimation techniques should be designed to enable the study of hydrogen reduction at higher flowrates and concentrations of iron(III) acetylacetonate.

6 REFERENCES

ABC, (2013). Ore and coal waste reclamation and agglomeration group. <http://agglomeration-binder.com/iron-ore-fines/>. Accessed 04 October 2013.

Alibaba, (2014). http://www.alibaba.com/product-detail/red-powder-Ferric-acetylacetonate_658718175.html. Accessed 12 July 2014.

Alibaba, (2014). http://www.alibaba.com/product-detail/Acetylacetone-Pentane-2-4-dione-Diacetylmethane_1740117054.html. Accessed 12 July 2014.

Allimann-Lecourt, C., Bailey, T.H., Cox, M., Gilby, L.M., and Robinson, J., (1999). Extraction of heavy metals from sediments using the SERVO process. *Land Contamination & Reclamation.* vol. 7, pp. 265-269.

Allimann-Lecourt, C., Bailey, T.H., and Cox, M., (2002). Purification of combustion fly ashes using the SERVO process. *Journal of Chemical Technology and Biotechnology*, vol 77, pp. 260-26.

Amara, D., Felner, I., Nowik, I., and Margel, K., (2009). Synthesis and characterization of Fe and Fe_2O_3 nanoparticles by thermal decomposition of tri-irondodecarbonyl. *Colloids and Surface A: Physiochem. Eng. Aspects.* vol. 339, pp. 106-110.

Anon, (2011). Chemical engineering plant cost index. http://www.nt.ntnu.no/users//magnehi/cepci_2011_py.pdf. Accessed 22 December 2013.

Apblett, A.W., and Barber, K., (2010). Green technology for extraction of iron from ores and other materials. *Advances in Materials Science for Environmental and Nuclear Technolog.* pp. 169-176.

Ball, D.F., and Dartnell,J., (1973). Agglomeration of iron ores. *New York. American Elsevier Publishing Company Inc.* 1-20.

Biswas, A.K., (1981). *Principles of blast furnace ironmanking,* Cootha Publishing House. Brisbane, Australia.

Brunauer, S., (1943). *The Adsorption of gases and vapors*, Oxford University Pressvol.1, pp. 201-205.

Burkert., (2007). Fluid control system: chemical resistance chart. http://www.buekert.com/media/COM_Chemical_Resistance_Chart.pdf. Accessed 09 Febuary 2014.

Cao, Y., Harjanto, S., Shibayama, A., and Naitoh, I., (2006). Kinetic study of the leaching of Pt, Pd and Rh from automotive catalyst residue using chloride solutions.*Materials Transactions*, vol. 47, pp 2015-2024.

Charles, R.G., and Harverlack, P.G., (1969). The chemical vapour decomposition of cobalt metal from cobalt(II) acetylacetonate. *Journal of Inorganic and Nuclear Chemistry,* vol 31, pp. 995-1005.

Cox, M., Duke, P.W., and Gray, M.J., (1985). Extraction of metals by the direct thermal attack of organic reagents. *Extraction Metallurgy. Institute of Mining and Metallurgy,* pp. 33-42.

Daniel, C., (1959). Use of half normal plots in interpreting factorial two level experiments. *Hydrometallurgy,* vol.39, pp 321-335.

Demopoulos, G.P., and Distin, P.A., (1985). Direct copper precipitation from a loaded chelating extractant by pressure hydrogen stripping, *Metallurgical Transaction B.* vol. 16B.

De Dietrich, (2013), Introductory guide to glass-lined steel equipment, http://cdn2.hubspot.net/hub/47823/file-24022062pdf/docs/ddpsintroduction_to_glass-lining_.pdf. Accessed 15 December 2013.

ETSAP. (2010.). Iron and Steel. Technology brief 102. http://www.iea-etsap.org/web/e-techds/pdf/i02-iron&steel-gs-ad-gct.pdf available on 12-June-2013. Accessed 03 August 2013.

Exchange Rates Uk. (2014), http://www.exchangerates.org.uk/South-African-Rand-ZAR-currency-table.html. Accessed 21 July 2014.

Fogler, H.S., (2006). *Elements of Chemical Reaction Engineering,* Prentice-Hall Inc. pp. 813-852.

Geological survey of India (GSI).(2002). Government India.http://www.portal.gsi.gov.in/gsiDoc/pub/DID_iron_full_mark.pdf. Accessed 04 October 2013.

Gielen, D., Newman, J., and Patel, M.K., (2008). Reducing industrial energy use and CO_2 emissions: The role of materials science. *Mrs Bulletin*, vol.33. 751-769.

Habashi, F., (1969). *Principles of Extractive Metallurgy.* Gordon and Breach Science Publishers, Inc. vol. 2. pp. 142-149.

Hamblin, A P., and Posner A M., (1979). The use of acetylacetone as a selective extractant of organically bonded metals in soils. *Journal of Soil Science*. vol.30, pp.175-181.

Huheey, J.E., Keiter, E.A., and Keiter, R.L., (1993). *Inorganic Chemistry: Principles of Structure and Reactivity*. Harper Collins College Publishers, pp. 522-537.

Jamei, M.R., Khosravi, M.R., and Anvaripour, B., (2013). Investigation of ultrasonic effect on synthesis of nano zero valent iron particles and comparison with conventional method. *Asia-Pacific Journal of Chemical Engineering*, vol.8. pp 767-774.

Joburg Municipality, (2014). http://joburg.org.za/bylaws/water. Accessed 15 July 2014.

Kamiri, H., and Gheadi, M., (2002). Solvent extraction of iron from aluminium sulphate leach solution using acetylacetone-chloroform. *Asian Journal of Chemistry.* vol. 19, pp. 4173-4176.

Karl, J., (1997), Choice of X-ray target. http://pd.chem.ucl.ac.uk/pdnn/inst1/filters.htm. Accessed 01 September, 2014.

Katsuta, S., and Yanagihara, H., (1997). Extraction of Zirconium (IV) and Hafnium (IV) with acetylacetone in the presence of 3,5Dichlorophenol: remarkable hydrogen

bond acceptor ability of tetrakis (acetylacetonato) chelates. *Solvent Extraction and Ion Exchange,* vol. 15, pp. 577-589.

Knorr, T., Markus, K., Glenk, F., and Etzold, J.M., (2011). Shrinking core like fluid solid reactions: A dispersion model accounting for fluid phase volume change and solid phase particle size distributions. *Chemical Engineering Science,* vol.69, pp. 492-502.

Kolodynska, D., (2013). Application of a new generation of complexing agents in removal of heavy metals ions from different wastes, *Environmental Science and Pollution Research,* vol. 20, pp. 5939-5949.

Lamprey, (2006). Properties and applications of metal acetylacetonates, *Annals of The New York Academy of Science*, vol.88, pp 519-525.

Lee, H Y., and Kim, S G., (2003). Kinetic study on the hydrogenation reduction of ferrous chloride vapours for the preparation of iron powder. *Powder Technology,*vol. 152, pp. 16-23.

Levenspiel, O., (1972). *Chemical Reaction Engineering*. John Whiley and Sons, New York.

Luidold, S., and Antrekowitsch, H., (2007). Hydrogen as a reduction agent: state of the art science and technology. *Journal of Materials*, vol. 59, pp. 20-26.

Mariba, E.R.M., (2010), Gas phase extraction of metals from oxides using the ligand acetylacetone. *University of the Witwatersrand*.

Montgomery, D C., (2005). *Design and Analysis of Experiments*, John Wiley and Sons, New Jersey, USA.

Morgan G.T., and Drew H.D.K., (1920). Researches on residual affinity and co-ordination. *Journal of the Chemical Society*, pp. 117, 1456.

Mpana, N.R., (2012). The extraction of aluminium from fly ash using acetylacetone in gaseous phase. *University of the Witwatersrand.*

Myers, R.H., Montgomery , D.C., and Anderson-Cook, C.M., (2009). *Response surface Methodology*, 3rd ed, Whiley and sons, New Jersey, USA, pp. 75-109.

NIST (2013). http://webbook.nist.gov/cgi/cbook.cgi?ID=C123546&Mask=1EFF. Accessed December 2013.
NIST (2013). http://webbook.nist.gov/cgi/cbook.cgi?ID=C1317608&Mask=2. Accessed 14 December 2013.

OECD, (2010). Challenges and opportunities for the steel industry in moving towards green growth.http://www.oecd.org/sti/ind/45010081.pdf. Accessed 01 September 2014

Peter Brouwer., (2003). Theory of XRF.PANalytical. http://www.cl.eps.manchester.ac.uk/seaes/documents/research/agu/xrf_theory_booklet.pdf. Accessed 17-05-2013.

Peters, M.S., and Timmerhaus, K.D., (1991). *Plant Design and Economics for Chemical Engineers.* 4th ed. New York: McGraww-Hill Inc.

Plaul, F.J., Bohm, C., and Schenk, J.L., (2009). Fluidised-bed technology for the production of iron products for steel making. *The Journal of the Southern African Institute of Mining and Metallurgy,* vol. 108, pp. 121-128.

Potgieter, J.H., Kabemba, M.A., Teodorovic, A., Potgieter-Vermaak, S.S., and Augustyn, W.G., (2006). An investigation into the feasibility of recovering valuable metals from solid oxide compounds by gas phase extraction in a fluidised. *Minerals Engineering,* vol. 19, pp. 140-146.

Richardson, J.F., Harker, J.H., and Backhurst, J.R., (2002).*Chemical Engineering: Particle Technology and Separation processes*. Butter-Heinemann, vol. 2, 4th ed. pp. 407-410.

Rogers G.F.C., and Mayhew Y.R., (1995). *Thermodynamic and Transport Properties of Fluids.* 5th ed. Blackwell Publishing.

Salmi, T., Grenman, H., Bernas, H., Warna, J., and Murzin, D.Y., (2010). Mechanistic modelling of kinetics and mass transfer for a solid-liquid system: Leaching of zinc with ferric iron. *Chemical Engineering Science*, vol. 65, pp. 4460-4471.

Salary survey, (2014). http://www.mywage.co.za/main/salary/Paycheck. Accessed 20 July 2014.

SARS, (2013). http://www.sars.gov.za/TaxTypes/PAYE/Pages/PAYE-statutory-rates-and-tax-tables.aspx. Accessed 10 December 2013.

Sievers, R E., and Sadlowski J E., (1978). Volatile metal complexes, *Science*, vol. 201, pp. 217-223.

Sinnott, R. K., (2005). *Coulson & Richardson's Chemical Engineering: Chemical Engineering Design.* 4th ed. Oxford: Elsevier Butterworth-Heinemann.

Spencer J.N., Holmboe. E.S., Kirshenbaum R.M., Firth D.W., and Pinto P., (1982). Solvent effects on the tautomeric equilibrium of 2.4-pentanedione. *Canadian Journal of Chemistry,* vol.60.

Stabnikov, P.A., Pervukhina, N.V., Baidina, I.A., Sheludyakova, L.A., and Borisov, S.V., (2007). On the symmetry of iron(III) tris-acetylacetonate crystals, *Journal of Structural Chemistry*. vol. 48, pp. 186-192.

Trading Economics, (2014). South Africa interest rate, www.tradingeconomics.com/south-africa/ineterest-rate. Accessed 12 February 2014.

Turton, R., Bailie, R.C., Whiting, W.B., and Shaeiwitz, J.A., (2008). *Analysis, Synthesis, and Design of Chemical Processes*, 3rd ed. Prentics Hall PTR.

USGS, (2008). Iron ore statistics and information. US Geological Survey Minerals Information, US Department of interior, Available at http://minerals.usgs.gov/minerals/pubs/commodity/iron_ore. Accessed 15 August 2013.

vanDyk, L., Mariba, E.R., Chen, Y., and Potgieter, J.H., (2010). Gas-phase extraction of iron from its oxide in a fluidized bed reactor, *Minerals Engineering,* vol.1, pp. 58-60.

Wagner, D., Devisme, O., Patisson, F., and Ablitza, D., (2006), A laboratory study of the reduction of iron oxides by hydrogen. *Proceedings of SOhn International Symposium*, vol.2, pp.27-31.

Willis, A.L., Chen Z., He, J., Turro, N.J., and O'Brien, S., (2007). Metal acetylacetonates as general precursors for the synthesis of early transition metal oxide nanomaterials. *Journal of Nanomaterials,* pp. 1-7.

Wright, J.K., and Taylor, I.F., (1991). A review of progress of the development of new ironmaking technology, *Minerals Engineering.* vol. 4, pp. 983-1001.

Yamada, (2014), Air operated double-diaphragm pumps, http://www.yamadapump.com/literature/guides/Yamada_Corrosion_Guide_CR0214.pdf, Accessed 20 June 2014.

Yellishetty, M., Ranjith, P G., and Tharumarajah, A., (2010). Iron ore and steel production trends and material flow in the world: is this really sustainable?, *Resources, Conservation and Recycling.* vol.54, pp. 1084-1094.

Zervas T., McMullan J T., and Williams B C., (1996). Direct Smelting and alternative processes for the production of iron and steel, *International Journal of Energy Research,* vol.20, pp. 1103-1128.

Zhang, H., Wang, H., Tao, G., Chai, Y., and Que, G. (2011). Chemical synthesis of Fe nano-crystals via hydrogenation of ferric acetylacetonate. *materials for Renewable Energy & Environment,* vol.2, pp. 2066-2070.

APPENDICES

Appendix A: Characteristics of solid samples

Table A.1: Particle size distribution of the iron ore fines sample

Class Range (microns)	Mass Fraction
+5600	0.0341
-5600+4750	0.0645
-4750+4000	0.1054
-4000+3350	0.1286
-3350+2000	0.2897
-2000+1180	0.1786
-1180+600	0.1029
-600+400	0.0274
-400+300	0.0191
-300+212	0.0069
-212+150	0.0134
-150+106	0.0169
-106+75	0.0101
-75+45	0.0019
-45	0.005

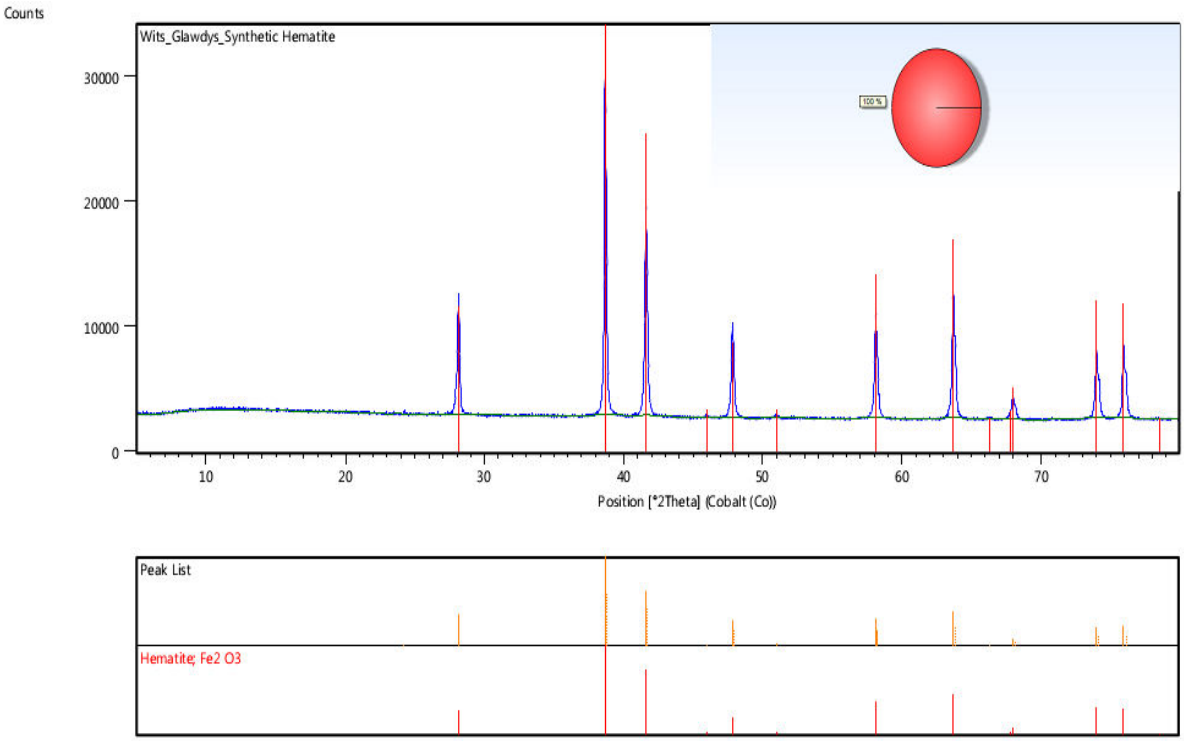

Figure A.1: XRF Diffractogram of synthetic hematite

Appendix B: Gas phase extraction

B.1 Analysis

The samples collected during the experimental test work were diluted and analyzed using the ICE 3000 series atomic absorption spectrophotometer (AAS) shown in Figure B.1. The appropriate lamp (Fe) was used, and the wavelength was chosen based on the concentration range. The calibration of the instrument was performed using standards prepared from synthetic Iron(III) acetylacetonate (>99.9%). Using distilled water all samples were diluted to the desired concentration range, and measurements were done in duplicate. The results of each analysis were used to calculate the extraction of iron from iron ore fines. This was performed as explained below.

Figure B.1: ICE 3000 series atomic absorption spectrophotometer

B.2 Calculations

During gas phase extraction experiments, samples were collected at specific time intervals. From each sample, 10 ml was collected, diluted and analyzed with an atomic adsorption spectrometer (AAS) as described above. The results from AAS analysis were then used to calculate iron extraction (%), and the calculation process is explained below.

The calculation was performed in the following sequence.

Mass of iron extracted

- The concentration of iron the in collected sample was determined from the AAS analysis results as presented below.

$$C_{Fe}\ \text{in sample solution} = C_{Fe}\ \text{in diluted solution} \times \text{dilution ratio} \qquad \text{B - 1}$$

$$\text{Where dilution ratio} = \frac{\text{Total volume of diluted solution}}{\text{volume of collected sample}}$$

- Using the concentration of iron in the collected sample, the mass of iron extracted and the mass of iron(III) acetylacetonatewas determined as follow.

$$m_{Fe} = C_{Fe} \times V_{sample} \qquad \text{B - 2}$$

$$m_{Fe-extracted} = m_{Fe} \times \frac{Mm_{Fe(acac)_3}}{Mm_{Fe}} \qquad \text{B - 3}$$

$\text{Where} m_{Fe(acac)_3} = \text{mass of iron (III) acetylacetonate (mg)}$

$C_{Fe} = \text{concentration of iron in collected sample (ppm)}$

$V_{Sample} = \text{Volume of collected sample (ml)}$

$Mm_{Fe} = \text{molar mass of iron (g.mol}^{-1}\text{)}$

$Mm_{Fe(acac)_3} = \text{molar mass of iron (III) acetylacetonate (g.mol}^{-1}\text{)}$

Mass of iron in weighted iron oresample

- The mass of iron contained in the amount of iron ore used was calculated as follows.

$$m_{Fe}\ \text{in iron ore} = \text{mass of iron ore} \times X_{Fe_2O_3} \times \frac{2 \times Mm_{Fe}}{Mm_{Fe_2O_3}} \qquad \text{B - 4}$$

Where $X_{Fe_2O_3}$ = mass fraction of hematite in iron ore = 0.93

$Mm_{Fe_2O_3}$ = molar mass of hematite (g.mol^{-1})

Iron extraction

Equations B-3 and B-4 were combined to calculate iron extraction or recovery as follows:

$$\text{Iron extraction } (\%) = \frac{\text{mass of iron extracted (mg)}}{\text{mass of iron in iron ore sample (mg)}} \times 100 \qquad \text{B - 5}$$

B.3 Experimental results

The experimental results for gas phase extraction are presented in Tables B1-B6. For each experimental run, samples were collected at the time interval specified in the tables below. The dilution ratio used is specified underneath each table.

Items listed in each table are defined as follow:

- Total volume of each sample collected during the experiment
- Concentration of Fe in the diluted solution is the concentration of iron as obtained from AAS analysis.
- Concentration of Fe in the collected sample is the concentration of iron in the collected sample, and was calculated from the concentration of the diluted solution.
- Mass of Fe $(Acac)_3$, Mass of Fe extracted and cumulative extraction of Fe were calculated using equations B-1 to B-7.

Table B.1: Gas phase extraction of iron from 20 g of iron ore fines at 250 °C and 9 mL/min acetylacetone flowrate.

Time	**Volume collected sample**	**Conc of Fein collected sample**	**Conc of Fein diluted solution**	**Mass of $Fe(Acac)_3$ extracted**	**Mass of Fe extracted**	**Cumulative extraction of Fe**
[min]	[mL]	[ppm]	[ppm]	[mg]	[mg]	[%]
15	143	258.096	25.8096	233.44	36.91	0.28
30	168	265.656	26.5656	282.27	44.63	0.63
45	172	290.944	29.0944	316.49	50.04	1.01
60	170	257.936	25.7936	277.34	43.85	1.35
90	303	193.845	19.3845	371.51	58.74	1.80
120	298	135.351	13.5351	255.07	40.33	2.11
150	300	109.533	10.9533	207.83	32.86	2.36
180	305	89.643	8.9643	172.92	27.34	2.57
210	285	94.507	9.4507	170.32	26.93	2.78
240	295	93.059	9.3059	173.61	27.45	2.99
300	610	95.450	9.545	368.22	58.22	3.44
360	602	96.176	9.6176	366.20	57.90	**3.88**

- **Dilution ratio: 10; Mass of iron ore sample: 20.003 g**

Table B.2: Gas phase extraction of iron from 20 g of iron ore at 250 °C and 6 mL/min acetylacetoneflowrate.

Time	**Volume collected sample**	**Conc of Fein collected sample**	**Conc of Fein diluted solution**	**Mass of $Fe(Acac)_3$ extracted**	**Mass of Fe extracted**	**Cumulative extraction of Fe**
[min]	[ml]	[ppm]	[ppm]	[mg]	[mg]	[%]
15	105	378.170	37.817	251.15	39.71	0.30
30	128	227.390	22.739	184.11	29.11	0.53
45	124	134.960	13.496	105.88	16.74	0.65
60	128	70.490	7.049	57.05	9.02	0.72
90	222	220.520	22.052	309.66	48.96	1.10
120	218	152.830	15.283	210.74	33.32	1.35
150	220	20.130	2.013	28.02	4.43	1.38
180	217	18.040	1.804	24.73	3.91	1.41
210	215	16.550	1.655	22.52	3.56	1.44
240	218	14.810	1.481	20.43	3.23	1.47
300	432	12.900	1.29	35.23	5.57	1.51
360	438	11.780	1.178	32.64	5.16	**1.55**

- **Dilution ratio: 10; Mass of iron ore sample: 20.123 g**

Table B.3: Gas phase extraction of iron from 20 g of iron ore at 275 °C and 6 mL/min acetylacetoneflowrate.

Time	**Volume collected sample**	**Conc of Fein collected sample**	**Conc of Fein diluted solution**	**Mass of $Fe(Acac)_3$ extracted**	**Mass of Fe extracted**	**Cumulative extraction of Fe**
[min]	[mL]	[ppm]	[ppm]	[mg]	[mg]	[%]
15	102	276.364	27.6364	178.29	28.19	0.22
30	120	156.289	15.6289	118.59	18.75	0.36
45	128	128.709	12.8709	104.17	16.47	0.49
60	124	113.650	11.365	89.11	14.09	0.60
90	220	110.710	11.071	154.07	24.36	0.78
120	222	102.830	10.283	144.39	22.83	0.96
150	216	80.130	8.013	109.48	17.31	1.09
180	218	79.284	7.9284	109.29	17.28	1.22
210	220	69.125	6.9125	96.20	15.21	1.34
240	218	50.432	5.0432	69.51	10.99	1.42
300	436	55.856	5.5856	154.01	24.35	1.61
360	430	48.652	4.8652	132.31	20.92	**1.77**

- **Dilution ratio: 10; Mass of iron ore sample: 20.018 g**

Table B.4: Gas phase extraction of iron from 50 g of iron ore at 275 °C and 6 mL/min acetylacetoneflowrate.

Time	**Volume collected sample**	**Conc of Fein collected sample**	**Conc of Fein diluted solution**	**Mass of $Fe(Acac)_3$ extracted**	**Mass of Fe extracted**	**Cumulative extraction of Fe**
[min]	[mL]	[ppm]	[ppm]	[mg]	[mg]	[%]
15	105	473.395	9.4679	314.40	49.71	0.15
30	123	408.915	8.1783	318.13	50.30	0.31
45	128	289.130	5.7826	234.08	37.01	0.42
60	127	266.105	5.3221	213.77	33.80	0.53
90	218	272.905	5.4581	376.26	59.49	0.71
120	220	221.930	4.4386	308.77	48.82	0.86
150	222	211.550	4.231	297.01	46.96	1.00
180	219	152.180	3.0436	210.80	33.33	1.10
210	220	75.225	1.5045	104.67	16.55	1.16
240	216	86.205	1.7241	117.77	18.62	1.21
300	441	59.025	1.1805	164.63	26.03	1.29
360	438	26.685	0.5337	73.94	11.69	**1.33**

- **Dilution ratio: 50; Mass of iron ore sample: 50.012 g**

Table B.5: Gas phase extraction of iron from 20 g of iron ore at 250 °C and 2 mL/min acetylacetoneflowrate.

Time	Volume collected sample	Conc of Fein collected sample	Conc of Fein diluted solution	Mass of $Fe(Acac)_3$extracted	Mass of Fe extracted	Cumulative extraction of Fe
[min]	[mL]	[ppm]	[ppm]	[mg]	[mg]	[%]
15	35	211.413	8.4565	46.80	7.40	0.02
30	51.5	350.820	14.0328	114.29	18.07	0.08
45	48	394.245	15.7698	119.66	18.92	0.11
60	52	252.860	10.1144	83.17	13.15	0.12
90	79.5	294.403	11.7761	148.00	23.40	0.19
120	78	242.513	9.7005	119.66	18.92	0.25
150	81	233.468	9.3387	119.60	18.91	0.31
180	79	200.880	8.0352	100.37	15.87	0.36
210	82	197.160	7.8864	102.27	16.17	0.41
240	81.5	174.270	6.9708	89.81	14.20	0.45
300	144	144.020	5.7608	131.17	20.74	0.51
360	138	140.083	5.603	122.26	19.33	0.57

- **Dilution ratio: 25; Mass of iron ore sample: 20.006 g**

Table B.6: Gas phase extraction of iron from 20 g of iron ore at 160 °C and 6 mL/min acetylacetoneflowrate.

Time	**Volume collected sample**	**Conc of Fein collected sample**	**Conc of Fein diluted solution**	**Mass of $Fe(Acac)_3$ extracted**	**Mass of Fe extracted**	**Cumulative extraction of Fe**
[min]	[mL]	[ppm]	[ppm]	[mg]	[mg]	[%]
15	105	219.071	219.0709	145.47	23.00	0.18
30	128	148.847	148.8468	120.49	19.05	0.32
45	124	56.400	56.3996	44.21	6.99	0.37
60	128	49.910	49.9099	40.41	6.39	0.42
90	222	36.874	36.8736	51.80	8.19	0.49
120	218	21.543	21.5431	29.73	4.70	0.52
150	220	12.813	12.8132	17.84	2.82	0.54
180	217	7.426	7.4255	10.18	1.61	0.56
210	215	6.880	6.8799	9.36	1.48	0.57
240	218	5.681	5.6809	7.84	1.24	0.58
300	432	4.626	4.6263	12.65	2.00	0.59
360	438	4.246	4.2456	11.76	1.86	**0.61**

- **Dilution ratio: 1; Mass of iron ore sample: 20.093 g**

Table B.7: Gas phase extraction of iron from 20 g of iron ore at 250 °C and 2 mL/min acetylacetoneflowrate.

Time	**Volume collected sample**	**Conc of Fein collected sample**	**Conc of Fein diluted solution**	**Mass of $Fe(Acac)_3$ extracted**	**Mass of Fe extracted**	**Cumulative extraction of Fe**
[min]	[mL]	[ppm]	[ppm]	[mg]	[mg]	[%]
15	102	3576.854	143.074	2307.50	364.84	2.61
30	121	3384.758	135.390	2590.33	409.56	5.54
45	123	3667.012	146.680	2852.68	451.04	8.77
60	128	2811.638	112.466	2276.19	359.89	11.35
90	214	1853.305	74.132	2508.43	396.61	14.18
120	218	1852.228	74.089	2553.84	403.79	17.07
150	222	1735.205	69.408	2436.39	385.22	19.83
180	216	1489.160	59.566	2034.40	321.66	22.13
210	220	1417.523	56.701	1972.35	311.85	24.37
240	216	1474.903	58.996	2014.92	318.58	26.65
300	436	1263.010	50.520	3482.81	550.67	30.59
360	439	448.950	17.958	1246.53	197.09	**32.00**

- **Dilution ratio: 25; Mass of hematite sample: 19.994**

Appendix C: Liquid phase extraction

C.1 Calculations

Calculation of main and interaction factors

The main and their interaction effects of the operating parameters were calculated using equations presented below (Myers et al., 2009). The main effects are; solid concentration (A), particle size (B) and temperature (C).

$$A = \frac{1}{4n}[a - (1) + ab - b + ac - c + abc - bc]$$

$$B = \frac{1}{4n}[b + ab + bc + abc - (1) - a - c - ac]$$

$$C = \frac{1}{4n}[c + ac + bc + abc - (1) - a - b - ab]$$

$$AB = \frac{1}{4n}[abc - bc + ab - b - ac + c - a + (1)]$$

$$AC = \frac{1}{4n}[(1) - a + b - ab - c + ac - bc + abc]$$

$$BC = \frac{1}{4n}[(1) + a - b - ab - c - ac + bc + abc]$$

$$ABC = \frac{1}{4n}[abc - bc - ac + c - ab + b + a - (1)]$$

The significance of each effect was estimated by the use of sum of square, and these were calculated using Equation C-1:

$$SS = \frac{(Contrast)^2}{8n} \qquad C - 1$$

Where contrasts can be calculated as follows:

For example contrast of A = $A/\frac{1}{4n}$ or = $[a - (1) + ab - b + ac - c + abc - bc]$

The contribution of each sum of square was calculated as the as a percentage of the total sum of squares.

The letters shown in the equations above correspond to the results of the experimental runs shown in Table C.1 below.

The calculations described above were performed using the Matlab code in Appendix F

Table C.1: Experimental conditions for the identification of influencing factors

Parameter	**Solid to liquid ratio**	**Particle size**	**Temperature**	**Run N°**
		[µm]	[°C]	
(1)	0.025:1	+106-150	120	1
a	0.127:1	+106-150	120	2
b	0.025:1	+400-600	120	3
ab	0.127:1	+400-600	120	4
c	0.025:1	+106+150	140	5
ac	0.127:1	+106-150	140	6
bc	0.025:1	+400-600	140	7
abc	0.127:1	+400-600	140	8

C.2 Experimental results

Identification of influencing factors

The experiments performed for the identification of influencing factors were performed according to experimental conditions shown in Table C.1.

Table C.2: Experimental data for identification of influencing liquid phase extraction parameters.

Run	Solution analyzed	Volume collected sample	Dilution Ratio	Conc. of Fe in collected sample	Conc of Fe in diluted solution	Mass of Fe extracted	Extraction of Fe	Total Fe extraction
		[ml]	-	[ppm]	[ppm]	[mg]	[%]	[%]
1	FS	250	25	6800.0	272.0	1700.0	52.27	52.27
	WS	250	1	0.0	0.0	0.0	0.00	
2	FS	250	25	23545.0	470.9	5886.3	36.20	39.63
	WS	250	1	474.6	474.6	118.7	0.73	
3	FS	250	25	4300.0	172.0	1075.0	33.05	33.05
	WS	250	1	0.0	0.0	0.0	0.00	
4	FS	250	25	24285.3	485.7	6071.3	37.34	38.20
	WS	250	1	564.6	564.6	141.2	0.87	
5	FS	250	50	12463.9	249.3	3116.0	95.81	97.72
	WS	250	1	248.4	248.4	62.1	1.91	
6	FS	250	50	20080.2	401.6	5020.1	30.87	34.52
	WS	500	2.5	1186.6	474.6	593.3	3.65	
7	FS	250	50	11592.1	231.8	2898.0	89.11	90.21
	WS	250	1	143.7	143.7	35.9	1.10	
8	FS	250	50	21780.0	435.6	5445.0	33.49	36.62
	WS	500	2.5	1020.1	408.0	510.0	3.14	

Effect of temperature

Table C.3: Effects of temperature on leaching of iron at 0.025:1 solid to liquid ratio.

T	Solution analyzed	Volume collected sample	Dilution Ratio	Conc of Fe in collected sample	Conc of Fe in diluted solution	Mass of Fe extracted	Extraction of Fe	Total Fe extraction
[ºC]	-	[ml]	-	[ppm]	[ppm]	[mg]	[%]	[%]
100	FS	500	25	2291.8	91.7	1145.9	35.23	35.23
	WS	250	1	0.0	0.0	0.0	0.00	
120	FS	250	25	6800.0	272.0	1700.0	52.28	52.27
	WS	250	1	0.0	0.0	0.0	0.00	
140	FS	250	50	12463.9	249.3	3116.0	95.81	97.72
	WS	250	1	248.4	248.4	62.1	1.91	
160	FS	250	50	12041.2	240.8	3010.3	92.56	94.75
	WS	250	1	285.2	285.2	71.3	2.19	

FS: Filtrate solution, WS: Wash solution

Table C.4: Effects of temperature on leaching of iron at 0.127:1 of solid to liquid ratio

T	Solution analyzed	Volume collected sample	Dilution Ratio	Conc of Fe in collected sample	Conc of Fe in diluted solution	Mass of Fe extracted	Extraction of Fe	Total Fe extraction
[ºC]	-	[ml]	-	[ppm]	[ppm]	[mg]	[%]	[%]
100	FS	250	50	15704.1	314.1	3926.0	24.14	24.71
	WS	250	1	368.4	368.4	92.1	0.57	
120	FS	250	25	6800.0	272.0	1700.0	52.27	52.27
	WS	250	1	0.0	0.0	0.0	0.00	
140	FS	250	50	20080.2	401.6	5020.1	30.87	34.52
	WS	500	2.5	1186.6	474.6	593.3	3.65	
160	FS	250	50	19382.2	387.6	4845.5	29.80	33.11
	WS	500	2.5	1078.4	431.3	539.2	3.32	

FS: Filtrate solution, WS: Wash solution

Effect of solid to liquid ratio

Table C.5: Effects of solid to liquid ratio on leaching of iron at 140 ^{0}C ,on 106 to 150 microns particles .

S/L Ratio	Solution analyzed	Volume collected sample	Dilution Ratio	Conc of Fe in collected sample	Conc of Fe in diluted solution	Mass of Fe extracted	Extraction of Fe	Total Fe extraction
	-	[ml]	-	[ppm]	[ppm]	[mg]	[%]	[%]
0.025	FS	250	50	12463.9	249.3	3116.0	95.81	97.54
	WS	250	1	12463.9	248.4	62.1	1.91	
0.038	FS	250	50	13067.5	261.4	3266.9	66.97	69.28
	WS	250	2.5	450.4	180.1	112.6	2.31	
0.051	FS	250	50	13617.5	272.4	3404.4	52.34	56.59
	WS	250	5	1105.7	221.1	1105.7	4.25	
0.076	FS	250	50	14426.0	288.5	3606.5	36.96	40.42
	WS	250	5	1350.4	270.1	1350.4	3.46	
0.127	FS	250	50	20080.0	401.6	5020.0	30.87	34.52
	WS	500	5	1186.6	474.6	593.3	3.65	

FS: Filtrate solution, WS: Wash solution

Table C.6: Effects of solid to liquid ratio on leaching of iron at 140 ^{0}C on +400 to -600 µm particlesize..

S/L Ratio	Solution analyzed	Volume collected sample	Dilution Ratio	Conc of Fe in collected sample	Conc of Fe in diluted solution	Mass of Fe extracted	Extraction of Fe	Total Fe extraction
	-	[ml]	-	[ppm]	[ppm]	[mg]	[%]	[%]
0.025	FS	250	50	11592.1	231.8	2898.0	89.11	90.21
	WS	250	1	143.7	143.7	35.9	1.10	
0.038	FS	250	50	13280.0	265.6	3320.0	51.04	51.87
	WS	500	1	108.2	108.2	54.1	0.83	
0.076	FS	250	50	14256.7	285.1	3564.2	36.53	37.11
	WS	500	1	112.3	112.3	56.2	0.58	
0.127	FS	250	50	21780.0	435.6	5445.0	33.49	36.62
	WS	500	2.5	1020.1	408.0	510.0	3.14	

FS: Filtrate solution, WS: Wash solution

Kinetic analysis

Table C.7: Kinetic data for leaching experiment at 80 ^{0}C.

Time	**Volume collected sample**	**Conc of Fein collected sample**	**Conc of Fein diluted solution**	**Mass of $Fe(Acac)_3$ extracted**	**Mass of Fe extracted**	**Fe extraction**
[Hours]	[ml]	[ppm]	[ppm]	[mg]	[mg]	[%]
3	250	603.60	12.07	333.75	150.9	4.64
6	250	950.94	19.02	525.80	237.7	7.31
12	250	2176.32	43.53	1203.36	544.1	16.73
18	250	3538.30	70.77	1956.45	884.6	27.20
24	250	4638.82	92.78	2564.96	1159.7	35.66
36	250	5849.89	117.00	3234.60	1462.5	44.97
48	250	6800.78	136.02	3760.38	1700.2	52.28

TableC.8: Kinetic data for leaching experiment at 100 ^{0}C.

Time	**Volume collected sample**	**Conc of Fein collected sample**	**Conc of Fein diluted solution**	**Mass of $Fe(Acac)_3$ extracted**	**Mass of Fe extracted**	**Fe extraction**
[Hours]	[ml]	[ppm]	[ppm]	[mg]	[mg]	[%]
3	250	547.66	10.95	302.82	136.9	4.21
6	250	898.89	17.98	497.02	224.7	6.91
12	250	1723.62	34.47	953.05	430.9	13.25
18	250	2649.83	53.00	1465.18	662.5	20.37
24	250	3036.18	60.72	1678.80	759.0	23.34
36	250	4059.94	81.20	2244.88	1015.0	31.21
48	250	4582.88	91.66	2534.03	1145.7	35.23

Table C.9:Kinetic data for leaching experiment at 120 ^{0}C.

Time	**Volume collected sample**	**Conc of Fe(Acac)3in collected sample**	**Conc of Fe(Acac)3in diluted solution**	**Mass of $Fe(Acac)_3$ extracted**	**Mass of Fe extracted**	**Fe extraction**
[Hours]	[ml]	[ppm]	[ppm]	[mg]	[mg]	[%]
3	250	304.40	6.09	168.31	76.1	2.34
6	250	517.74	10.35	286.27	129.4	3.98
12	250	1056.29	21.13	584.06	264.1	8.12
18	250	1724.92	34.50	953.77	431.2	13.26
24	250	2111.28	42.23	1167.40	527.8	16.23
36	250	2528.85	50.58	1398.28	632.2	19.44
48	250	3432.93	68.66	1898.18	858.2	26.39

Kinetic analysis graphs

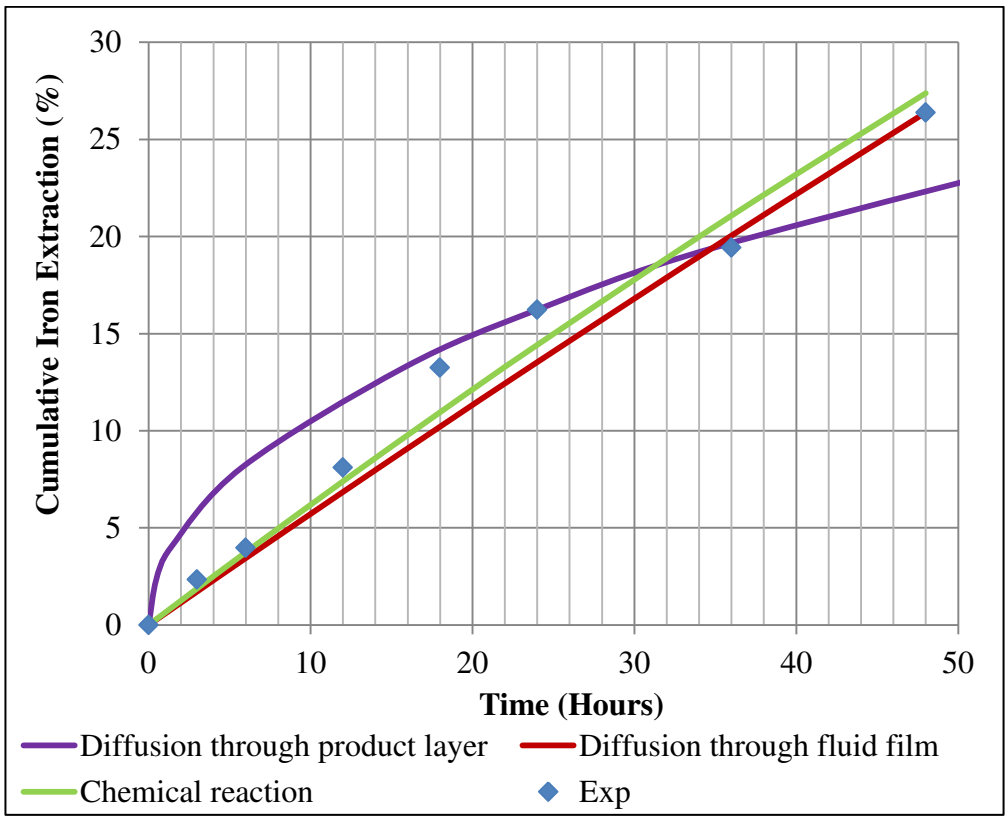

Figure C.1: Experimental extraction kinetic data and fitted shrinking core kinetics models at 80 °C (+106 to -150 µm particle size and 0.025:1 solid to liquid ratio).

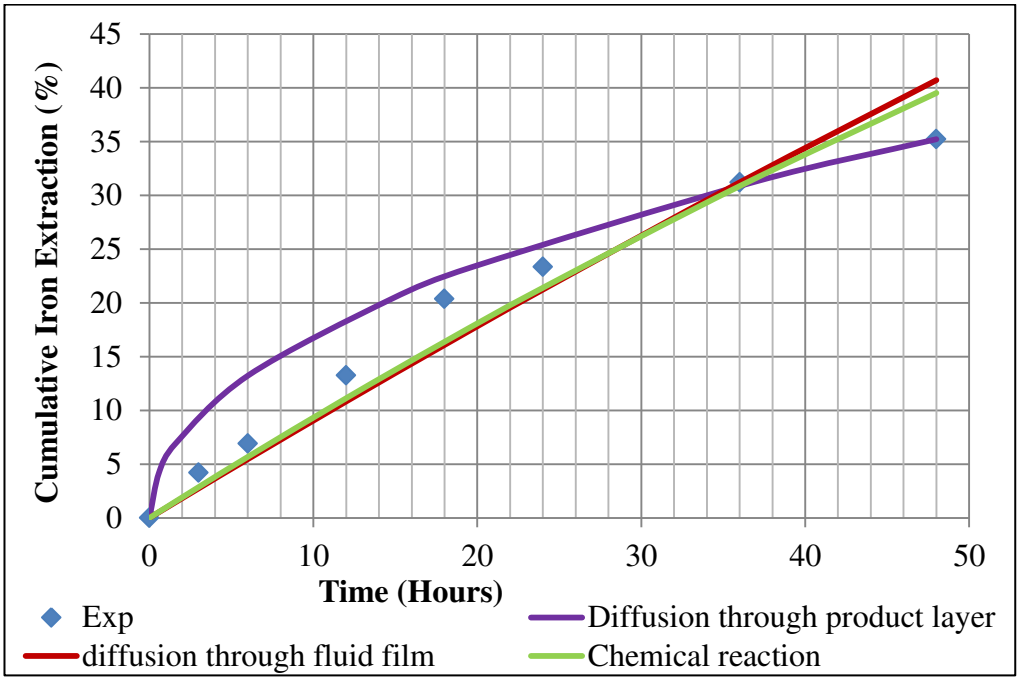

Figure C.2: Experimental extraction kinetic data and fitted shrinking core kinetics models at 100 °C (+106 to -150 µm particle size and 0.025:1 solid to liquid ratio).

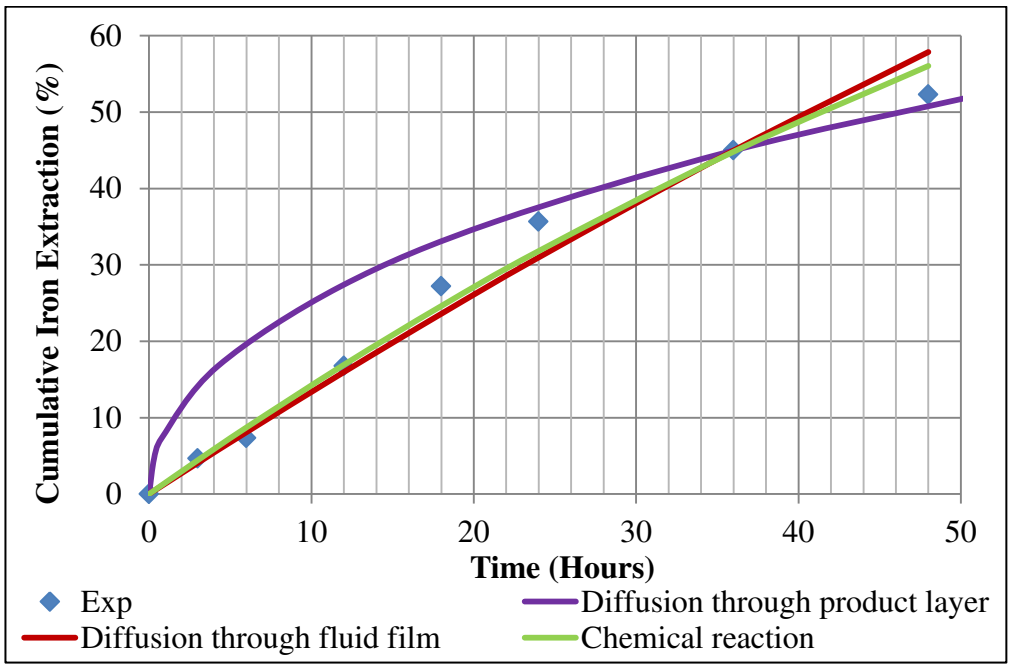

Figure C.3: Experimental extraction kinetic data and fitted shrinking core kinetics models at 120 °C (+106 to -150 µm particle size and 0.025:1 solid to liquid ratio).

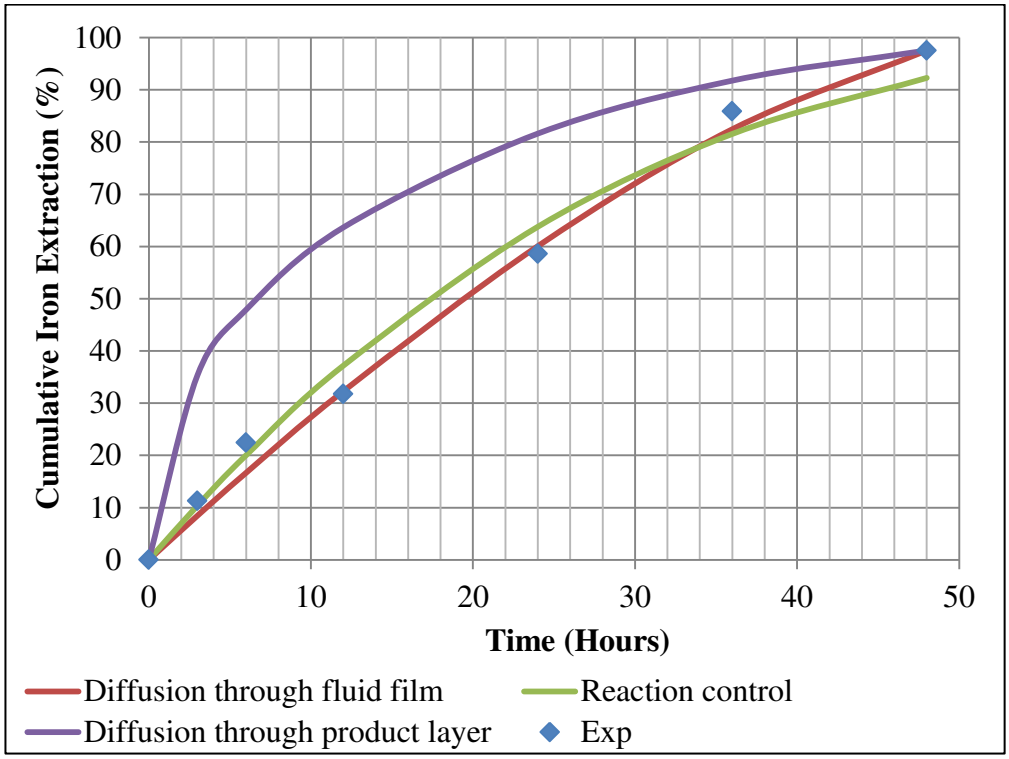

Figure C.4: Experimental extraction kinetic data and fitted shrinking core kinetics models at 140 °C (+106 to -150 µm particle size and 0.025:1 solid to liquid ratio).

Appendix D: Hydrogen reduction

D.1 Analysis and calculations

The hydrogen reduction experiment was conducted as described in section 3.5 of the report. To determine the amount of $Fe(acac)_3$ sublimated, the remaining $Fe(acac)_3$ was dissolved in a known volume of acetylacetone, and the resulting solution was analyzed using atomic adsorption analysis (AAS). The iron formed during the process was captured on the surface of glass beads. To quantify this amount, the glass beads were dissolved in 60mL of HCl, and the resulting solution was also analyzed using AAS. The procedure used to calculate recovery of iron is explained below.

The mass of $Fe(acac)_3$ in the acetylacetone solution is determined according to EquationD-1.

$$m_{Fe(acac)_3}\text{ in solution} = C_{Fe} \times V_{Solution} \times \frac{Mm_{Fe(acac)_3}}{Mm_{Fe}} \qquad \text{D-1}$$

Using the result of Equation D-1, the mass of $Fe(acac)_3$sublimated is then calculated as follow.

$$m_{Fe(acac)_3}\text{ sublimated} = \text{Initial } m_{Fe(acac)_3} - m_{Fe(acac)_3}\text{ in solution} \qquad \text{D-2}$$

$$m_{Fe-sublimated} = m_{Fe(acac)_3}\text{sublimated} \times \frac{Mm_{Fe}}{Mm_{Fe(acac)_3}} \qquad \text{D-3}$$

The concentration of Fe formed is determined in ppm using AAS on the hydrochloric acid solution. The mass of Fe is calculated using the equation:

$$m_{Fe} = C_{Fe}\text{ in } FeCl_3\text{ solution} \times V_{Solution} \qquad \text{D-4}$$

The recovery of iron is determined using Equation D-5.

$$\text{Iron recovery} = \frac{m_{Fe}}{m_{Fe-sublimted}} \times 100\% \qquad \text{D-5}$$

D.2 Experimental results

The results of hydrogen reduction are presented in Table D.1below. The dilution ratio for the iron(III) acetylacetone solution and the iron chloride solution were 10 and 1 respectively.

Table D.1: lists the results of the experiments conducted at different temperatures.

Temperature	**Initial mass of $Fe(acac)_3$**	**Conc of Fe in $Fe(acac)_3$ solution**	**Conc of Fe in $FeCl_3$ solution**	**Fe recovery**
[°C]	[mg]	[ppm]	[ppm]	[%]
250	1	308.644	48.83	46.38
270	1	291.704	48.48	23.67
290	1	301.834	34.86	28.96

Appendix E: Cost estimation

E 1: Physical properties of chemical components and utilities

The properties presented in Table E.1 were used for energy balance calculations.

Table E.1: Properties of chemical components

Compound	Enthalpy of formation (kJ/mol)	Heat capacity (kJ/mol°C)	Heat of vaporization (kJ/kmol)
Acetylacetone	-427.6 (NIST, 2013)	0.2323	45.254
Water	-285.83	0.0754	40.657
Iron ore ($Fe_2 O_3$)	-825.5(NIST, 2013)	0.1048 (NIST, 2013)	-
Iron (III) acetylacetonate	-72.473	0.4299	-

The flow rate of medium pressure steam required to provide the heat needed by the various heat exchanger units was calculated using the physical properties presented in Table E.2. These values were obtained from

Table E.2: Properties of medium pressure steam (5 bar) (Rogers and Mayhew, 1995)

Boiling temperature	151.8 °C
Enthalpy at 160 °C	2767
Enthalpy at 151.8 °C	2749
Enthalpy of condensation at 151.8°C	2109

Cooling water

The specific heat capacity of the water at 25 °C is 4.184 J/kmol. This property was used to calculate the flowrate of cooling water as described in section E.3.

E.2: Investment capital

The investment capital of the processing plant shown in Figure 4.20 was performed using the total module cost technique. This method uses the purchased cost of the

various pieces of equipment to calculate the total fixed investment (Turton et al., 2008). Equations 4.20 and 4.21 were used to calculate the total fixed investment as described in the results section.

$$C_{TM} = \sum_{i=1}^{n} C_{TM,i} = 1.18 \sum_{i=1}^{n} C_{Bm,i} \qquad 4.20$$

$$C_{GR} = C_{TM} + 0.50 \sum_{i=1}^{n} C^{o}_{BM,i} \qquad 4.21$$

The bare module cost was calculated for each piece of equipment as described below.

Equipment sizing and costing

The total cost of equipments is a major contributor to the capital investment required for a processing plant. The size of each piece of equipment was determined and used to estimate the purchased cost and the bare module cost. This was performed as highlighted below.

Conveyor

A screw conveyor was chosen for this process. Because the process is designed for 106 to 150 µm particles, a conveyor diameter of 0.1524 m (6inches) was chosen as it is most suited to handle particle smaller than 19 mm (3/4 inches) (Stanley, 1990). The bare module cost was estimated for a maximum length of (150 ft). The purchased cost was calculated using Equation E-1.

$$\log_{10} C_p^0 = K_1 + K_2 \log(A) + K_3 [\log(A)]^2 \qquad \text{E-1}$$

Where A is the area

$$Area = \pi DL = 21.82 m^2$$

K_1, K_2, and K_3 were taken as 3.6062, -0.7341, and 0.1982 (Turton et al., 2008).

The purchased cost in the year 2001 was found to be $ 951.98.

The module cost was estimated using a bare module factor for field installation of 1.10 (Turton et al., 2008).

$$C_{BM} = C_p^o F_{BM} \qquad \text{E-2}$$

Where C_{BM} is the bare module cost, C_p^o is the purchased cost, and F_{BM} is the module factor (1.1).

C_{BM} = R 11058.168 ($ 1047.175)

The 2001 module cost was then updated to the current year using Equation E-3, and then converted to the local currency (Rand) at an exchange rate of 10.56 (Exchange Rates UK, 2014). Using chemical engineering plant indexes (CEPCI), the bare module cost obtained is presented below.

$$\text{Cost in year A} = \text{Cost in year B} \times \frac{\text{Cost index in year A}}{\text{Cost index in year B}} \qquad \text{E-3}$$

$$\text{Cost} = 11058.168 \times \frac{595}{397}$$

Bare module cost of screw conveyor = R 16573.32

Mixer

The total cost of the mixer was constituted as the cost of the vessel and that of the impeller. A liquid retention time of 1 hour was chosen, and the volume of the vessel was estimated as described below.

Volumetric flow of Liquid = 9.523 m^3hr^{-1}

The mass flowrate and density of the stream were obtained from the simulation using the Aspen plus v8.4 software package.

Volume of vessel = $Q \times t = 9.284 \times 1 = 9.523$ m^3

Equation E-1 was then used to estimate the purchased cost of the vessel.

$$\log_{10} C_p^0 = K_1 + K_2 \log(A) + K_3 [\log(A)]^2 \quad \text{E-1}$$

Where A is the vessel size in m^3

K_1, K_2, and K_3 are the constants, and for a process vessel the value of 3.4947, 0.4485, and 0.1074 were used respectively (Turton et al., 2008).

C_p^0 = R 115541.32 ($10941.41)

The cost the impeller was calculated based on the power requirement. The power requirement for the mixing of slurries is roughly estimated as 10 HP per 1000 gallons (Stanley, 1990).

V= 9.523 m^3 = 2515.604 gallons.

P = 2.515 hp = 18.77 kw.

The mixing power was then used to calculate the purchased cost according to Equation E-1.

Where A is the mixing power in kw

The cost constants K_1, K_2, and K_3, were taken as 3.8511, -0.2911, and -0.0003 respectively (Turton et al., 2008).

C_p^0 = R 31883.90 ($3019.31)

The total purchased cost of the mixer was calculated as the sum of the vessel and agitator cost as shown below.

C_p= R 115541.32 + R 31883.90 = R 147425.21

To account for the installation cost F_{BM} factor of 1.38 was used according to Equation E-2.

The bare module cost of the mixer is R 203446.79

The cost was then projected to current data as shown below

$$\text{Cost= } 203446.79 \times \frac{595}{397} \textbf{= R 304913.96}$$

Heat exchangers

The purchased cost of heat exchanger was calculated based on the surface area required for heat transfer.

The surface area for the heat exchanger unit (E-101) was estimated using Equation E-4.

$$A = \frac{Q}{U\Delta T_{LM}} \qquad \text{E-4}$$

In this heat exchanger, stream 4 containing acetylacetone, water and iron ore (hematite) mixture is heated from 75 °C to 130 °C. The energy balance around this process unit can be summarized as follow

$$Q = \Delta H_{acetylacetone} + \Delta H_{Water} + \Delta H_{hematite} \qquad \text{E-5}$$

$$\Delta H_{acetylacetone} = \dot{m}_{acetylacetone} \times \int_{25}^{130} Cpdt \qquad \text{E-6}$$

$$\Delta H_{water} = \dot{m}_{water} \times (H_{\text{water at 25C}} - H_{\text{steam at 140C}}) \qquad \text{E-7}$$

$$\Delta H_{Hematite} = \dot{m}_{Hematite} \times \int_{25}^{130} Cpdt \qquad \text{E-8}$$

Using equations shown above heat duty was calculated.

The log mean temperature was calculated as follow.

$$\Delta T_{LM} = \left(\frac{\Delta T_2 - \Delta T_1}{\ln \frac{\Delta T_2}{\Delta T_1}} \right) \qquad \text{E - 9}$$

The equations shown above were combined to find the heat transfer area.

The same approach was used to size all heat exchanger units and the results are tabulated below.

Table E.3: Characteristics of heat exchanger units

Unit	**Q(KW)**	**U(KW/m^2°C)**	**ΔT_{LM}(°C)**	**A(m^2)**
E-101	872	0.75	65.0	17.88
E-102	-1254	0.5	56.4	44.49
E-103	-1089	0.85	87.3	14.68
E-104	-174	0.85	57.2	3.58
E-105	-297	0.50	57.2	10.41

The purchased cost was calculated using the equation Equation E-1.

Where A is the heat transfer area in m^2

K_1, K_2, and K_3 are the constants, and for a process vessel the value of 4.8306, 0.8509, and 0.3187 were used respectively.

The cost calculated using Equation E-1 was for carbon steel as material of construction. For the purchased cost of glass-lined heat exchangers, a material factor of 4.8 was used. The cost were then projected to the current year using CEPI indexes and converted to the local currency (Rand).

The procedure described above was applied to all the heat exchanger units and the results are tabulated below.

Table E.4: Module costs of heat exchanger units

Heat Exchanger Unit	Costs (millions Rand)
E-101	1.338
E-102	1.431
E-103	1.359
E-104	0.221
E-105	1.434

Reactors

The leaching of iron ore fines with acetylacetone is performed in a series of four autoclave operated as a continuous stirred reactor (CSTR). Experimental results showed that the maximum iron extraction was obtained at 140°C, a solid to liquid ratio of 0.025:1 and for a total reaction time of 48 hours. The leaching reactor are of equal size, hence a residence time of 12 hours per reactor. The total cost of the reactor was constituted of the cost of the reactor vessel and that of the agitator.

The volume of the reactor was then as estimated as follow.

V = volumetric flowrate (Q) $\times$ density

Q = mass flowrate $\times$ density

The density of the slurry was calculated using Equation E-10

$$\rho_{Slurry} = \frac{100}{\left(\frac{\%_{Solid}}{\rho_{Solid}} + \frac{\%_{Liquid}}{\rho_{Liquid}} \right)} \qquad \text{E-10}$$

The density of the liquid was taken as 0.885 ton/m^3, it was obtained from Aspern plus v8.4. The density of iron ore was taken as 5.049 ton/m^3 and the density of the slurry was found to be 0.904 ton/m^3. The density of the slurry was then used to calculate the volumetric flowrate as described.

$$Q_{Slurry} = 9.583 m^3 h^{-1}$$

$$V_{Reactor} = 9.583 m^3 h^{-1} \times 12h = 114.99 m^{-3}$$

The purchased cost of the reactor vessel operating at ambient pressure and constructed with carbon steel was estimated using Equation E-1 (Turton et al., 2008).

Where A is the vessel size in m^3

K_1, K_2, and K_3 are the constants, and for a process vessel the value of 3.4947, 0.4485, and 0.1074 were used respectively.

$$C_p^0 = \text{R } 795973.58 \ (\$75376.29)$$

The cost the impeller was calculated based on the power requirement. The power requirement for the mixing of slurries is roughly estimated as 10 HP per 1000 gallons (Stanley, 1990).

V= 114.99 m^3 = 30376.1 gallons.

P = 232.44 hp = 226.61 kw.

The mixing power was then used to calculate the purchased cost of the turbine mixer according to Equation E-1.

Where A is the mixing power in kw

The cost constants K_1, K_2, and K_3, for the turbine mixer were taken as 3.4092, -0.5104, and 0.003 respectively (Turton et al., 2008).

$$C_p^0 = \text{R } 1767.56 \ (\$167.38)$$

The total purchased cost was then estimated as follows.

$$C_p^0 = 795973.58 + 1767.56 = \text{R } 797741.14$$

Because the reactor is glass lined, a factor of material of construction had to be used. A cost factor of 4.8 was used (Turton et al., 2008). An average bare module factor of 4 was used to account for installation costs. These factors were used according to Equation E-2.

The bare module was of the reactor in the year 2001 was found to be R 15316629.85.

The cost was then projected to current data using Equation E-3.

$$\text{Cost} = 15316629.85 \times \frac{595}{397} = \textbf{R 22955654.3}$$

Filter (F-101)

A top feed drum filter was chosen for this process. This is because it is the most suitable for slurries with high solid concentration, with free draining solids of fast settling velocity (Richardson, et al., 2002). The usual maximum area for such a filter is 10 m^2, and this area served as basis for the estimation of the filter cost. Equation E-1 was once again used to estimate the purchased cost.

Where A is the filter area (10 m^2)

4.8123, -0.7142 and 0.042 were used for K_1, K_2, and K_3 respectively

The purchased cost in the 2001 was found to be **$** 13,807.02**.**

Using the bare module factor to account for installation cost, the module cost was estimated as follows.

Where F_{BM} is for drum filter is estimated at 1.65 (Turton et al, 2008).

The module cost was found to be **$** 22,781.59**.**

The 2001 cost was then projected to current data and converted to local currency.

$$\text{Filter cost} = 503{,}481.99 \times \frac{595}{397}$$

Filter cost = $ 34,143.69 = R 360,557.32

Crystallizer (C-101)

The cost of a crystallizer is dependent on the production rate. A forced convection crystallizer was chosen for this process, and its purchased cost was calculated using Equation E-11(IFP, Chemical Engineer's Handbook, p. 19.40).

$$C = f \exp\left[4.868 + 0.3092 \ln W + 0.0548\left(\ln W^2\right)\right] \qquad \text{E-11}$$

Where W is the klb/h of crystals

The monthly iron(III) acetylacetonate production rate of 800 tons corresponds to 2.45 klb/h. The purchased cost of the crystallizer in the year 1985 was estimated at $ 448,237.56.

To account for the material of construction and installation costs, Equation E-2 was used. A material cost factor of 4.8 and the installation cost factor of 1.6 were used (Turton et al., 2008).

The bare module was found to be $ 3,442,464.49.
The total module cost obtained above was of the year 1985. The calculated cost was then projected to current data according to Equation E-3.

$$\text{Bare module of Cost= } \$3{,}442{,}464.49 \times \frac{595}{325} = \$\ 6{,}032{,}257$$

Bare module of crystallizer = 63.7 million Rand

Flash drum (V-101)

A horizontal separator without a demister pad was chosen for vapour-liquid separation. In order to estimate the bare module cost of the flash drum, the purchased cost was determined first and combined with module factors. The purchased cost is dependent of the vessel size, and the preliminary sizing of the separator was performed as described below.

The settling velocity of the liquid droplets was calculated using Equation E-12.

$$u_t = 0.07\left[\frac{\rho_{liq} - \rho_{gas}}{\rho_{gas}}\right]^{1/2} \qquad \text{E-12}$$

Where the liquid density (ρ_{liq}) and the gas density (ρ_{gas}) were obtained from Aspen as 885.26 kg.m^{-3} and 1.27 kg.m^{-3} respectively.

The settling velocity was found to be 1.85 m.s^{-1}.

For a flash drum without a demister pad, the recommended gas velocity is calculated as follows.

Gas velocity $u_a = 0.15 \times u_t = 0.278$ m.s^{-1}

For preliminary design, the gas and liquid are assumed to occupy equal volume inside the vessel (Sinnot, 2005).

Height of gas $h_g = 0.5D_v$

Where D_v is the diameter of the vessel.

For operating pressure of 0-20 bar, a length to diameter ratio of 3 is recommended (Sinnot, 2005).

Gas volumetric flowrate =0.143 m^3.s^{-1} (Aspen plus v8.4)

Cross sectional area for the flow of gas = $0.5 \times \frac{\pi D^2}{4} = 0.393D^{-2}$ E-13

The gas linear velocity $u_g = \frac{0.143}{0.393D_v^2} = 0.364D_v^{-2}$ E-14

The gas residence time required for the droplet to drop to the liquid surface is calculated using Equation E-15.

$$\frac{h_v}{u_a} = \frac{0.5D_v}{0.278} = 1.801D_v \quad \text{E-15}$$

The actual residence time is calculated using Equation E-16 (length of vessel/linear velocity of gas).

$$\frac{L_v}{u_g} = \frac{3D_v}{0.364D_v^{-2}} = 8.248D_v^3 \quad \text{E-16}$$

Equating Equation E-15 and Equation E-16, the following is obtained.

$D_v = 0.467$ m

$L_v = 3D_v = 1.401\text{m}$

The Volume of the vessel was then calculated as follows.

$$V_v = \pi\left(\frac{0.467}{2}\right)^2 1.401 = 0.240m$$

The volume of liquid in the vessel $V_{liq} = 0.5V_v = 0.120m^3$

Volumetric flow of liquid is 0.161 m^3. min.

The liquid residence time is then calculated as follows.

$$t = \frac{0.120}{0.161} = 0.75\,\text{min}$$

This is below the minimum allowable time of 10 minutes. The vessel diameter has to be increased to obtain a satisfactory residence time. The diameter was then increased by a factor estimated as follows.

$$r = \left(\frac{10}{0.75}\right)^{0.5} = 3.65$$

New diameter = $0.467 \times 3.65 = 1.7$ m

New length = $1.7 \times 3 = 5.11$ m

New volume of liquid = $0.5 \times \left(\frac{1.7}{2}\right)^2 \times \pi \times 5.11 = 5.80$ m^3

New residence time = $\frac{5.80}{0.161} = 36$ min

The new residence time is higher than the minimum required. Hence, the volume of flashdrum =11.60 m^3

The volume of the flash drum obtained above was then used to estimate the purchased cost of the flashdrum. This was performed using Equation E-1.

Where A is the flashdrum volume (11.60 m^3).

3.5567, 0.3776 and 0.0903 were used for K_1, K_2, and K_3 respectively. (Turton et al., 2008)

The purchased cost in year the 2001 was found to be **$** 11,506.83

Using the bare module factor to account for the material of construction, the module cost was estimated using Equation E-2. The module factorF_{BM} is for glass-lined vessels was taken as 4.8 (Turton et al, 2008).

The module cost was found to be **$** 55,232.78

The purchased cost presented above was based on the 2001 data, the cost was then projected to current data and converted to local currency.

$$\text{Flash drum cost} = 55{,}232.78 \times \frac{595}{397}$$

Flashdrum cost = $ 79231.9035= 0.837 million Rands

E.3. Manufacturing Cost

The major contributors to the manufacturing cost are; raw material cost, labour cost, utilities cost and waste treatment cost.

$$COM = 0.280FCI + 2.73C_{OL} + 1.23\left(C_{UT} + C_{WT} + C_{RM}\right)$$

The factors mentioned above were calculated as described below.

Labour cost

The labour cost was calculated using the method illustrated below (Turton et al., 2008)

$$N_{OL} = \left(6.29 + 31.7P^2 + 0.23N_{np}\right)^{0.5} \quad \text{E-17}$$

Where: $N_{OL}$is the number of operators per shift, $P^2$is the number of processing steps involving the handling of particulate solids, and $N_{np}$is the number of non-particulate processing steps

$$\text{Therefore Cost of operating labour} = \text{operating labour} \times \text{wages per year}$$

For the proposed plant $P^2$is 3, and N_{np} is 9

$$N_{OL} = \left(6.29 + 31.7(3)^2 + 0.23N_{np}\right)^{0.5} = 17.137$$

Assumptions

- A single operator works on average 49weeks a year, five 8hour shifts a week. This amounts to 245shifts/year/operator.
- The chemical plant operates 24 hours/day. 3 shifts will be carried out per day. This amounts to 1095 operating shifts per year.
- The number of operators required for a shift was calculated as follows

$$\frac{1095\ \text{shifts per year}}{2458\ \text{shifts per operator per year}} \approx 4.5\ \text{operators (Turton et al., 2008)}$$

Operating labour = $N_{OL} \times\ 4.5\ operators$

= 78 operators

Plant operators earn a monthly income of around R13500 according to (Salary survey, 2014).

Hence the annual cost of operating labour = 78× R13500 × 12 = **12.636 million Rands**

Cost of utilities

The cost of utilities was constituted of cooling water, steam, and electricity. The requirement of each of the mentioned utility was obtained from energy balance calculations. Cooling water was obtained at ambient temperature (25 °C), and was heated to the recommended maximum temperature of 45 °C (Turton et al, 2008). The total power consumption was calculated as the sum of the estimated power consumption of the mixer, all the reactors and conveyor.

The feed rate of water was calculated using Equation E-18. Where Q is the heat duty of the heat exchanger unit, C_P was taken as 0.004184 kJ/kg°C, and a ΔT of 15 °C (30 °C to 45 °C). .

$$m_{water} = \frac{Q}{C_P \Delta T} \qquad \text{E-18}$$

The cooling water requirements for the various heat exchanger units are presented in Table E.5.

Table E.5: Feed rates of cooling water

Heat exchanger unit	**Duty (Q) kW**	**Water feed rate (m^3 /year)**
E-102	-1254	606147.493
E-103	-1089	526352.116
E-104	-174	84255.988
E-105	-297	143730.804
Total cooling water requirement		**1360486.402**

The feedrate of steam required to provide the amount of heat needed for the various was calculated using Equation E-19 and Equation E-20. The results obtained are presented in Table E.6.

$$m_{Steam} = \frac{Q}{\Delta H_{Steam}} \qquad \text{E.19}$$

$$\Delta H_{Steam} = (\text{H at } 160°C - \text{H at } 151.8\ °C) + \Delta H \text{ of condensation} \qquad \text{E-20}$$

The enthalpies mentioned in Equation E-20 can be found in Table E.2.

Table E.6: Feedrate of medium pressure steam

Process Unit	**Duty (Q) (kW)**	**Steam feed rate (ton/year)**
E-101	871.882	12673046
CR-101	1923.167	27953759
Total steam requirement		**40626805**

The various utilities costs described above are summarized in Table E.7

Table E.7: Summary of utilities costs

Item	**Costs (million Rands)**
Water	29.808
Steam	16.233
Electricity	8.133
Total	**54.175**

Once the Raw materials costs, operating labour costs, utilities costs, and waste treatment was determined the total manufacturing cost was determined using Equation 4.24 and Table E.8 gives a summary the results.

Table E.8: Summary of manufacturing costs

Costs	**Cost (million Rands)**
Raw materials	377.938
Operating labour	12.636
Utilities	54.175
Waste treatment	62.821
Total Manufacturing costs	**724.963**

E.4 Profitability and sensitivity analysis

The profitability of the proposed process was analyzed using the cash flow diagram and IRR criteria. The annual net cash flow was calculated as described in the result section.

Table E.7: Cash flow distribution

Year	**Net cash flow**
0	Cost of Land
1	30 % of FCI
2	70% of FCI + Working Capital
3-12	Net cash flow (Equation 4.28)

The sensitivity of the process profitability to fluctuations in raw material costs, product price and plant capacity was investigated, and the results were presented and discussed in section 4.5. Figure E.1 shows the cash flow diagram at various prices of acetylacetone.

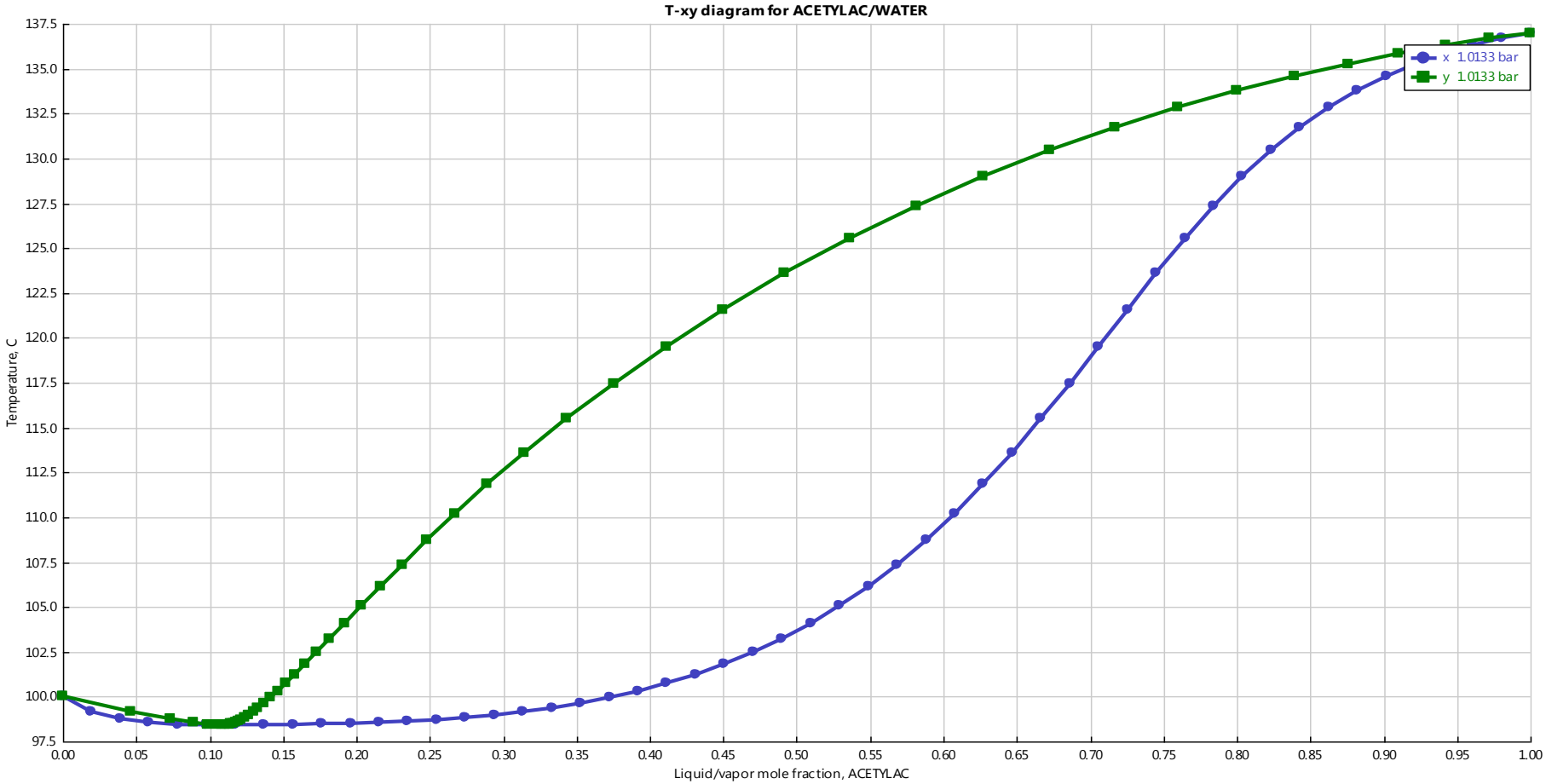

Figure E.1: Txy phase diagram of the acetyl-acetone mixture

Appendix F: Matlab codes

F.1 Program for determining dimensions of fluidized bed reactor

```
size=input ('size class range:')

dp=(sqrt(size(1)*size(2)))/10000      % ....size in cm

Qliquid = input('Q in ml/min:')

Mass = input('M iron ore sample in grams:')

dens_sol = 4.8500                    ;%.... g/cubiccm

dens_liq = 0.980                     ;%.....9/cubiccm

dens_gas = 0.0035                    ;%.....g/cubiccm

visc_liq = 7.67e-04                  ;%.....Pa.s

visc_gas = 1.29e-04                  ;%.....gram/cm-s

Qliq = Qliquid/(60*1000000)          ;% Q...cubic meters/s

sph = 1                              ;

emf = 0.484                          ;


%.... calculation of minimum fluidizing velocity using assumed voidage....

umf_1          =(((dp^2)*(dens_sol-dens_gas)*981)*(emf^2)*(sph^2))/(150*visc_gas*(1-
emf));       %....cm/sec

Remf=dp*umf_1*dens_gas/visc_gas                                    ;

Qgas=Qliq*dens_liq/dens_gas                                ;       %..... volumetric flow
in m3/sec
```

```
RequiredArea=Qgas/(umf_1/100)          ;    %..... Area for minimum fluidising velocity m2

Diam = sqrt(RequiredArea*4/3.14)                    ; %..... tube diameter in meters

%.... calculation of minimum fluidizing velocity using Archimede number ifdp< 0.06

Ar = (dp^3)*dens_gas*(dens_sol-dens_gas)*980/(visc_gas^2)          ;

Remf_2 = (((33.7^2)+0.0408*Ar)^(0.5))-33.7                    ; %.....Reynold number

Umf_2 = visc_gas*Remf_2/(dp*dens_gas)                    %.....Minimum fluidizing velocity in cm/sec

Uo_2=1.5*Umf_2                                %.....Operating velocity

Area_2=Qgas/(Uo_2/100)                    ;

Diam_2=sqrt(Area_2*4/3.14)                    %.....Maximum allowed diameter

% if dealing with coarse particles... the following equations are used.

else

Ar = (dp^3)*dens_gas*(dens_sol-dens_gas)*980/(visc_gas^2)          ;

Remf_2 = (((28.7^2)+0.0494*Ar)^(0.5))-28.7                ;

Umf_2 = visc_gas*Remf_2/(dp*dens_gas)

Uo_2=1.5*Umf_2

Area_2=Qgas/(Uo_2/100)                    ;

Diam_2=sqrt(Area_2*4/3.14
```

```
end

%.... calcuation of terminal velocity

dpt = dp*(((dens_gas*(dens_sol-dens_gas)*980)/(visc_gas^2))^(1/3))

ut=((1/18)*(dens_sol-dens_gas)*((size(1)/10000)^2)*980)/visc_gas% terminal velocity

Ga=(dp^3)*dens_gas*(dens_sol-dens_gas)*980/(visc_gas^2)

Re_o= ((2.33*(Ga^0.018))-(1.53*(Ga^(-0.016))))^13.3

Ust=visc_gas*Re_o/(dens_sol*dp)

r=Ust/Umf_2

Diam = sqrt((Qgas/(Ust/100))*4/3.14)
```

F.2 Program for the identification of influencing factors

```
n = 1      ;     %.... number of replicate

i = 52.3   ;     %.... extraction at low level for all factors

a = 35.5   ;     %.... extraction % for run II

b = 33.1   ;     %.... extraction % for run III

ab = 36.7  ;     %.... extraction % for run IV

c = 97.7   ;     %.... extraction % for run V

ac = 34.5  ;     %.... extraction % for run VI

bc = 90.2  ;     %.... extraction % for run VII

abc = 36.6 ;     %.... extraction % for run VIII
```

```
%..... Calculation of Effect estimates

A=(1/(4*n))*(a-i+ab-b+ac-c+abc-bc)

B=(1/(4*n))*(b+ab+bc+abc-i-a-c-ac)

C=(1/(4*n))*(c+ac+bc+abc-i-a-b-ab)

AB=(1/(4*n))*(abc-bc+ab-b-ac+c-a+i)

AC=(1/(4*n))*(i-a+b-ab-c+ac-c+abc)

BC=(1/(4*n))*(i+a-b-ab-c-ac+bc+abc)

ABC=(1/(4*n))*(abc-bc-ac+c-ab+b+a-i)

%..... Calculation of Sum of Squares

SSA=((a-i+ab-b+ac-c+abc-bc)^2)/(8*n)

SSB=((b+ab+bc+abc-i-a-c-ac)^2)/(8*n)

SSC=((c+ac+bc+abc-i-a-b-ab)^2)/(8*n)

SSAB=((abc-bc+ab-b-ac+c-a+i)^2)/(8*n)

SSAC=((i-a+b-ab-c+ac-c+abc)^2)/(8*n)

SSBC=((i+a-b-ab-c-ac+bc+abc)^2)/(8*n)

SSABC=((abc-bc-ac+c-ab+b+a-i)^2)/(8*n)

SSTOT= SSA+SSB+SSC+SSAB+SSAC+SSBC+SSABC

%.... Calculation of Sum of Square percent contribution

SSA_Contribution = (SSA/SSTOT)*100

SSB_Contribution = (SSB/SSTOT)*100
```

SSC_Contribution = (SSC/SSTOT)*100

SSAB_Contribution = (SSAB/SSTOT)*100

SSAC_Contribution = (SSAC/SSTOT)*100

SSBC_Contribution = (SSBC/SSTOT)*100

SSABC_Contribution = (SSABC/SSTOT)*100